



**Politecnico
di Torino**

Politecnico di Torino

Corso di Laurea Magistrale in Ingegneria Meccanica

Tesi di Laurea Magistrale

ROTOR DYNAMICS WITH PASSIVE MAGNETIC BEARINGS

Relatore:
Prof. Alessandro Vigliani

Correlatori:
Prof. Elvio Bonisoli
Dr. Domenico Lisitano

Candidato:
Salvatore Paolo Cavallaro

A.a. 2020/2021

Index

Index.....	1
Abstract.....	2
Introduction.....	3
1. Magnetic rotor.....	4
1.1 Rotor components	5
2. Structural modifications	7
2.1 Structural stiffness.....	7
2.2 Threaded connections	8
2.3 Ball transfer unit.....	11
2.3.1 Current configuration.....	11
2.3.2 First alternative solution.....	12
2.3.3 Second alternative solution	12
2.3.4 Third alternative solution	13
2.3.5 Comparison between the four configurations	14
3. Positioning of optical sensors	16
3.1 Position sensors.....	16
3.2 Speed sensor.....	19
4. Motor and clutch assembly	21
4.1 Preliminary design	21
4.2 Optimised design.....	25
5. Measurement of the vertical force component.....	30
5.1 Load cell configuration	30
5.2 Scale configuration	32
6. Final layout	35
7. Rotor Oscillation Analysis	40
8. Electrical components of the test bench.....	44
8.1 Driver setting.....	45
8.2 System wiring	47
8.3 Modification of system wiring.....	50
9 Pre-test of optical sensors	51
9.1 Pre-test layout	51
9.1.1 Magnetic rotor.....	51
9.1.2 Laser tachometer.....	53
9.1.3 Support structure for keyence optical sensors.....	54
9.2 Post-processing analysis of pre-test data	56
9.2.1 Post-processing analysis of displacements	56
9.2.2 Post-processing analysis of voltage pulses	59
9.3 Tests results.....	61
9.3.1 Test 1-9 (plastic plate, drifting).....	62
9.3.2 Test 10-16 (plastic plate, no drifting).....	63
9.3.3 Test 17-21 (glass plate, no drifting).....	65
9.3.4 Analysis of dynamic rotor behaviour.....	66
9.3.5 LUPOS model	70
9.3.6 Analysis in frequency domain.....	70
Appendix.....	73
Reference	84

Abstract

The aim of this thesis is to design a test bench to study the dynamic behaviour of a rotor with passive magnetic bearings characterized by the minimisation of the energy dissipated due to friction. This rotor is connected to an actuation system consisting of a magnetic clutch and an electric motor in order to simulate its behaviour as a kinetic energy accumulator. The first part of the thesis describes the optimisation of the original rotor design, the layout of the support structure for measuring displacements and angular velocity, the project of the actuation system and the electrical wiring to control it. The second part concerns experimental analysis and consists of the collection and post-processing of displacement and speed data of another magnetic rotor in order to carry out preventive tests before studying the rotor designed in this thesis.

Introduction

The term "rotordynamics" refers to the specialised branch of applied mechanics that studies the behaviour and diagnosis of rotating structures. A rotor is a body suspended by a set of cylindrical hinges or bearings that allows it to rotate freely around an axis. Rotordynamics represents a complex engineering problem because of the difficulties involved in meeting specifications for different operating conditions. There are many ways of employing rotational motion: to achieve translation, to store energy, to transfer power from one point to another and to obtain kinetic energy from other kinds of energy. Even if rotors used in machines and mechanisms provide numerous advantages, as regards efficiency, wear, and easy adjustments, "mechanical side effects" are related to the rotational movements: the rotor rotation can be accompanied by various vibration modes that depend on the structure of the rotor and its unbalance.

For this reason, the first part of the thesis aims to implement a series of modifications to the initial design of the rotor, in order to optimise its operation, and the development of the structures necessary to measure its displacement and speed. Then, it is possible to characterise the dynamic behaviour of the rotor by identifying its main vibrational modes and to study its motion by creating different types of rotor parameterisation. These different settings are achieved by introducing dynamic imbalances, varying the number of magnetic bearings used and changing the relative position between their fixed and mobile rings by setting the vertical location of the rotor with respect to that of the stator. The purpose of studying the operation of the rotor is to be able to use it as a kinetic energy accumulator, which is why the mechanical couplings and electrical connections of the actuation system for transferring torque to the rotor are also designed in this first part.

The second part of the thesis is experimental and aims to analyse the displacement and speed data measured by the optical sensors. Preliminary tests were carried out on a small magnetic rotor in order to understand its operation and to develop a Matlab script that allows the post-processing of the data acquired, before moving on to the analysis of the rotor initially presented.

1. Magnetic rotor

Following the ISO definition, a rotor is a body suspended through a set of cylindrical hinges or bearings that allow it to rotate freely about an axis fixed in space, while the part of the machine that does not rotate is called stator.

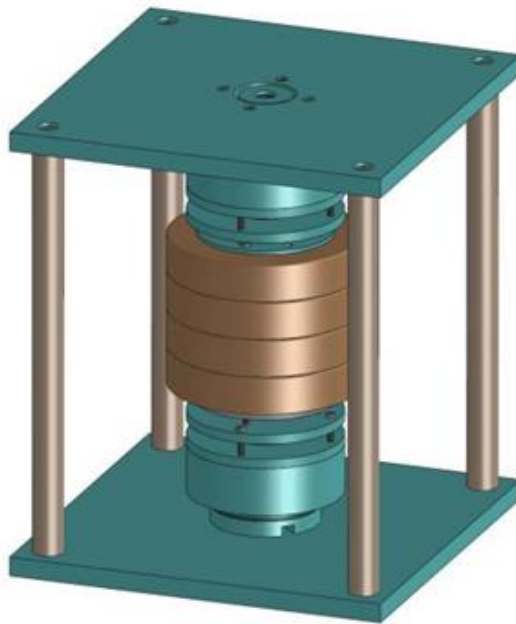


Figure 1.1 – Model of vertical magnetic rotor.

The typical behaviour of a rotor can be simplified through some fundamental aspects:

- the rotor shafts do not "vibrate", it spins and whirl;
- the rotor supports undergo vibrations;
- due to the rotation, the centre of the disk moves on a trajectory whose amplitude depends on the speed;
- as the speed of rotation increases there is an increase in the amplitude of the vibration. The maximum speed peak is called critical;
- if the amplitude of the vibration is excessive, catastrophic failures can occur.

The main elements of the rotor under study are:

- shaft
- hubs
- magnetic bearings

The stator structure is composed by polytetrafluoroethylene (PTFE known as Teflon) and Delrim elements. The choice to use these materials is due to their diamagnetic behaviour, in fact the magnetic susceptibility is negative and so it tends to exclude a magnetic field from its interior. Another

important feature is the possibility to change the rotating mass based on the number of hubs on the shaft.

1.1 Rotor components

The shaft is made of aluminium alloy, it has not a homogeneous distribution of the mass due to the presence of a flange, used as support for the brass hubs. Aluminium has been chosen because of its paramagnetic characteristic, in fact it is weakly attracted to a magnet: this effect is thousands of times weaker than in ferromagnetic materials.

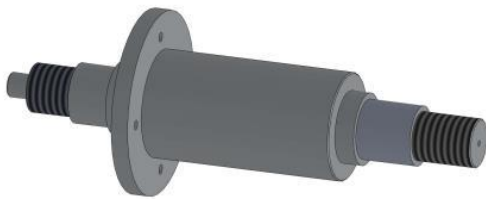


Figure 1.1.1 – Rotor shaft.

The mass of the rotor assembly is represented by the brass hubs which are positioned in abutment with the shaft flange. A higher number of disks mounted on the shaft corresponds to a higher value of inertia and mass of the rotor. Furthermore, there is a variation of the position of the centre of mass according to a fixed Cartesian reference.

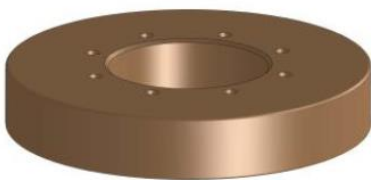


Figure 1.1.2 – Brass hub.

In this rotor model there are neodymium magnets. This type of magnets are permanent magnets made from an alloy of neodymium, iron and boron and they are the strongest type of permanent magnet commercially available. The neodymium magnets are graded according to their maximum energy product, which relates to the magnetic flux output per unit volume. They are classified by letter N followed by two numbers.

These elements have strong anisotropic characteristics which allow to obtain a residual magnetic induction three or four times stronger than that obtainable by the traditional permanent magnets.

They have a silvery-white colour, they are fragile, and they are easily damaged.



Figure 1.1.3 – Magnetic bearings.

2. Structural modifications

The first tests made with the rotor showed that it has some structural issues that need to be solved in order to take accurate measurements to characterize its motion. These criticalities are:

- structural stiffness
- threaded connections screws-Teflon
- ball transfer unit

2.1 Structural stiffness

The first problem is the low stiffness of the structure that does not allow an optimal functioning of the rotor during its rotation due to vibrations. These vibrations are linked to the bending of the four cylindrical elements which connect the lower base to the upper base. It was proposed not to produce these components made of a different material because a reinforcing structure, built using four L-shaped profiles in angular positions, is an easy solution to prevent undesirable vibrations.

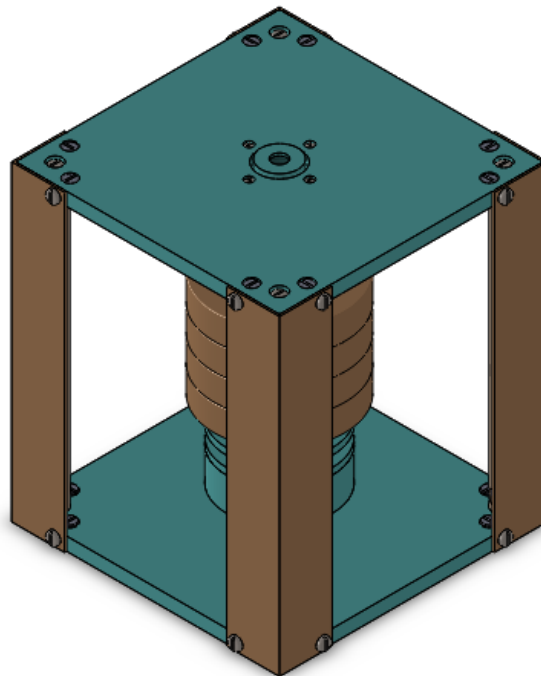


Figure 2.1.1 – Reinforcing structure made with L-shaped profiles.

We took into account a second possible solution, which involves the elimination of the L-profiles and the replacement of the cylindrical support elements with four parallelepipeds made of Delrim, a polymeric material that is more rigid than Teflon, thicker than the previous components. A further hole for an M5 screw is drilled in addition to the one in the centre of the base in order to avoid the rotation of these parallelepipeds.

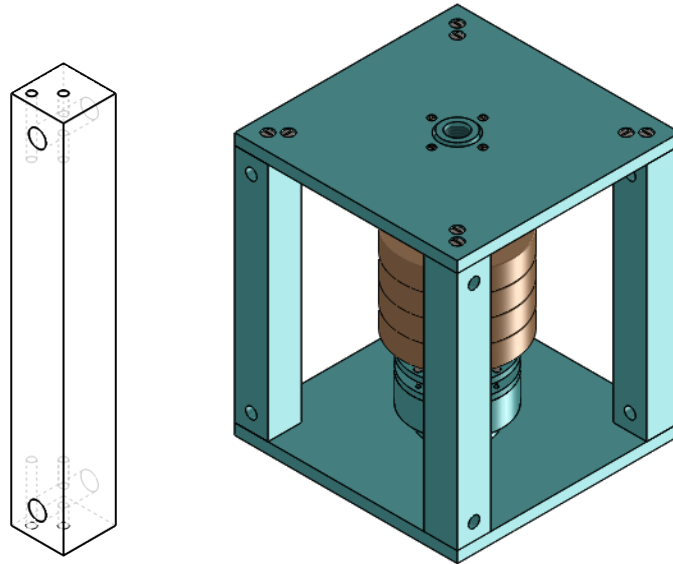


Figure 2.1.2 – Support bar (left) and second configuration (right).

2.2 Threaded connections

Many parts of the rotor and the structure where it is placed are made of Teflon and we decided to connect them with threaded elements screwed in the polymer. This simple solution does not allow to have a clamping force as high as in the case of connections between screw and nut both made of metallic material. In addition, this condition could worsen if the components are disassembled and reassembled many times, due to the progressive deterioration of the Teflon nut screws. The solution proposed to solve this problem consists in the use of barrel nuts M5 (small metal cylinders with a central threaded hole), to be inserted into the structure in such a way as to allow the correct tightening of the screws.



Figure 2.2.1 – Barrel nut.

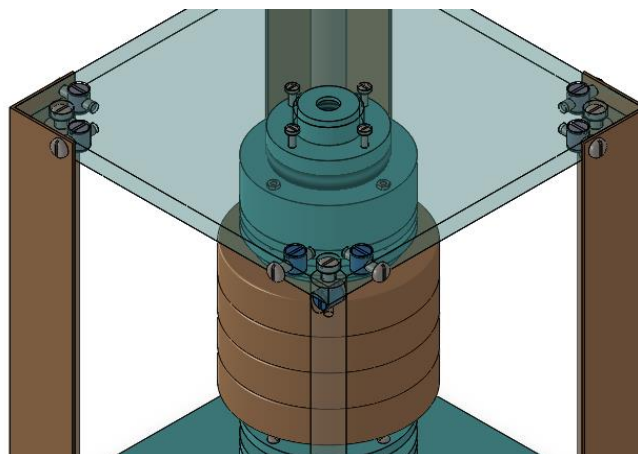


Figure 2.2.2 – Barrel nuts mounting.

This solution is not viable in the two Teflon supports (the lower one and upper one), due to the excessive thickness of the latter, which makes it hard to position the barrel nuts and the subsequent tightening of the screws. However, these are the most critical areas where to ensure an adequate clamping force. In fact, the force developed by the screw-Teflon coupling in the current assembly, is not sufficient to keep the stator rings of the magnetic bearings in the correct configuration, and sometimes it is necessary to reposition them manually before using the rotor again. Therefore, we deemed appropriate to implement a design modification of the two parts by making the threaded holes through and using M3×50 screws (in the lower bearing) and M3×45 screws (in the upper bearing) to be tightened by means of nuts.

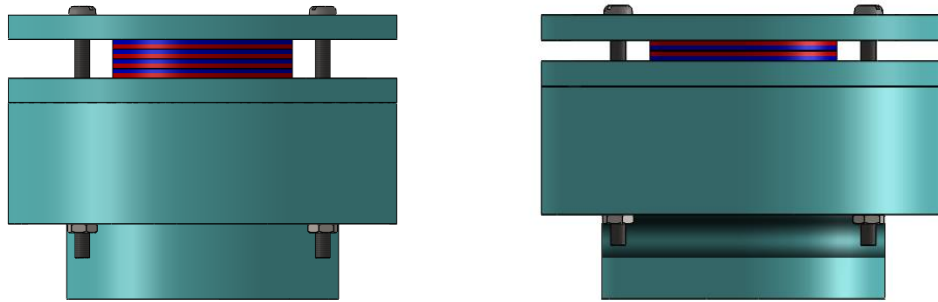


Figure 2.2.3 – Lower support (left) and upper support (right).

The same problem, regarding the difficult use of barrel nuts, also concerns the two platform rings, the upper one and lower one, due to their shape and positioning. In addition, since the solution of through holes and bolts is not viable there, two possible solutions are proposed below. The first solution consists of using M3 (DIN 562) square nuts.



Figure 2.2.4 – Square nut.

In order to make the mounting of the latter more practical and to minimise the amount of material removed, it was proposed to make four rectangular holes in the two components of the depth necessary to ensure correct positioning of the nuts in relation to the screws. These holes are only one millimetre wider than the nuts, so that these can be tightened without the use of any tools, just by screwing in the respective screws. This is possible because the sides of the holes act as restraints to prevent the nuts from turning.

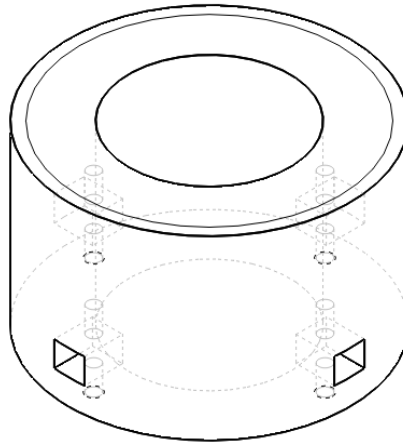


Figure 2.2.5 – Platform-ring holes.

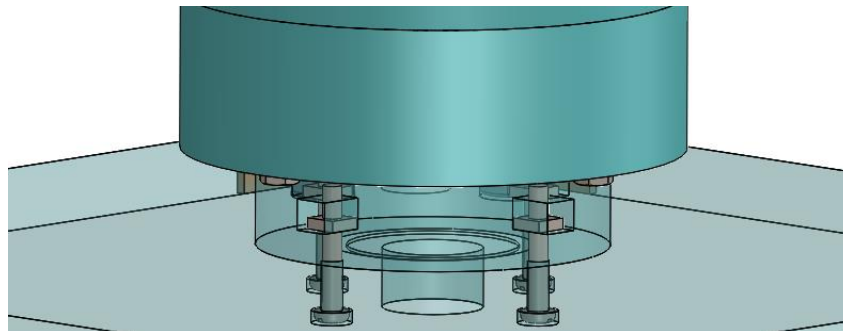


Figure 2.2.6 – Platform-ring mounting.

Due to the difficulty in making the rectangular holes described above, it was decided to use barrel nuts with a threaded hole for M3 screws in the two platform rings as well. This solution provides for the creation of four circular through holes where these metal cylinders are housed, which are positioned without an end stop element that facilitates their installation, unlike the previous case. The use of barrel nuts instead of square nuts also has an additional advantage concerning the absence of Teflon wear on the sides of the holes of the first solution which act as a constraint on their rotation in order to allow them to be tightened.

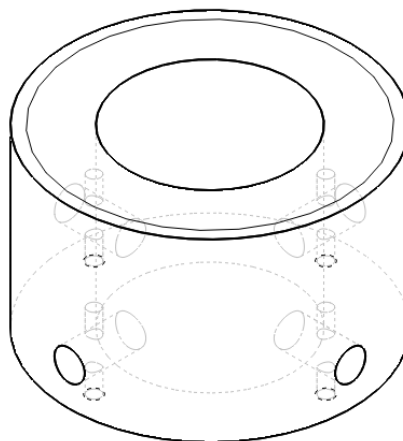


Figure 2.2.7 – Platform-ring holes.

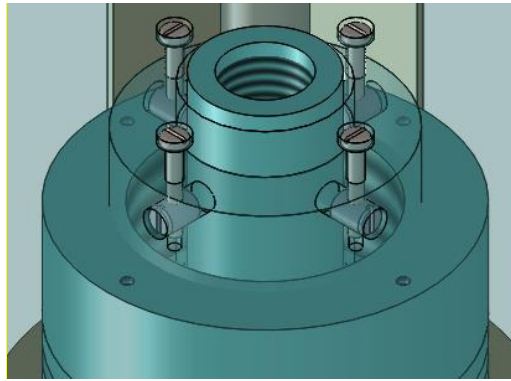


Figure 2.2.8 – Platform-ring mounting.

2.3 Ball transfer unit

We evaluated the possibility of finding a better solution for the rotating element interposed between the lower part of the rotor and the base of the structure, even though this is not a critical issue, taking into account that the contact should tend as much as possible to a point type in order to minimize friction. The current configuration consists in the interposition of a steel sphere between the base and the shaft, without any fixing method, making the assembly and disassembly phases of the rotor not very practical due to the interaction between the steel sphere and the magnetic rings. Three solutions are proposed, considering the different rotor height variation, since its position with respect to the stator rings of the magnetic bearings affects the compensation of the vertical force. Taking into account the current configuration, a lowering of the rotor, even by a few millimetres, would result in a lower downward force, with the consequence of a lower resistance to rotation.

2.3.1 Current configuration

The current configuration, as said before, consists in the interposition of a steel sphere between the base of the structure and the lower part of the rotor.

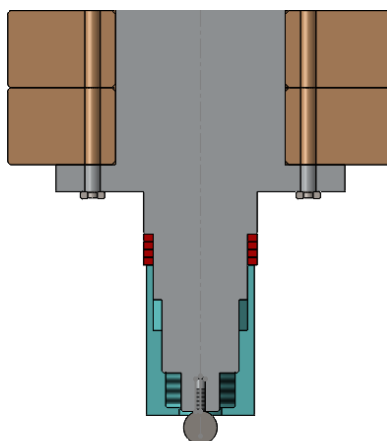


Figure 2.3.1.1 – Current configuration.

2.3.2 First alternative solution

The first proposed solution involves replacing the ball used in the initial configuration with a ball transfer unit, mounted by interference fit with the Teflon part at the bottom of the rotor and brought in contact with the shaft.



Figure 2.3.2.1 – Ball transfer unit.

There are no technical specifications about the ball transfer unit we own, and since these components have quite variable values of load capacity, depending on the model taken into consideration, maybe it is better not to use it. In fact, we found that some of these, similar to the one we already own, have a load capacity of just 3 kg, then less than the weight of the rotor.

This modification consists in producing this lower Teflon part again but with a length 9 mm longer with respect to the original component, and with the lower hole having a diameter of 18 mm. Then structural modifications to the shaft are not expected, although the rotor's height will result slightly higher.

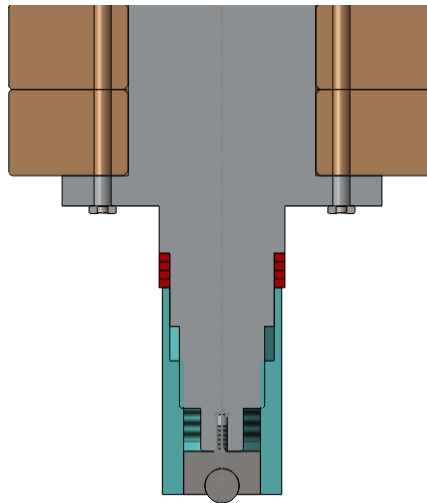


Figure 2.3.2.2 – First alternative solution.

2.3.3 Second alternative solution

The second solution proposed requires the use of the same ball transfer unit used in the first solution, but since the increase in height of the rotor is to be avoided, so as not to incur in a reduction of the vertical balance of the weight force generated by magnetic bearings, in the following configuration both the Teflon part and the rotor shaft are modified. The Teflon part needs to be produced again with a length 5.5 mm longer than the original part and with the lower hole having an internal diameter of 18 mm, while 3.5 mm of material has to be removed from the shaft in the direction of the rotor axis.

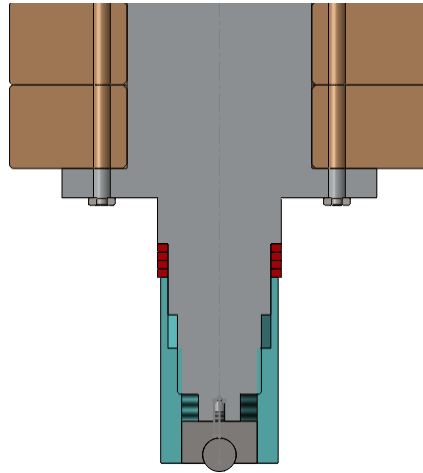


Figure 2.3.3.1 – Second alternative solution.

In this way, the height of the rotor is expected to be the same as in the initial configuration, thus not experiencing any reduction of the balancing effect of the vertical force component generated by the magnetic bearings. This second solution, although it is more invasive because of the modification on the shaft, has the advantage of a further reduction of the overall height of the rotor by removing more material from the lower part of the shaft, thus having a gain on the decrease in the resistance to rotation.

2.3.4 Third alternative solution

The third solution proposed involves the use of a ball transfer unit with threaded pin, made integral with the rotor shaft by a threaded screw joint. It has a load capacity of 35 kg that respects the design specifications.



Figure 2.3.4.1 – Ball transfer unit with threaded pin.

This configuration involves modifying both the shaft and the Teflon component at the bottom of the rotor. A 10 mm length of material should be removed from the shaft in the direction of the rotor axis, and then a blind threaded hole 20 mm deep should be made for the M8 pin of the ball transfer unit. It is not necessary to produce the Teflon part again, in contrast to the two solutions previously proposed, as it is sufficient to modify the lower hole to obtain an internal diameter of 22 mm and a depth of 11 mm.

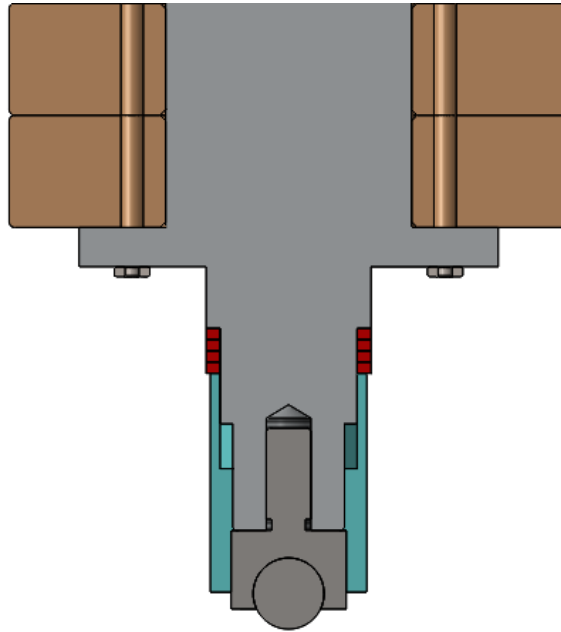


Figure 2.3.4.2 – Third alternative solution.

It is proposed an alternative option concerning the Teflon part screwed onto the lower part of the rotor, since using the original third solution layout would involve unscrewing the axial bearing every time the number of magnetic bearings on the shaft is to be changed. In order to avoid this issue, it is possible to produce this component again but with a different geometry to solve the problem described: the lower part allows screwing onto the 24.5 mm diameter part of the shaft (which needs to be threaded for a length of 7 mm), while the upper face stops at the lower magnetic bearing ring. We considered to produce this part made of aluminium instead of Teflon to ensure a good tightening force despite the small length of the threaded part. But on the other hand this choice creates problems linked to the interaction with magnetic bearings, so we preferred to use the previous option.

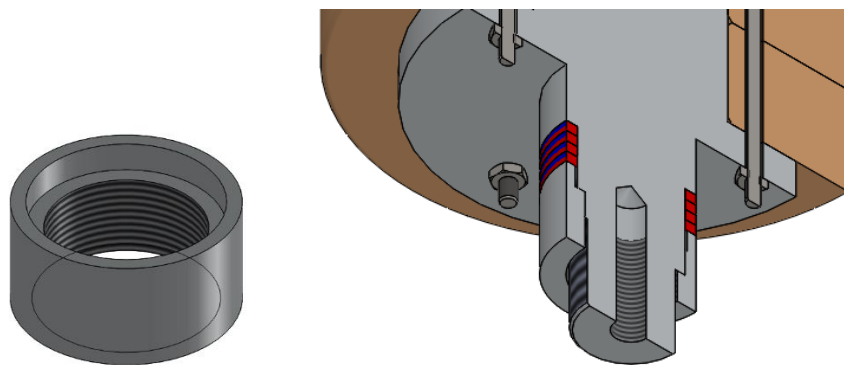


Figure 2.3.4.3 – Cup ring (left) and cup ring mounting (right).

2.3.5 Comparison between the four configurations

After describing the three proposed configurations in detail, the variation in height Δh of the rotor with respect to the initial configuration is analysed, since, as already highlighted, it is of fundamental importance for balancing the weight force of the rotor.

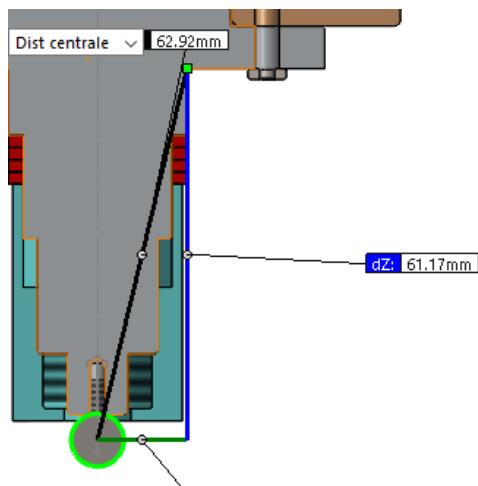


Figure 2.3.5.1 – Initial configuration.

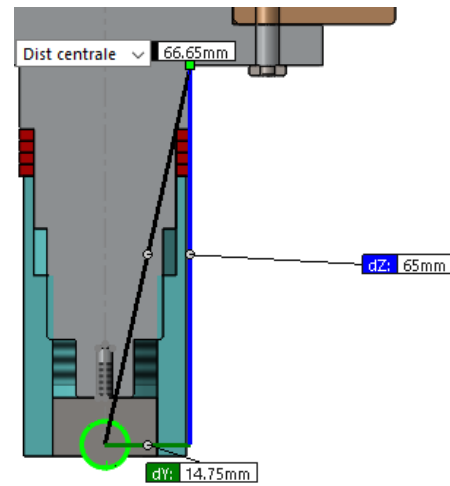


Figure 2.3.5.2 – First solution.

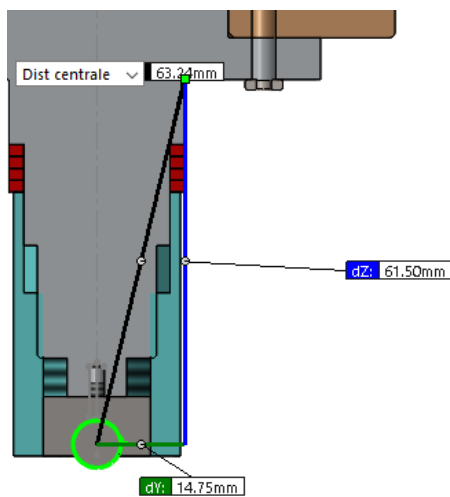


Figure 2.3.5.3 – Second solution.

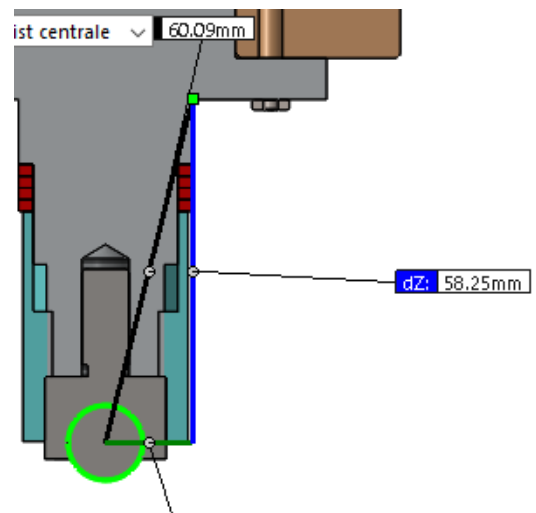


Figure 2.3.5.4 – Third solution.

Considering that the sum of dZ and the radius of the sphere used in the first configuration is 65.5 mm, it is possible to obtain the height variations.

Table 2.3.5.1 – Calculation of height variation.

Solution	dZ [mm]	r [mm]	$dZ+r$ [mm]	Δh [mm]
1	65.00	4.00	69.00	+ 3.50
2	61.50	4.00	65.50	+ 0.00
3	58.25	6.35	64.60	- 0.90

The third solution proposed allows a reduction in height of 0.9 mm by removing only the material of the lower part of the shaft with a smaller cross-section. The second solution does not present any variation in height since the length of material that has to be removed was calculated to compensate for the increase in height of the first proposed configuration (a further reduction in overall height can be obtained by removing more material).

3. Positioning of optical sensors

The following section describes the design of a structure made from Bosch 40×40 mm profiles for positioning optical sensors that detect the position and speed of the rotor.

3.1 Position sensors

Measurements of the position of the rotor during its rotation, to define its dynamic behaviour, are carried out by using optical sensors manufactured by Keyence. The following sensors are available:

- 1 sensor Keyence LK - 052
- 2 sensors Keyence LK - 082
- 1 sensor Keyence LK - 152

The first two digits of the number in the product name correspond to the distance at which the photocell of the sensor must be placed with respect to the measured element (expressed in tens of millimetres). Compliance with this specification is of fundamental importance for correct measurements, and the structure designed for correct positioning of the sensors during tests is based on it.



Figure 3.1.1 – Optical sensor Keyence.

Another specification to be taken into account when positioning these sensors is the angle of incidence of the laser on the component whose position is to be measured during rotation. For each component whose displacement is to be measured, it is necessary to have two sensors whose emitted laser beams are perpendicular to each other. Four sensors are required in order to obtain all the necessary information on the displacement of the rotor during its movement: two pairs of perpendicular laser beams have to carry out measurements at two different heights. In order to avoid creating a structure for the positioning of the sensors with cantilever beams and taking into account the size of the material required for the measurements, we considered appropriate to carry out the measurements on the brass rotor hubs instead of on the rotor shaft. Measuring the displacement of the hubs does not create any problems from the point of view of analysing the dynamics of the rotor, since they are integral with the shaft. The structure for positioning these sensors is made using Bosch 40×40L profiles, where the basic supports of the optical detectors are fixed. These supports have a lower plate for mounting the sensors on the profiles, and two registers that allow to adjust their position with an accuracy of a tenth of a millimeter.

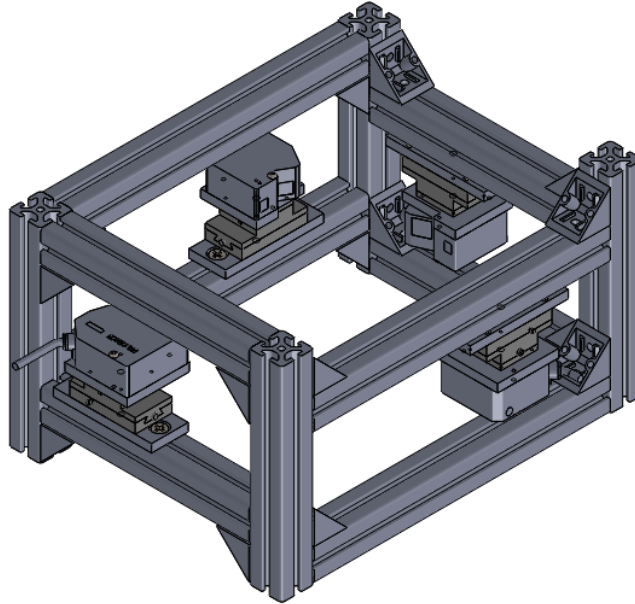


Figure 3.1.2 – Measurement structure.

This structure does not have a base on which to place the rotor, because it is necessary to keep the measured element separate from the measuring structure when taking measurements, so that the results are more accurate. To place this measuring structure with high precision, the correct position of the rotor in relation to the sensors is achieved by interposing an adjustment plate (46 mm in length) between the base of the rotor and the two horizontal profiles as showed in the following figure.

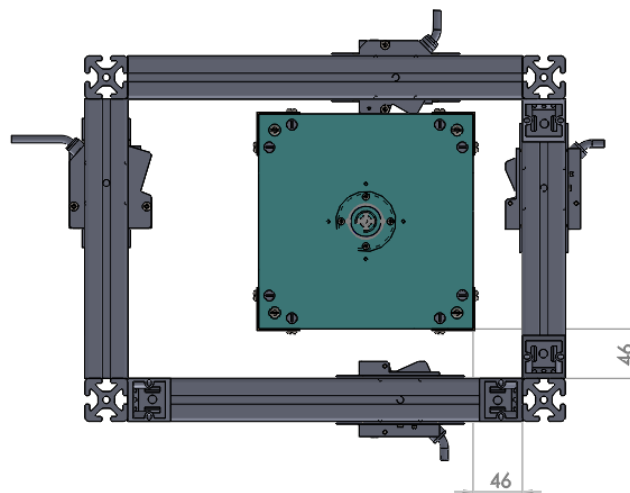


Figure 3.1.3 – Positioning of the rotor and measurement structure.

The choice of measuring on the rotor hubs means that it is impossible to analyse the dynamic behaviour of the rotor with this configuration in cases where there are fewer than four hubs. However, it is still possible to carry out measurements with fewer rotor hubs by simply changing the position of the LK - 052 and LK - 152 sensors (the sensors that measure the displacement of the hub positioned at the greater height), fixing them to the underside of the horizontal profiles at the top of the structure and positioning them at the correct height, as shown in the figure.

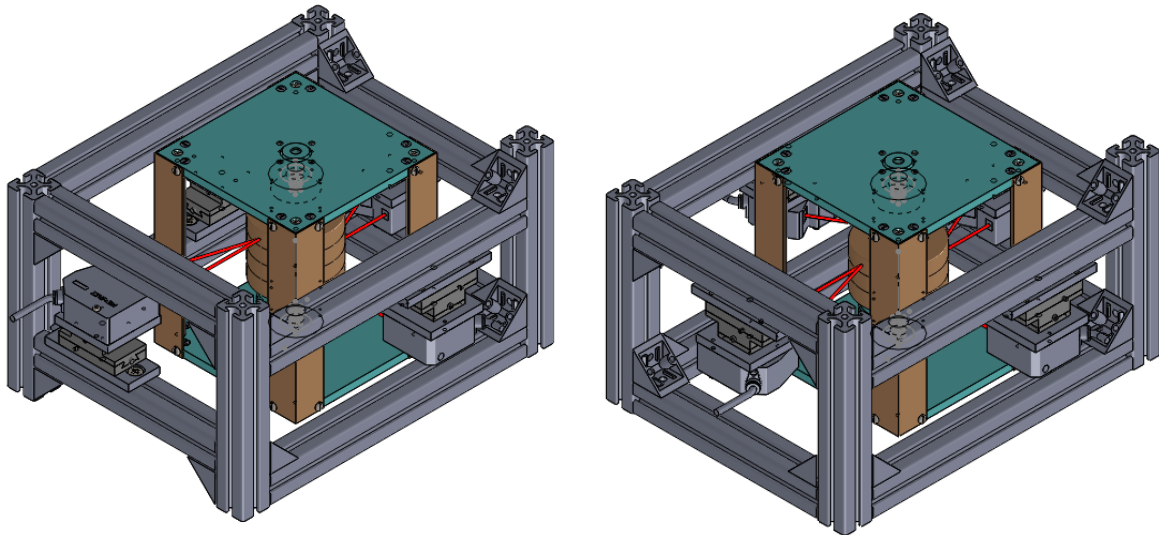


Figure 3.1.4 – Configuration with four hubs (left) and three hubs (right).

Some relevant views are shown below in order to clarify the layout of the 3D model made in Solidworks.

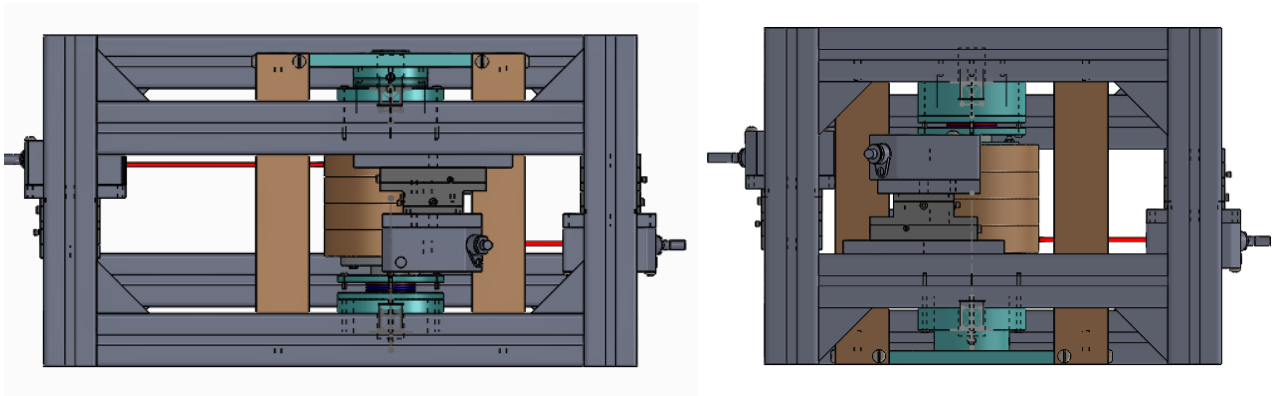


Figure 3.1.5 – Front view (left) and side view (right).

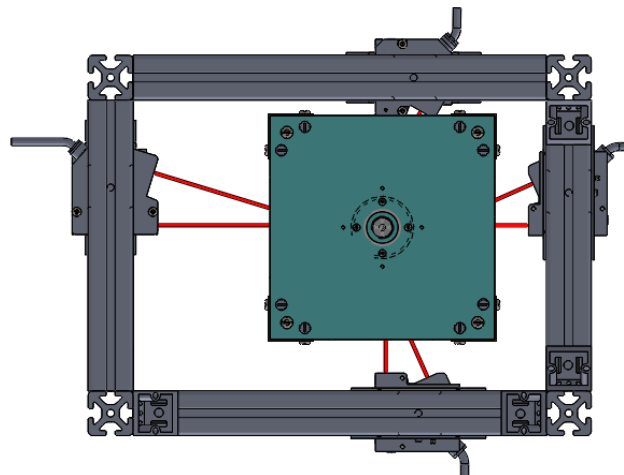


Figure 3.1.6 – Top view.

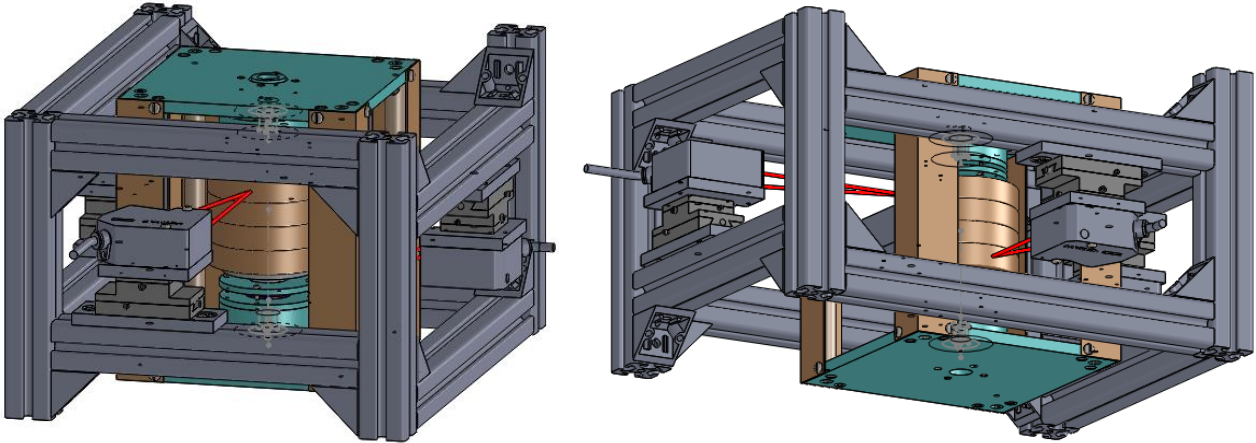


Figure 3.1.7 – Further relevant views.

3.2 Speed sensor

We decided to use a sensor from "The modal shop" (LaserTach LT2 ICP) to measure the rotational speed of the rotor, allowing measurements of up to 100000 rpm in a distance range of 5 to 51 cm. In order to respect the minimum distance limit stated in the sensor specifications, it was necessary to design a support bracket for mounting on the Bosch profile, whose length was dimensioned taking into account not only the distance limit, but also the size of the wiring behind the laser.



Figure 3.2.1 – LT2 Laser tachometer.

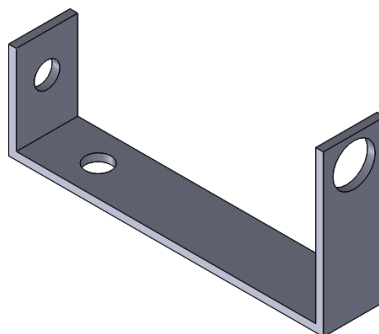


Figure 3.2.2 – Bracket.

The connection between the two components is made by means of two screws in order to bind their rotation and keep the laser of the sensor perpendicular to the surface on which the measurements are to be made.

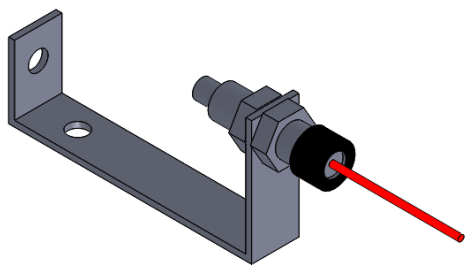


Figure 3.2.3 – Sensor assembly.

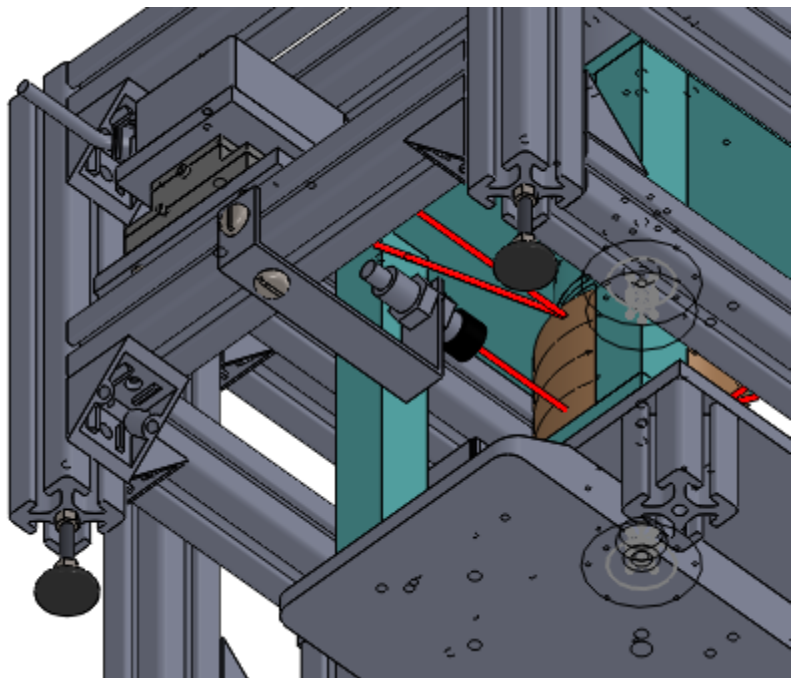


Figure 3.2.4 – Sensor mounting.

4. Motor and clutch assembly

We decided to use a DC brushless motor connected to an electromagnetic clutch in order to analyse the operation of the rotor connected to an external rotating element. The lower part of the clutch is made integral with the rotor shaft so that the latter can be moved or decoupled from the motor. The two parts of the clutch are free to rotate without any constraint until it is electrically powered and the two parts are made integral and held together by an electromagnetic force.

It was necessary to create 3D models of both elements in Solidworks, in accordance with the dimensions recorded, in order to design all the components necessary for the assembly of the motor and the clutch.

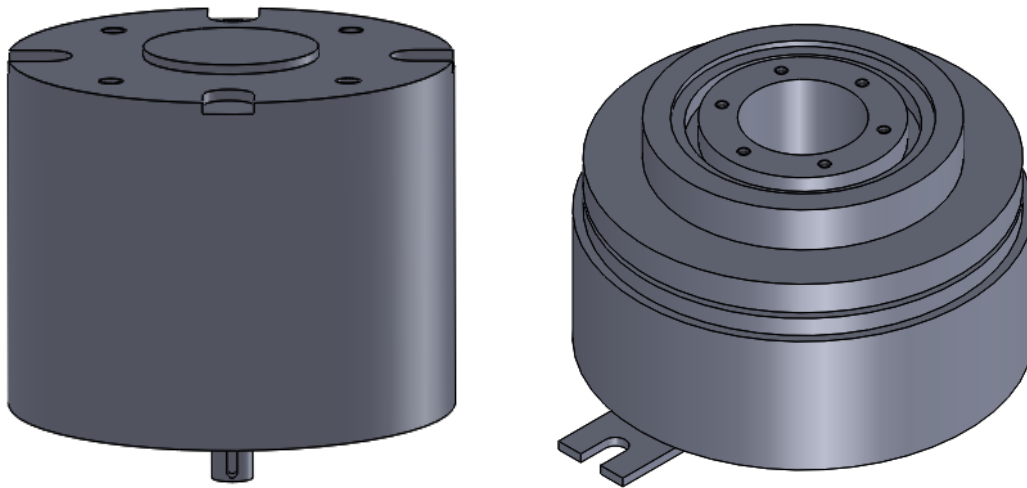


Figure 4.1 – Motor (left) and clutch (right).

4.1 Preliminary design

The following paragraph describes the preliminary design of the connections between the various parts, to which the optimisation modifications described in the next paragraph are subsequently made. In order to assemble the motor, the clutch and the rotor, it is necessary to use components which allow the connection of the various parts by means of threaded or keyed couplings.

Therefore, a cylindrical component was designed to be connected internally to the output shaft of the motor and externally to the clutch inlet to guarantee the rotation of the motor and the upper part of the clutch. Both couplings are keyed.

A shaft, threaded at the end to be coupled to the rotor and flanged at the other end to be coupled to the clutch by means of six M3 screws, was projected to connect the lower part of the clutch to the rotor without making any change to the latter. Part of the shaft is hexagonal in shape so that it can be tightened using an M6 hexagonal nut spanner.

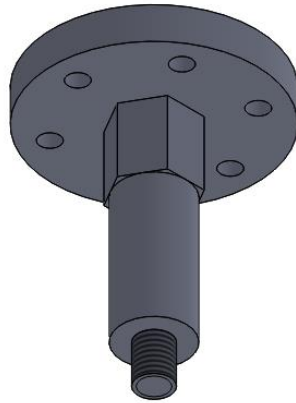


Figure 4.1.1 – Connection shaft clutch-rotor.

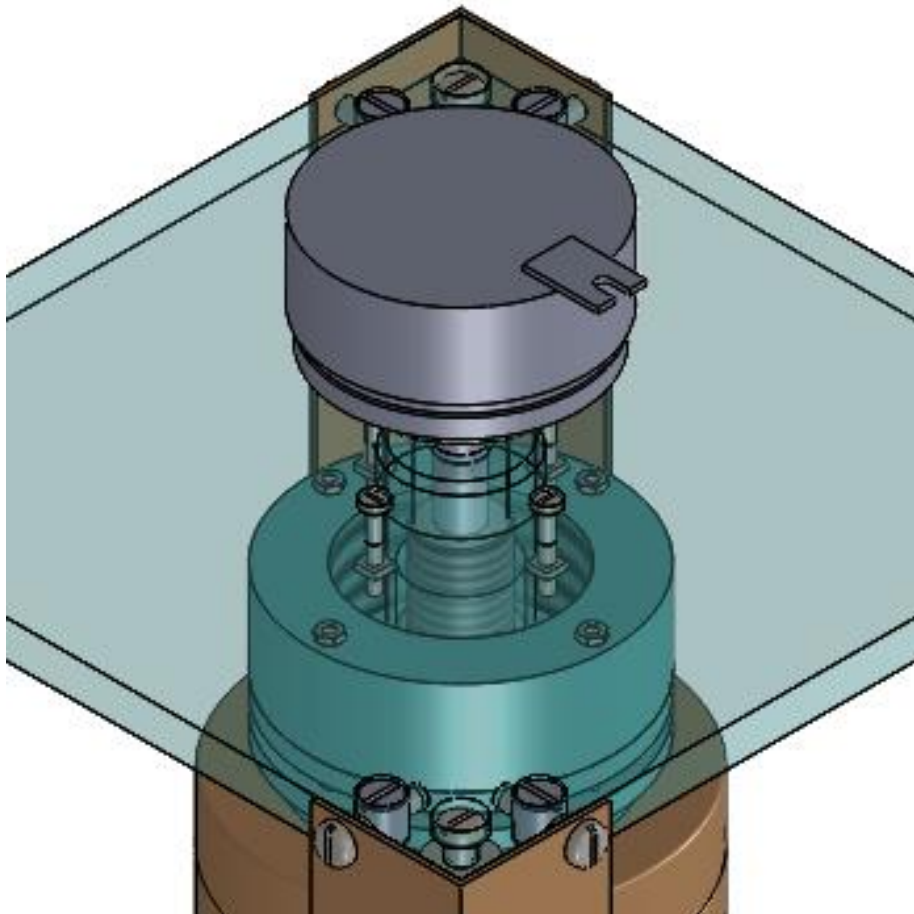


Figure 4.1.2 – Clutch-rotor connection.

In order to ensure that the motor rotates in conjunction with the upper part of the clutch, we decided to drill a hole in the clutch and connect it to the motor output shaft by means of a key.

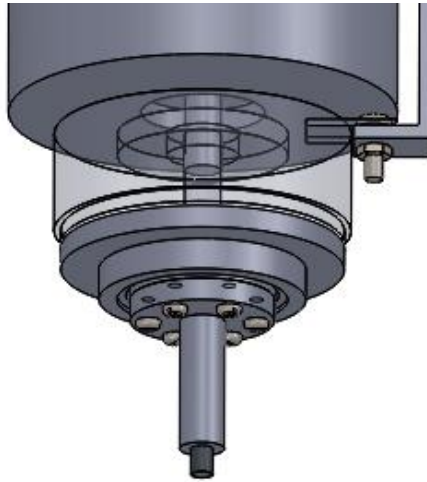


Figure 4.1.3 –Motor-clutch connection.

The support structure is made from Bosch 40×40 profiles in a gantry configuration to avoid overhanging unstable elements and allow a precise positioning of the motor. It is separated from the measuring structure described above so as not to alter the measurements taken by the optical sensors.

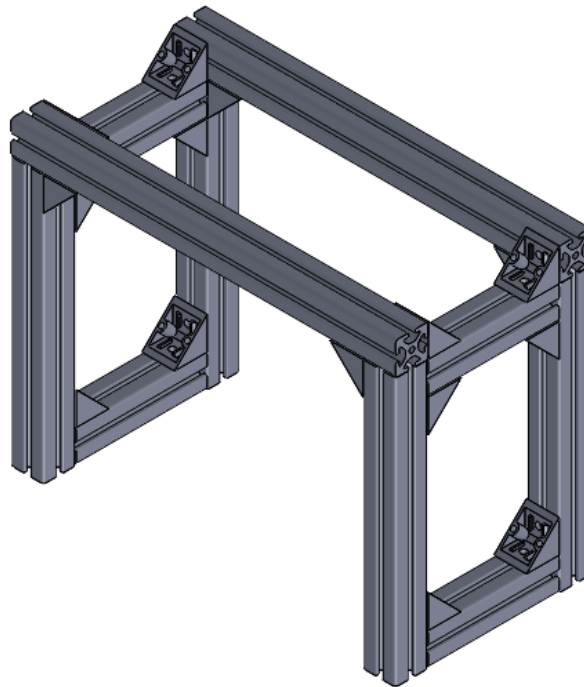


Figure 4.1.4 – Support structure.

A plate was projected in order to allow the motor to be mounted on it. There are four holes for flat countersunk M8 screws (ISO 7046-1) to fix it to the Bosch profiles, and six more holes: four are necessary for mounting the motor by mean of M6 screws and two for mounting a bracket connected to the clutch by means of a M4 screws.

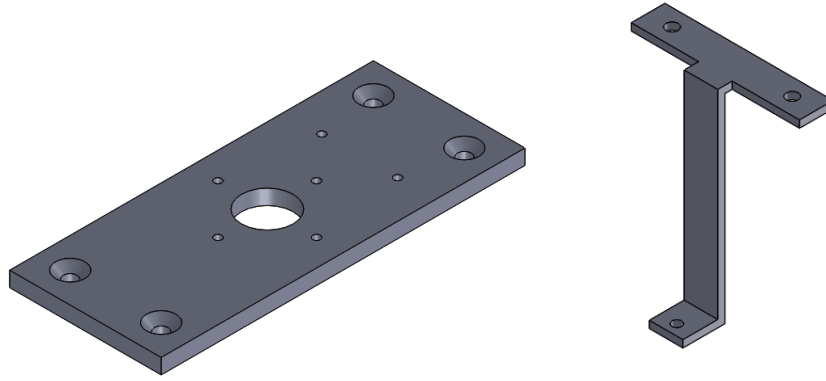


Figure 4.1.5 – Plate (left) and bracket (right).

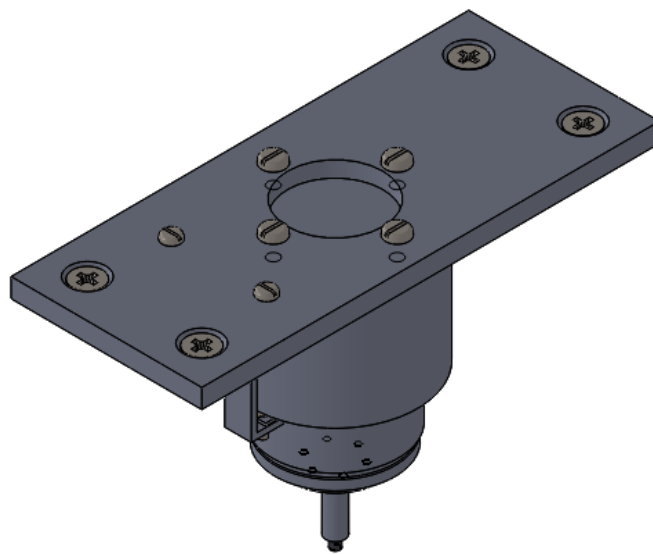


Figure 4.1.6 – Motor and clutch assembly.

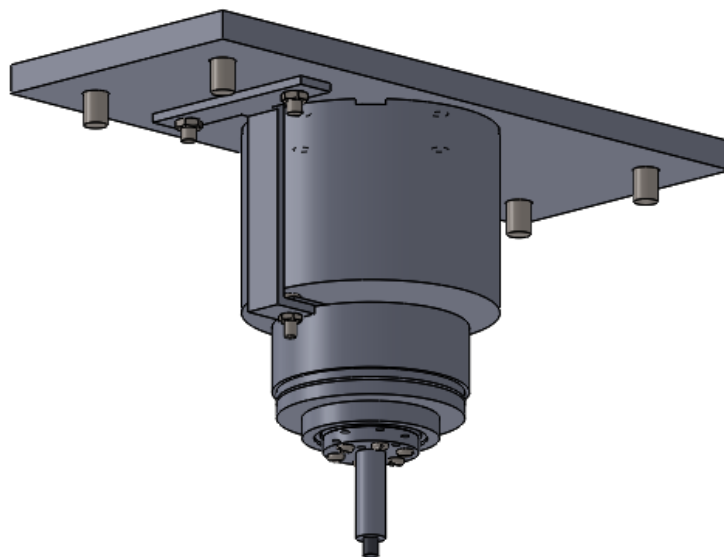


Figure 4.1.7 – Motor and clutch assembly.

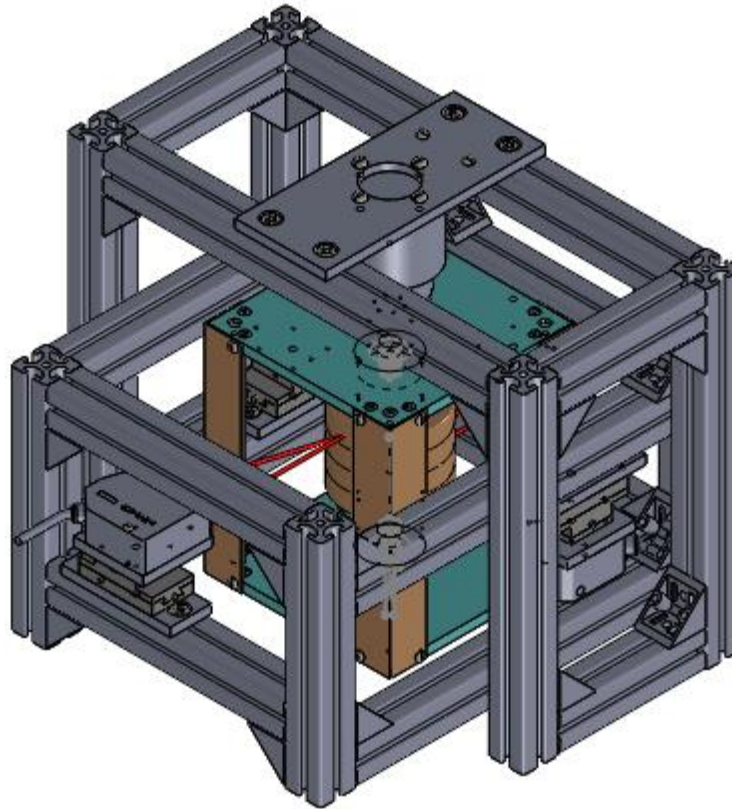


Figure 4.1.8 – Final mounting.

4.2 Optimised design

We deemed necessary to make changes to the preliminary design in order to optimise the assembly and simplify the production processes for making the designed components. The elements on which it was appropriate to carry out a partial redesign are shown below:

- Clutch-rotor connection element
- Motor-clutch connection
- Motor plate
- Base of the support structure

The previous connecting element between the clutch and the rotor has three main problems: the difficulty in machining the hexagonal part, the cost of machining it due to the excessive removal of material from a single aluminium cylinder, and finally the M3 threaded pin which is not suitable for transferring the necessary torque.

In order to solve the problem of the hexagonal part, we decided to replace it with two parallel flattenings on the cylindrical part, the two surfaces have a distance of 10 mm so that they can be tightened using a fork spanner for M6 nuts.

In addition we planned to produce this component as two different elements, to be connected to each other by means of an M6 hex socket head cap screw, in order to minimise the material removed during manufacture and reduce costs.

Finally, it was considered necessary to increase the diameter and length of the threaded pin at the base of this component, since we estimated that due to the high inertia of the rotor, the previous solution was not appropriate for transferring torque, especially in critical phases such as the start-up transient.

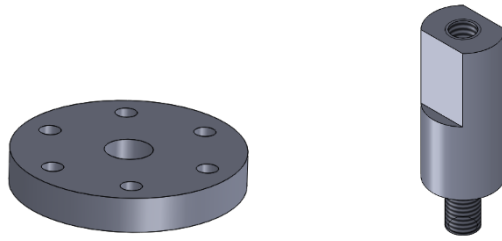


Figure 4.2.1 – Upper part (left) lower part (right).

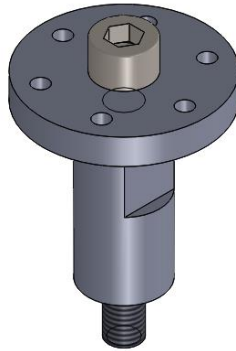


Figure 4.2.2 – Connection element clutch-rotor.

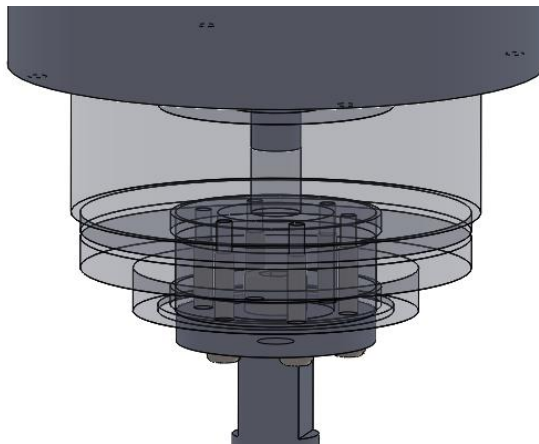


Figure 4.2.3 – Connection element mounting.

This modification involves the increase in the diameter of the lower cylindrical part and the subsequent increase in the diameter of the hole in the Teflon component screwed into the top of the rotor shaft (cup top).

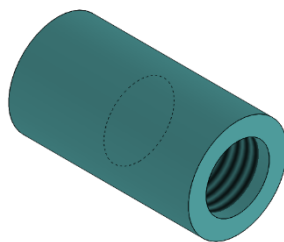


Figure 4.2.4 – Cup top.

A further change to be made in order to make the use of this new version of the component viable is to modify the upper threaded hole of the shaft by increasing its diameter and depth. In addition, the external diameter of the top of the shaft is the limit that does not allow the use of an M8 threaded pin for transferring motion, as making the respective hole would reduce its thickness too much.

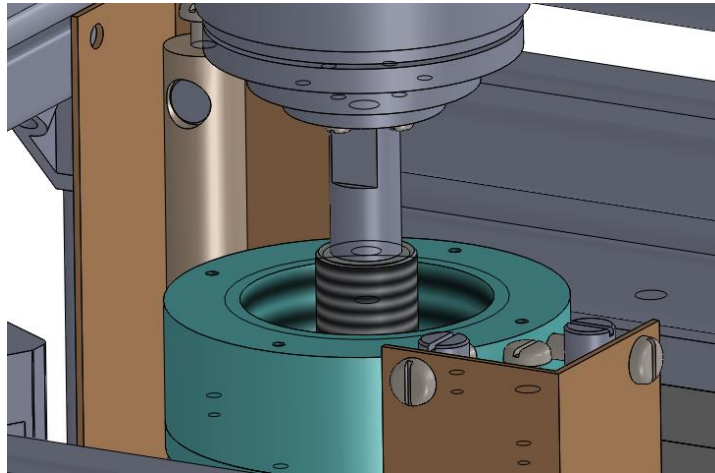


Figure 4.2.5 – Clutch-rotor connection (Cup top hidden).

With regard to the connection between the motor and the clutch, the bracket designed has a production feasibility problem due to the upper transverse part. Initially, in order not to change the preliminary design too much, we redesigned it so that it could be manufactured by bending and drilling a sheet metal. Subsequently, however, we deemed more convenient and practical to use the threaded holes on the underside of the motor, allowing a connection to the clutch by means of an M3 screw and a washer. In order to optimise the positioning of the clutch, it is advisable to insert a shim of the same height as the upper metal piece used for assembly, placed in an opposite position to the latter.

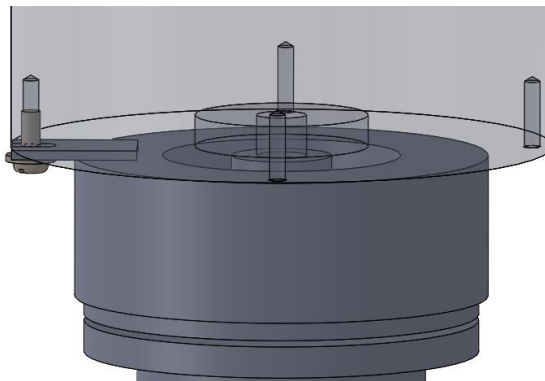


Figure 4.2.6 – Motor-clutch mounting.

Some design changes were made to the motor mounting plate: the two holes for mounting the clutch connection bracket were removed and the four countersunk holes were replaced with holes for hex socket head cap screws in order to simplify machining.

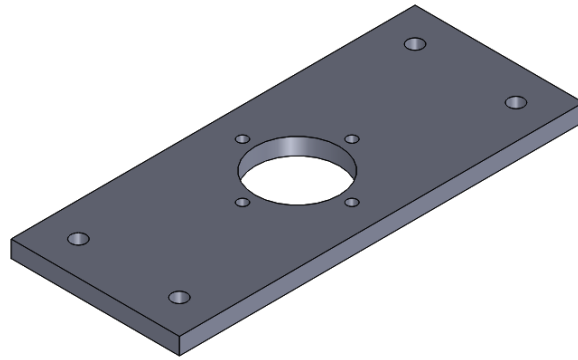


Figure 4.2.7 – Motor support plate.

The last modification, concerning the base of the support structure, involves the use of height-adjustable knuckle feet M8 screwed to the bottom of the Bosch profiles in order to ensure correct positioning of the various components. This is of particular importance for the clutch, as it is possible to guarantee the gap between the two fixed and moving parts according to the operating specifications.

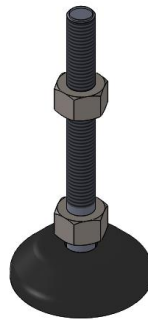


Figure 4.2.8 – Adjustable knuckle foot M8.

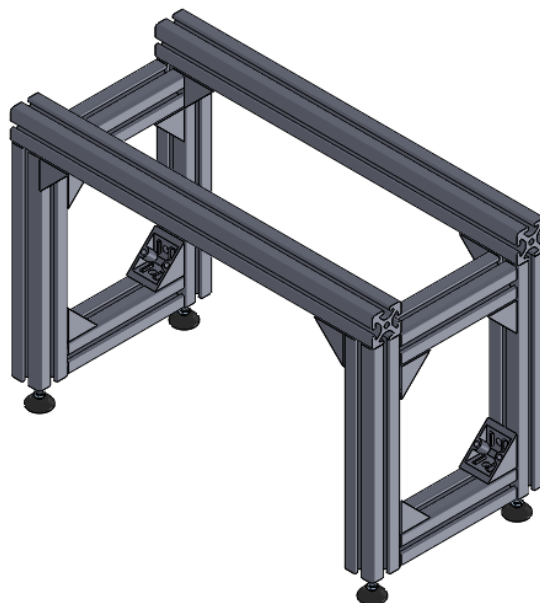


Figure 4.2.9 – Support structure.

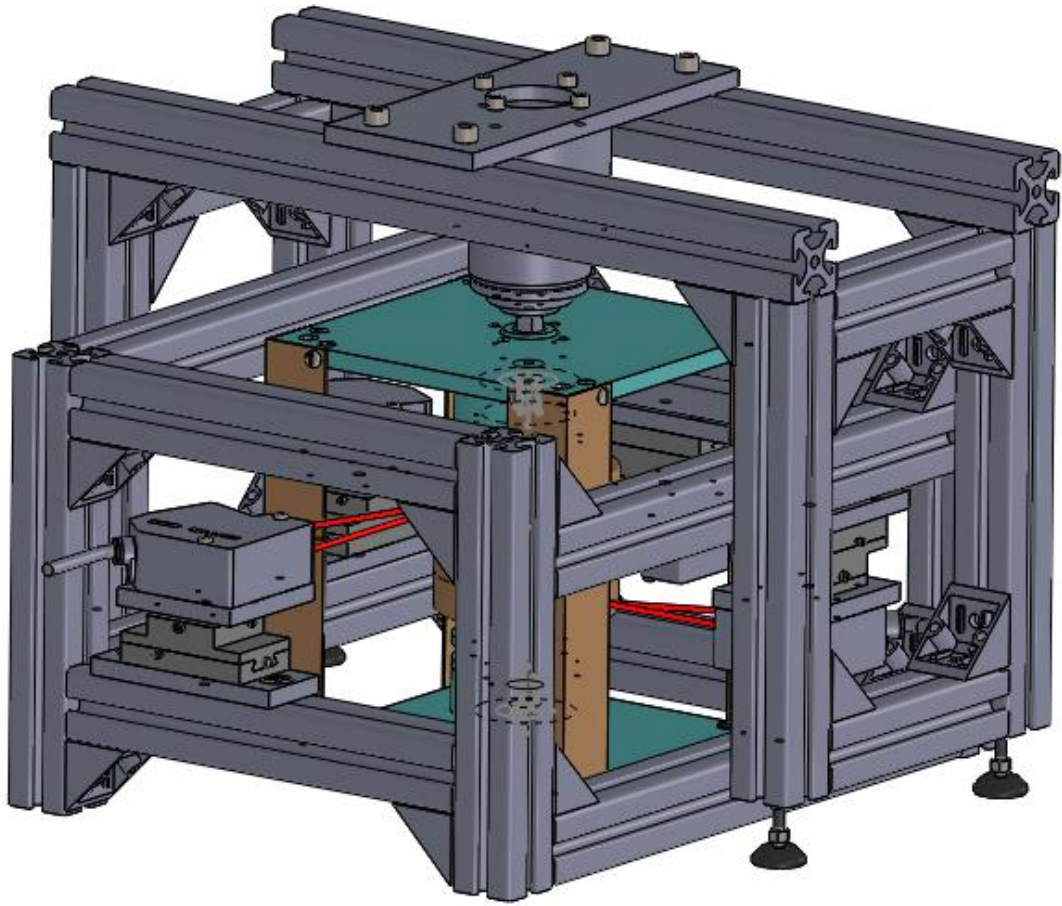


Figure 4.2.10 – Final mounting.

5. Measurement of the vertical force component

As previously mentioned, the balancing effect of the vertical component of the weight generated by the magnetic bearings is of fundamental importance, which is why it is interesting to evaluate its influence on the dynamics of the rotor. Two possible configurations are therefore described, the first one involves the use of a load cell, while the second involves a common scale.

5.1 Load cell configuration

In order to measure the compensation effect of the vertical force, in the first proposed solution we decided to use a load cell produced by S2Tech to evaluate the variation of the detected weight.

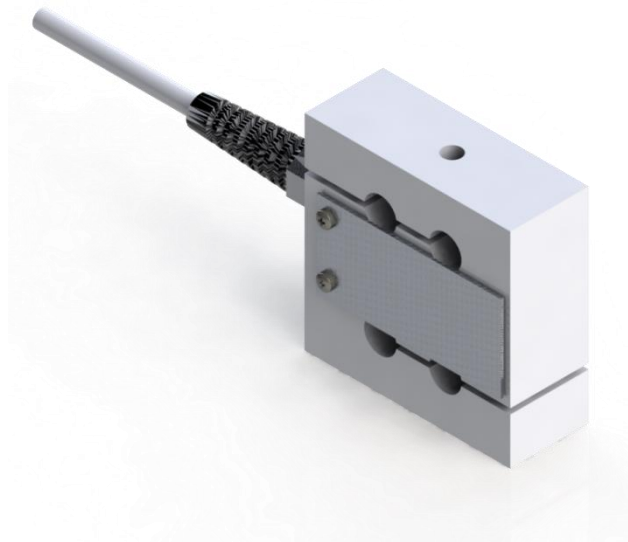


Figure 5.1.1 – Load cell S2Tech 546QD - A1.

From the technical specifications provided, we know that the maximum error of each measurement is equal to 0.05 kg while the sensitivity is equal to 0.22 kg.

In order to use the load cell during operation of the rotor, it is necessary for the latter to rest on an element directly connected to the load cell by means of a threaded pin. So, we decided to remove the steel disc previously positioned at the base of the rotor and to use a thumbscrew with an M8 threaded pin, since it is easily available and useful for our purpose.

This solution makes it possible to change the vertical positioning of the rotor by tightening the screw so as to obtain a better weight compensation due to the magnetic bearings.



Figure 5.1.2 – Thumbscrew.

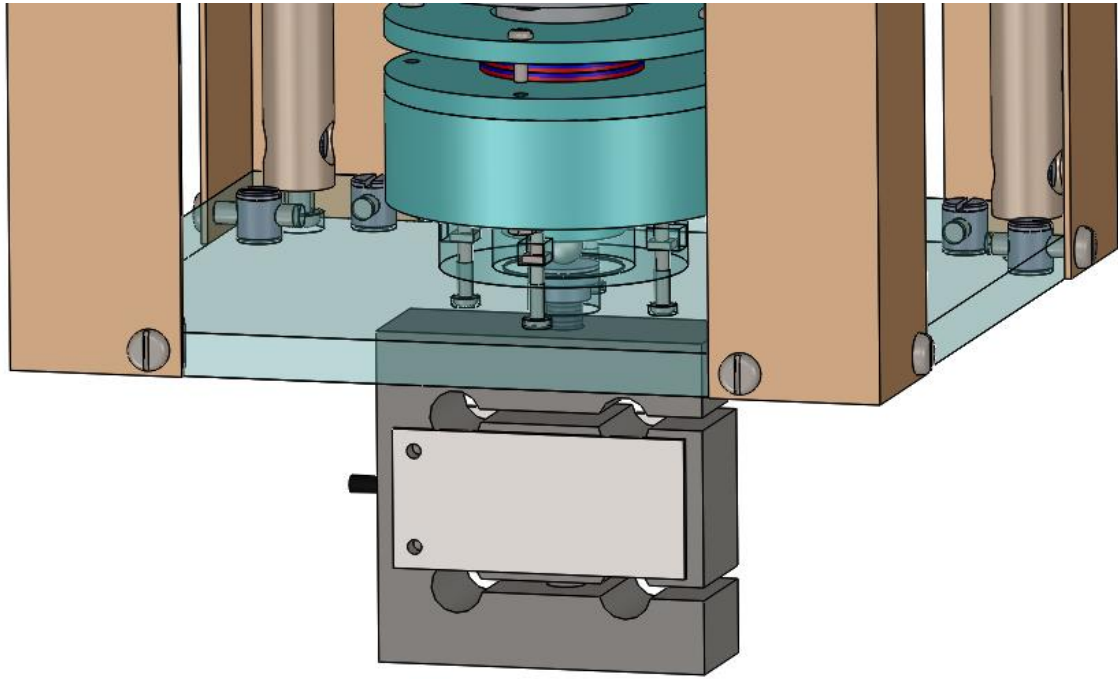


Figure 5.1.3 – Load cell mounting.

In order to carry out this measurement, it is also necessary to use a plane on which to place the Teflon structure where the rotor is housed, but in such a way that it does not come into contact with the structure where the optical sensors are mounted or with the support structure of the motor, in order to maintain accurate measurements. To this end, the following support has been designed (at the base of which there are the Bosch profiles already used previously).

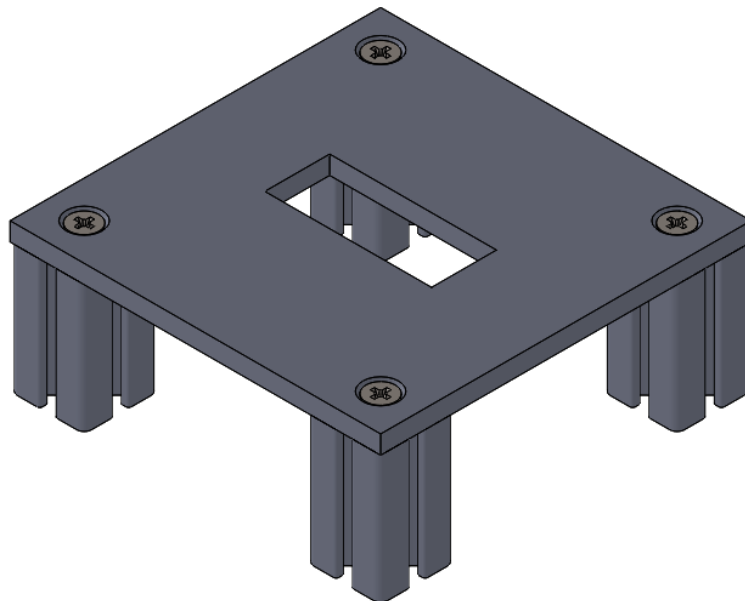


Figure 5.1.4 – Support lower base.

It is clear that all the previously designed structures can no longer be used unless a design modification is made to increase their height by 80 mm by replacing all the vertically positioned Bosch profiles with others of greater height. The final assembly configuration is shown below.

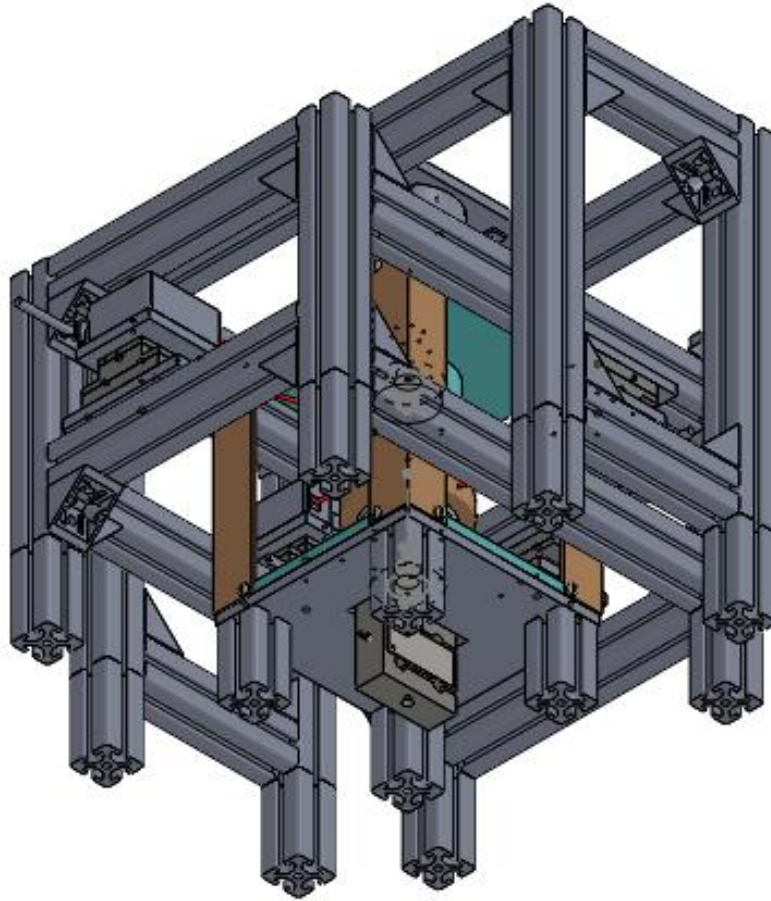


Figure 5.1.5 – Load cell configuration - final mounting.

5.2 Scale configuration

In the second solution it was decided to use a common scale to evaluate the compensation effect of the vertical force. The main advantage of using the latter is not only the low cost, but also the sensitivity equal to one gram, which provides more precise information than the load cell. This is motivated by the fact that the load cell used in the first configuration has a full scale of 110 kg instead of just 10 kg, as in this case, so it is not really intended for the use proposed here.



Figure 5.2.1 – Scale (left) and 3D model (right).

In order to be able to use the balance during operation of the rotor, it is necessary for the latter to rest on an element directly on it, which is why we chose to use a small metal cylinder with a variable cross-section, after removing the steel disc previously positioned at the base of the rotor. The base of this component has a larger diameter to provide better stability.

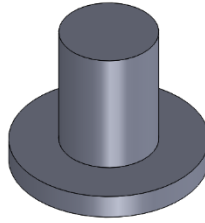


Figure 5.2.2 – Cylindrical base.

In order to carry out this measurement, it is also necessary to use a plane on which to place the Teflon structure where the rotor is housed, but in such a way that it does not come into contact with the structure where the optical sensors are mounted or with the support structure of the motor, in order to maintain accurate measurements. To this end, the following support has been designed (at the base of which there are the Bosch profiles already used previously).

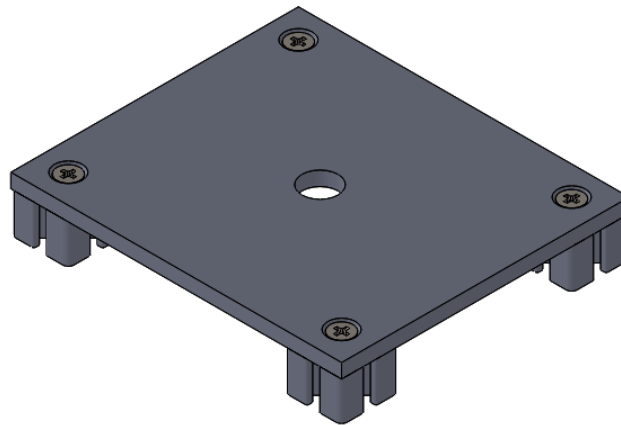


Figure 5.2.3 – Support lower base.

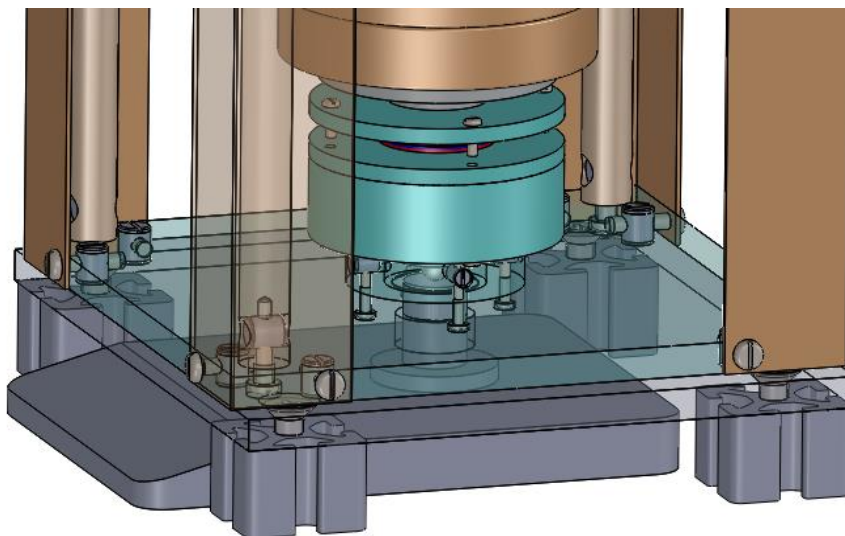


Figure 5.2.4 – Mounting example.

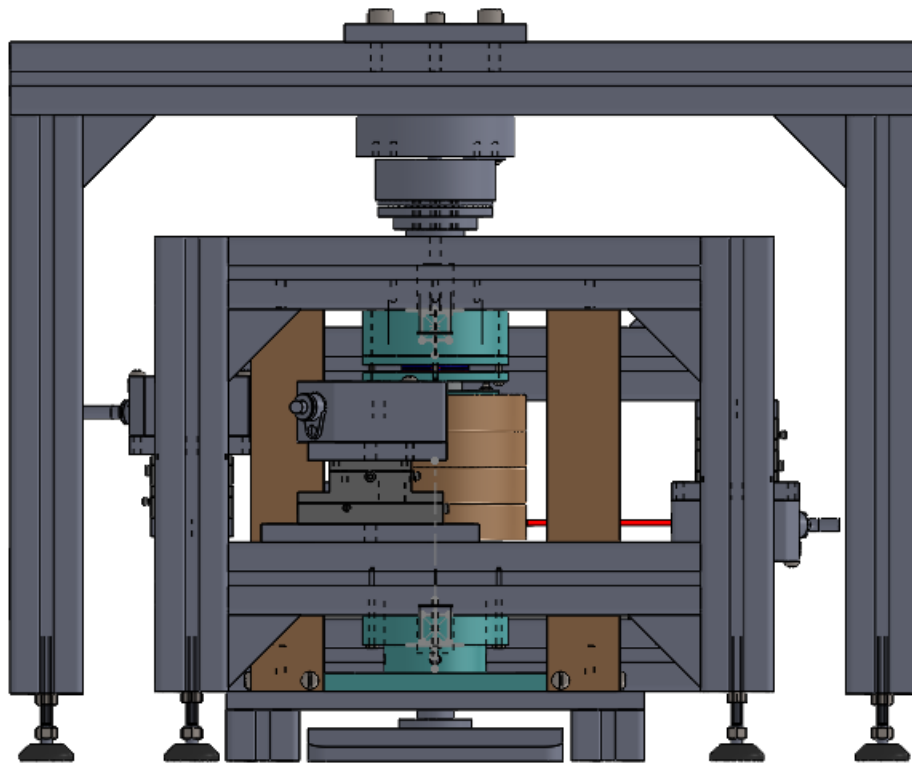


Figure 5.2.5 – Scale configuration (front view).

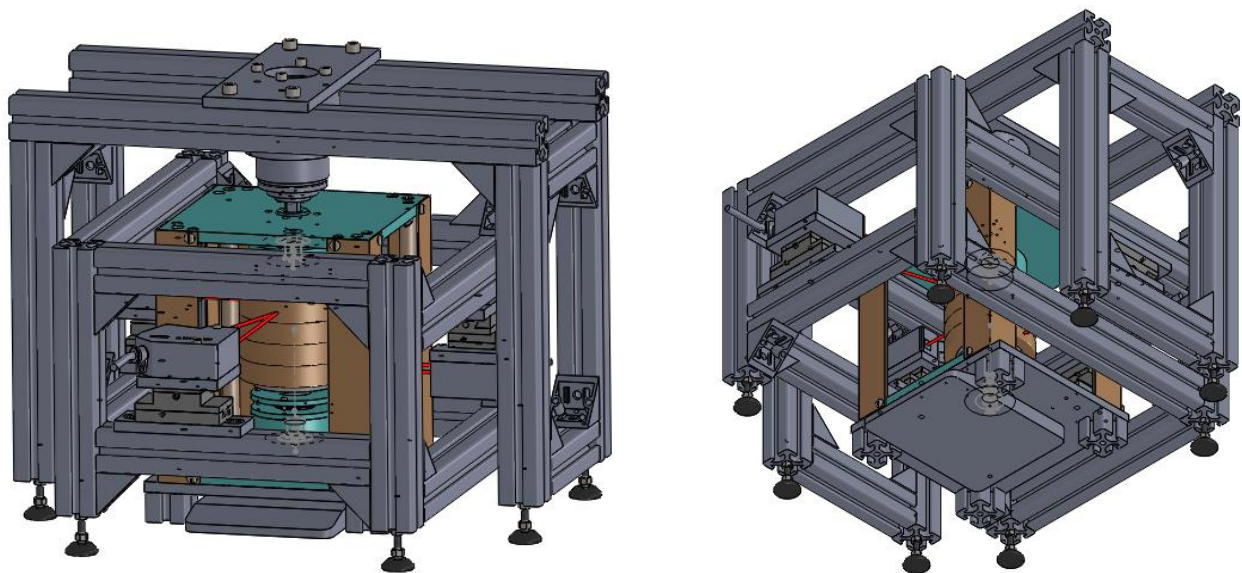


Figure 5.2.6 – Views of scale configuration.

6. Final layout

The final configuration of the rotor is based on the solutions previously proposed, but with further modifications to make its operation more efficient.

Regarding the solution for increasing stiffness, we decided to use the square section bars made of Delrim, but without the through holes for the barrel nuts. The problem of the screw-polymer connections is solved there by means of the installation of threaded inserts in the blind holes present in the two bases of each support bar.

These threaded inserts are also used for the assembly of the two platform rings, without proceeding to the drilling for the insertion of the barrel nuts.

With regard to the choice of the element at the base of the rotor, which allows it to rotate, the solution based on the ball transfer unit with threaded pin is considered to be the most advantageous, as it guarantees extremely low friction and a better assembly process than the other proposed configurations.

The first modification concerns the design of a clamping system for the two platform rings that constrains their rotation as soon as they reach the desired position. This component consists of a parallelepiped made of Delrim with two M5 holes in the lower base to mount it on the stator base, and a transverse M5 hole to be coupled to a screw which, when screwed in, reaches the platform ring exerting pressure to prevent its rotation. The height at which this transversal hole is to be drilled is chosen so as to be able to clamp the two stator components in configurations useful for the analyses we are carrying out. Finally, the choice of an M5 screw, instead of another with a smaller diameter (in order to reduce the overall dimensions), is due to the need to be able to distribute the tightening force over a larger surface area in order to avoid excessively damaging the surface of the polymer and also to increase the effectiveness of the clamping.

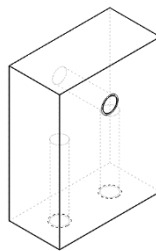


Figure 6.1 – Clamping block.

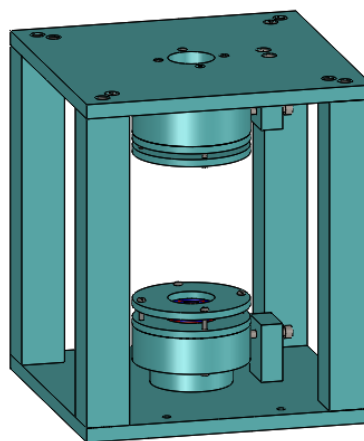


Figure 6.2 – Clamping blocks mounting.

Another modification was made to the element between the scale and the ball transfer unit, so that its height could be adjusted without having to disassemble the structure in order to remove it. To make this possible, it was first necessary to make a modification to Bosch profiles which are mounted vertically, increasing their length by 20 mm so that it was possible to realize the same increase in height of the upper part of this component. The purpose of this modification is to have enough space to make four flattenings on the cylindrical surface which, in pairs, allow the part to be screwed/unscrewed using an M10 nut spanner. The presence of two pairs of flattenings instead of just one is motivated by the need to guarantee a second alternative position to use the fork spanner when the first one is not practical due to the presence of the profiles of the structures around the rotor. Two additional flattenings have been made on the lower part to allow it to be blocked using a fork spanner for M30 nuts in order to prevent the upper part from rotating in solidarity with the lower one during height adjustment. We considered necessary a further increase in the diameter of the base to have a more stable support since the overall height of the component is higher with respect to the previous one. Another modification to this part is that it was made in two separate components, assembled with an M5 screw, in order to produce it more cheaply. At the base of the upper part there is an M3 through-hole to allow the two parts to be clamped by means of an M3×6 mm threaded grub screw as soon as the desired height is reached.

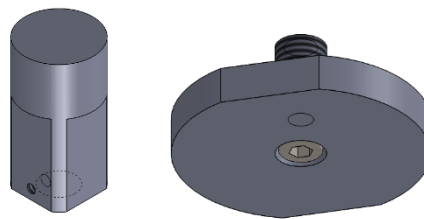


Figure 6.3 – Upper part (left) and lower part (right).

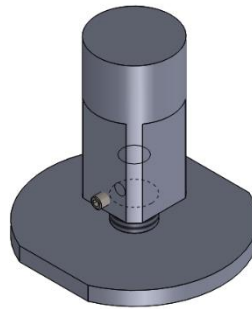


Figure 6.4 – Connection element scale - rotor.

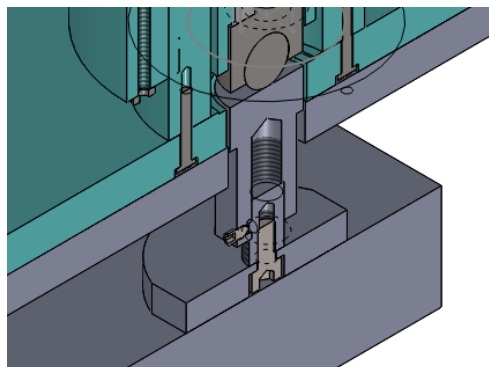


Figure 6.5 – Connection element scale - rotor mounting.

We decided to make the stator base integral with the plane on which it is positioned by four M5 screws screwed into eight holes that are coaxial in pairs: four unthreaded in the Teflon base, and four threaded in the metal base in order to keep the rotor in the correct position during its movement.

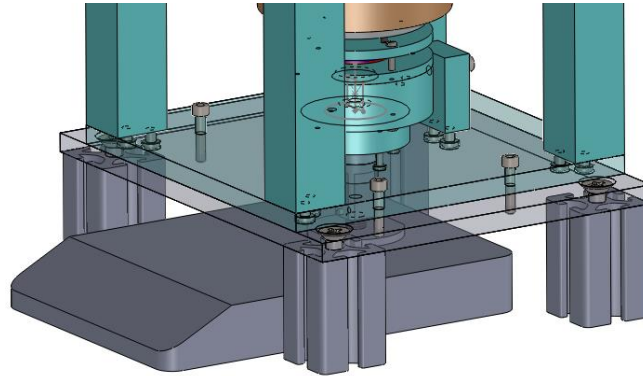


Figure 6.6 – Stator - aluminium plane connection.

Two further changes to the layout are proposed, aimed at improving the accuracy of the structure's final assembly, which could be partially compromised in the previous configuration due to imperfections in the profiles cutting process.

The first modification concerns the profiles at the base of the structure below the rotor, as it is not possible to guarantee total flatness of the cut and the same height for the four components. The solution proposed is to manufacture these parts with a lower height so that adjustable knuckle feet can be mounted at their bases to balance the geometric errors caused by the cuts.

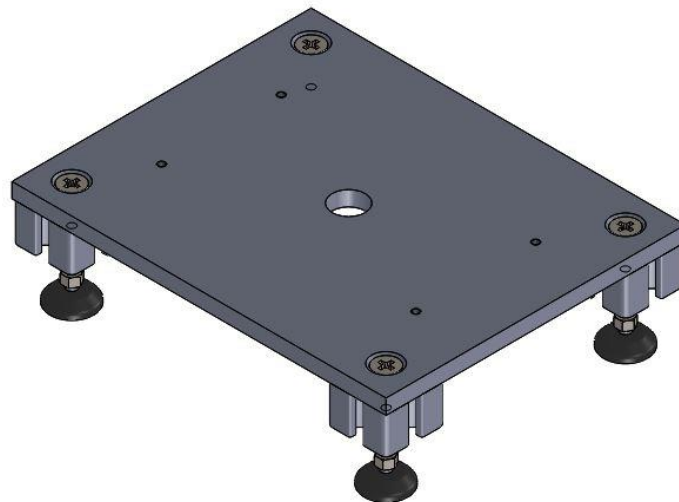


Figure 6.7 – Lower base modification.

The second modification consists in a different configuration for the gantry support structure on which the motor is mounted, so that the ends of the profiles obtained by the cutting process are not adjacent to the sides of the profiles perpendicular to them. If this contact is not avoided, the presence of errors in the inclination of the cuts, even of just a few degrees, could lead to non-negligible geometric problems after the final assembly of the entire structure. The proposed alternative layout (showing only the profiles, at the base of which adjustable knuckle feet will then be mounted) is shown below.

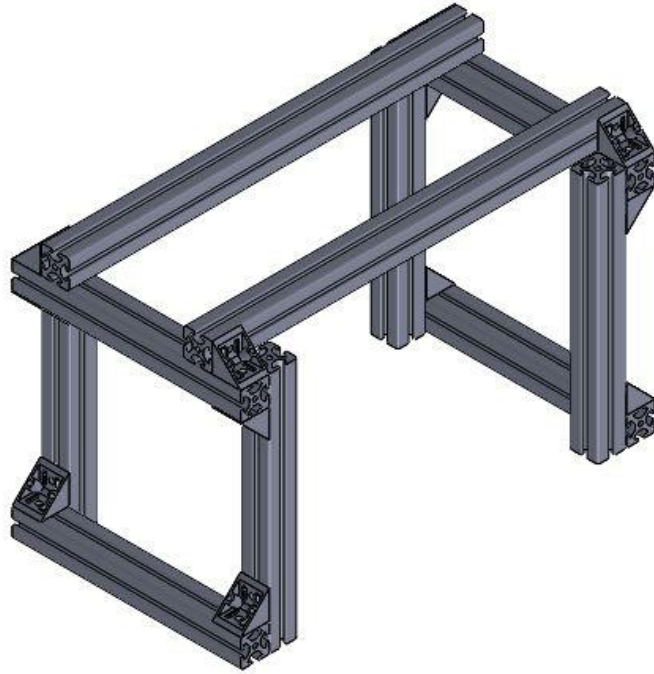


Figure 6.8 – Support structure alternative layout.

Finally, two additional transverse profiles are to be mounted to bind the two structures made by profiles as soon as they have been positioned in the correct configuration. In this way it is possible to prevent them from moving during motor operation.

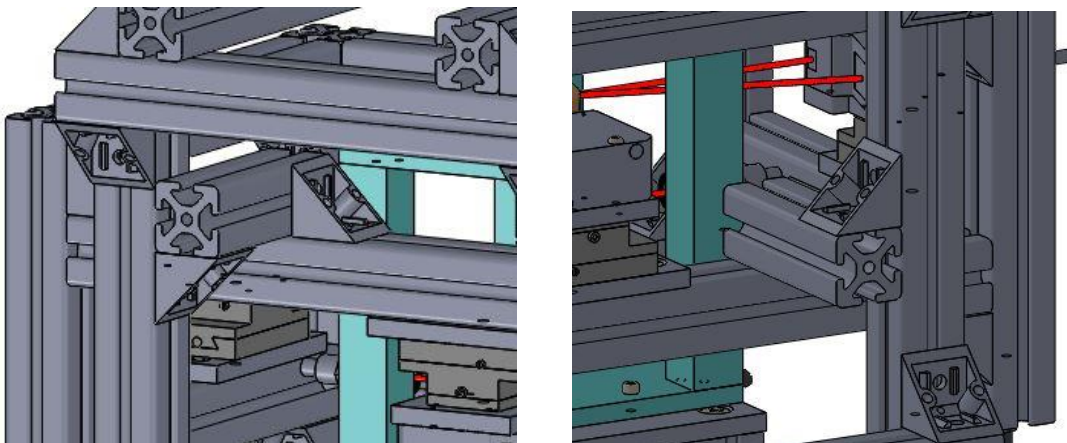


Figure 6.9 – Structures binding.

A cross-section of the final layout is shown below to make the assembly of the various parts clearer.

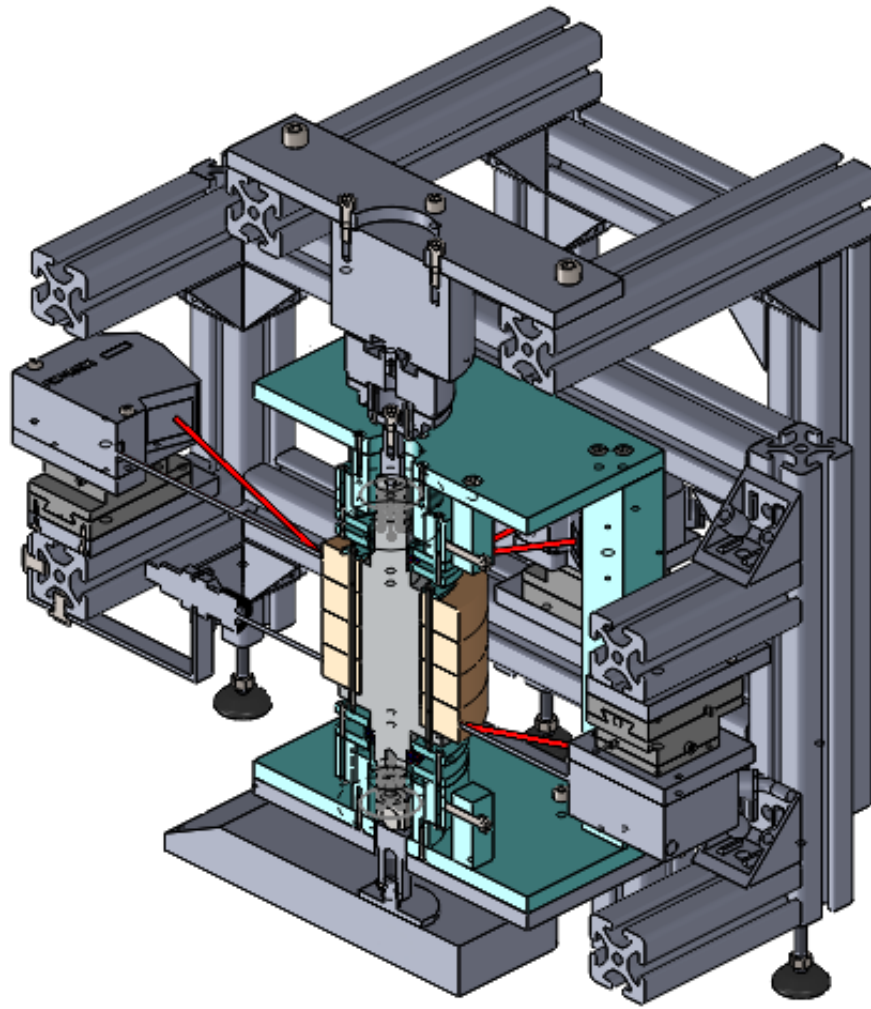


Figure 6.10 – Final configuration (cross section).

7. Rotor Oscillation Analysis

The rotor does not rotate with its axis perpendicular to the base plane, it also oscillates by varying the angle of inclination of the axis and moving in the plane. The most accurate mathematical model developed analyses the behaviour of the unbalanced rotor, in fact in real life, the centre of mass cannot be exactly coincident with the centre of the cross section of the shaft. The distance between the two points may be small, but the presence of the eccentricity (e) causes a static unbalance that can strongly affect the behaviour of the system. The modal analysis of this system was performed by using LUPPOS obtaining ten complex conjugated underdamped modes and two overdamped modes. The modes are coupled together at five different natural frequencies and those of particular interest for the following analysis are the cylindrical and conical modes.

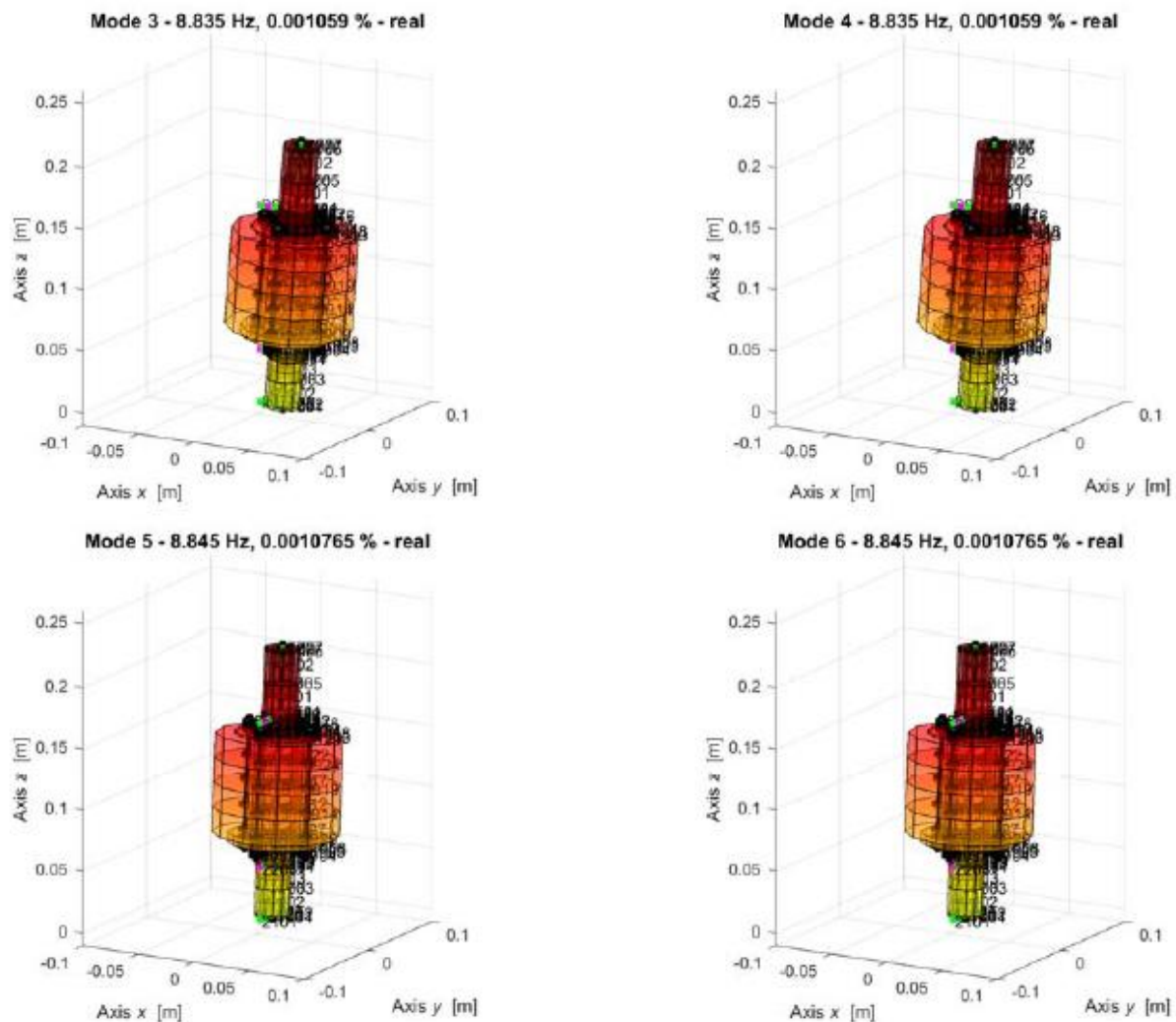


Figure 7.1 – Bounce modes.

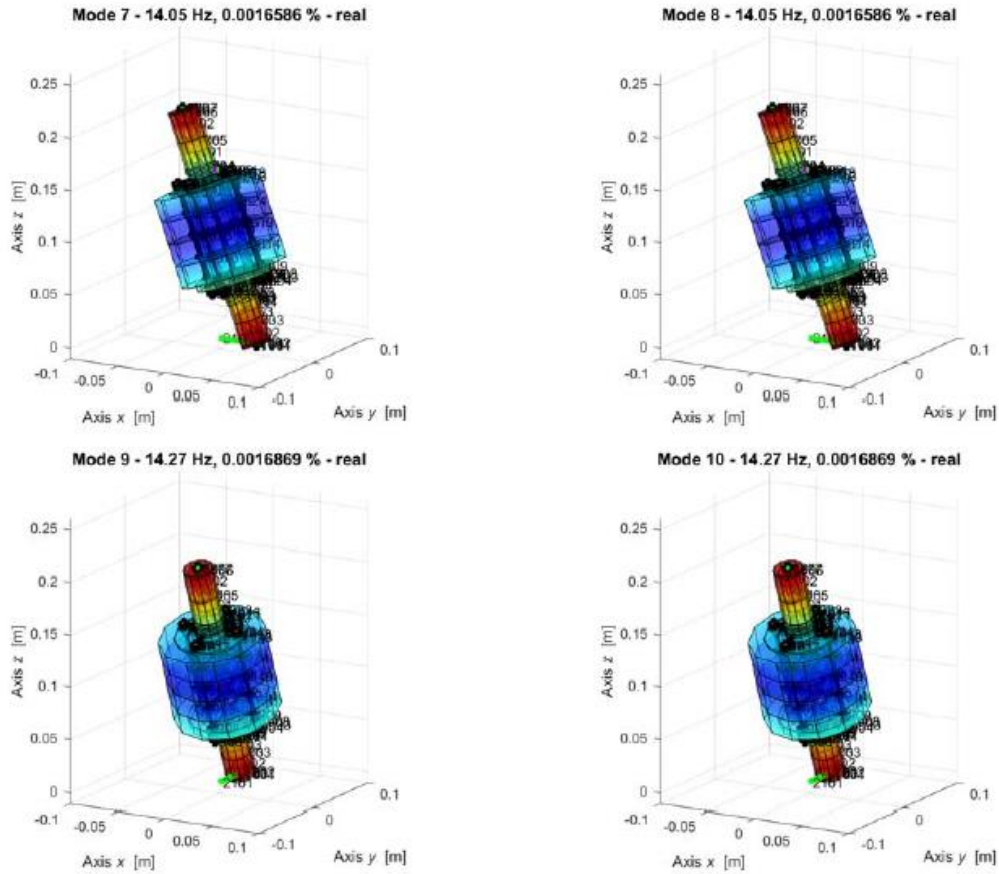


Figure 7.2– Conical modes.

These considerations are important in order to understand the following analysis aimed at studying the limiting conditions that would lead to contact between the stator and rotor bearing rings, due to the oscillation described above. Contact between these rings should be avoided as it would slow down the rotation of the rotor and it would generate sparks. It is therefore desired to verify that this condition does not occur due to an antecedent contact between the rotor and stator parts of the clutch whose gap is 0.2 mm.

The parameters evaluated for this analysis are the vertical distance z with respect to a starting position assumed as 0 (assumed positive upwards and negative downwards), the radial distance r and the angle of inclination θ of the axis. The limit value of the angle that leads to bearing contact for the configuration considered is defined as θ_{\max} .

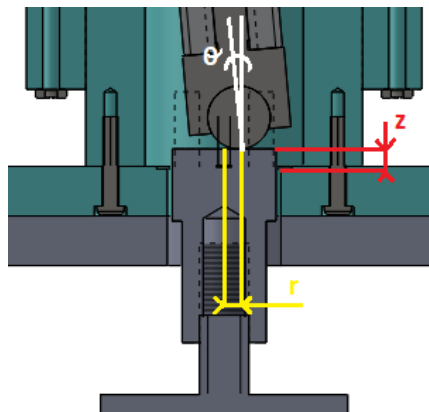


Figure 7.3 – Geometrical parameters.

The measurements taken are compared with the value of the angle of inclination of the rotor which leads to contact between the fixed part and the moving part of the clutch. A point on the perimeter of the upper part of the clutch is taken as a reference and a simple equation is used to determine the limit value of the angle ϑ , taking into account that the two parts touch as soon as the point under examination reaches a position 0.2 mm higher than the starting point.

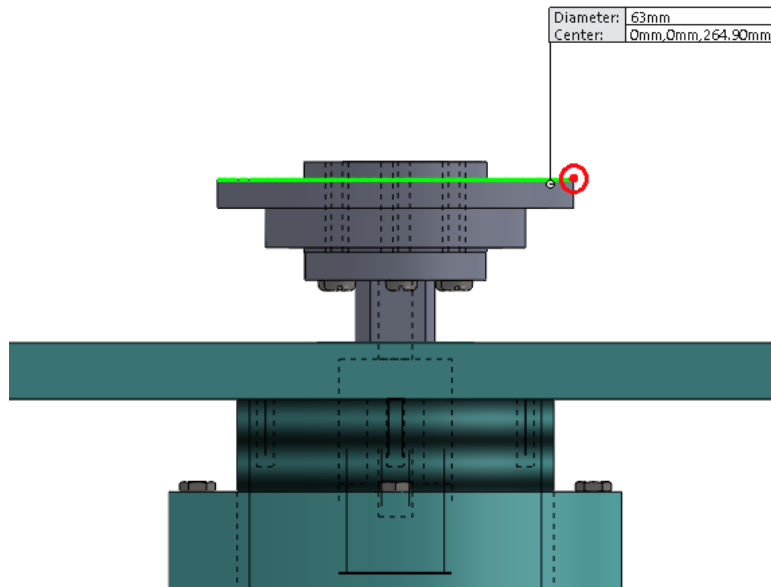


Figure 7.4– Reference point.

$$\vartheta_{limit} = \arcsin \left[0.2 \cdot \left(\frac{63}{2} \right)^{-1} \right] = 0.364^{\circ} \quad (6.1)$$

If sliding between the bearing rings occurs at inclination values greater than ϑ_{limit} , it will be prevented by prior contact between the two parts of the clutch.

The first part of the analysis involves keeping the value of r at zero, varying only z by adjusting the height of the base cylinder, and then changing the values of ϑ until the ϑ_{max} of the respective configuration is reached. The study of the variation of this parameter is important since the rotor is to be used in various configurations characterised by a different vertical position in order to obtain information on the different behaviour it assumes.

Table 7.1 – Variation of z .

z [mm]	r [mm]	ϑ_{max} [°]	Bearings contact
2,00	0,00	0.440	No
1,00	0,00	0.440	No
0,00	0,00	0.440	No
-1,00	0,00	0.440	No
-2,00	0,00	0.440	No

It can be seen from the values measured that the z parameter does not lead to any variation for ϑ_{max} in a range of values in the order of a few millimetres (for our analyses, it is not planned to test the operation of the rotor for height variations greater than those examined in the table). It should also be

pointed out that in this configuration with r equal to 0, possible contact between the magnetic rings would always occur in the bearings located at the top of the shaft.

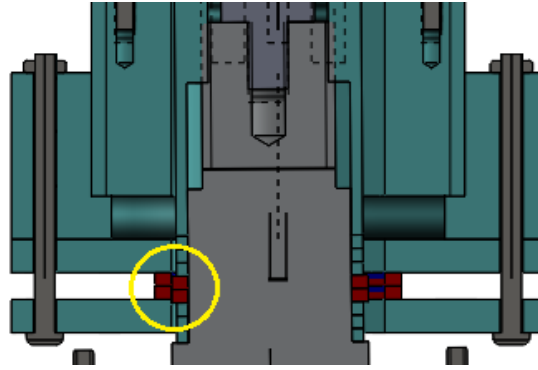


Figure 7.5 – $z=0$; $r=0$; $\vartheta=0.44^\circ$.

The next analysis involves varying the radial distance r while keeping the z parameter null as it was found to be non-influential for ϑ_{\max} in a range of values of a few millimetres.

Table 7.2 – Variation of r .

z [mm]	r [mm]	ϑ_{\max} [°]	Bearings contact
0,00	0,00	0.440	No
0,00	0,05	0.420	No
0,00	0,10	0.400	No
0,00	0,15	0.385	No
0,00	0,20	0.370	No
0,00	0,25	0.355	Yes

The bearing rings make contact for a value of r between 0.20 mm and 0.25 mm (considering the variation in that range of values, it is reasonable to think that sliding occurs for a value halfway between the two, around 0.225 mm). Inclining the rotor in the opposite direction to the radial displacement would increase the ϑ of the first series of measurements, shown in table 6.1, even more, so the inclination in the same direction to the radial displacement of the rotor is taken into consideration here. For this reason, the modes to be referred to, while taking into account this effect, are the cylindrical ones.

The case of contact between the bottom bearing rings is not shown in any table as it does not occur due to the geometry of the rotor.

8. Electrical components of the test bench

The following paragraph describes the electrical connections made in order to drive the rotor by means of an actuation system composed of a magnetic clutch (MWM "EMS 60") and a brushless DC motor (Northrop Grumman "BN34-25EN-02LH") controlled by an external driver (Litton "SCA-B4-70-10").

The magnetic clutch consists of two parts, one integral with the motor by means of a shaft-hub connection made with a key, and the other integral with the rotor: they are free to move independently of each other, but when the part connected to the motor is electrically powered, they rotate together thanks to the magnetic attraction force developed between them, thus allowing the transfer of the driving torque to the rotor shaft.



Figure 8.1 – Magnetic clutch.

The rotation of the shaft of the brushless motor is possible thanks to the magnetic interaction between a permanent magnet acting as a rotor and three stator windings which are 120° out of phase with each other and which are powered alternately (this is why it is necessary to use an external driver to modulate the control of the power supply to these windings). The hall sensors inside the motor are also fundamental to the operation of this type of control: they are externally powered by the driver and send back information on the position of the rotor as an output, thus allowing closed-loop modulation of the power supply to the windings.



Figure 8.2 – Brushless D.C. motor.



Figure 8.3 – Driver.

We decided to use a 10 kOhm potentiometer as a voltage divider in order to modulate the rotation speed of the rotor shaft. This solution was preferred to the impractical one of modifying the potential difference value via the "offset" potentiometer integrated in the driver itself. In fact, the latter alternative has several negative aspects: the use of a screwdriver for adjustment, reduced modulability and the lack of visual feedback of the adjustment level.



Figure 8.4 – Potentiometer.

8.1 Driver setting

When carrying out the wiring, it is important to consider that the driver operating mode chosen is the "Hall Mode", which uses the data received from the hall sensors in the brushless motor as input. To work in this mode it is necessary to short-circuit the jumpers J2, J7, J8 and J9 of the driver with appropriate connectors, as shown in figure 8.1.1.



Figure 8.1.1 – Driver setting.

Figure 8.1.1 also shows the setup of the integrated potentiometers which are used to configure the following parameters:

- Gain coarse and Gain fine potentiometers are adjusted in order to make the dynamical behaviour of the servo amplifier compatible to the particular connected motor.
- n max potentiometer is used to adapt the desired maximum speed to the amplitude of the present set value.
- I max decides the maximum possible motor current.
- Offset is adjusted to level the position at which the motor stands still.

If a setup with a motor with different specifications is used, it is necessary to set the values of these potentiometers again, information for this operation is shown in table 8.1.1.

Table 8.1.1 – Driver potentiometers setting.

Potentiometer	Function	Turning to the left (ccw)	Turning to the left (ccw)
Gain coarse	Gain	Factor lowered	Factor raised
Gain fine	Gain	Factor lowered	Factor raised
n max	Definition of max. number of revolutions	Value is decreased	Value is increased
I max	Set value for max. current	Upper limit lowered	Upper limit raised
Offset	Zero Offset (motor stands still)	Motor rotates counterclockwise	Clockwise rotation

The way in which the driver was set up involves the pre-setting of the potentiometers described in Table 8.1.2.

Table 8.1.2 – Driver potentiometers pre-setting.

Gain coarse	Gain fine	n max	I max	Offset
Left stop	Middle	Middle	Middle	Middle

After positioning the potentiometers as described, continue by setting the maximum value available for the set value (using our external potentiometer), and turn the potentiometer n max until the desired speed is reached. Next, set the value of potentiometer I max, ensuring that the maximum current allowed in the used motor is not exceeded. The gain potentiometers are then adjusted, starting with a progressive increase in the value of the coarse gain, ensuring that the motor does not start to work unsteadily, does not vibrate and does not cause excessive noise. Finally, set the set value to zero (using the external potentiometer we connected) and adjust the offset until the motor shaft stops.

8.2 System wiring

The connection of the electrical wiring was initially carried out following the circuit in figure 8.2.1, partly following the instructions provided by the driver manufacturer and integrating into the circuit the connection of the clutch to the same 24V power supply, adding a switch to allow its control.

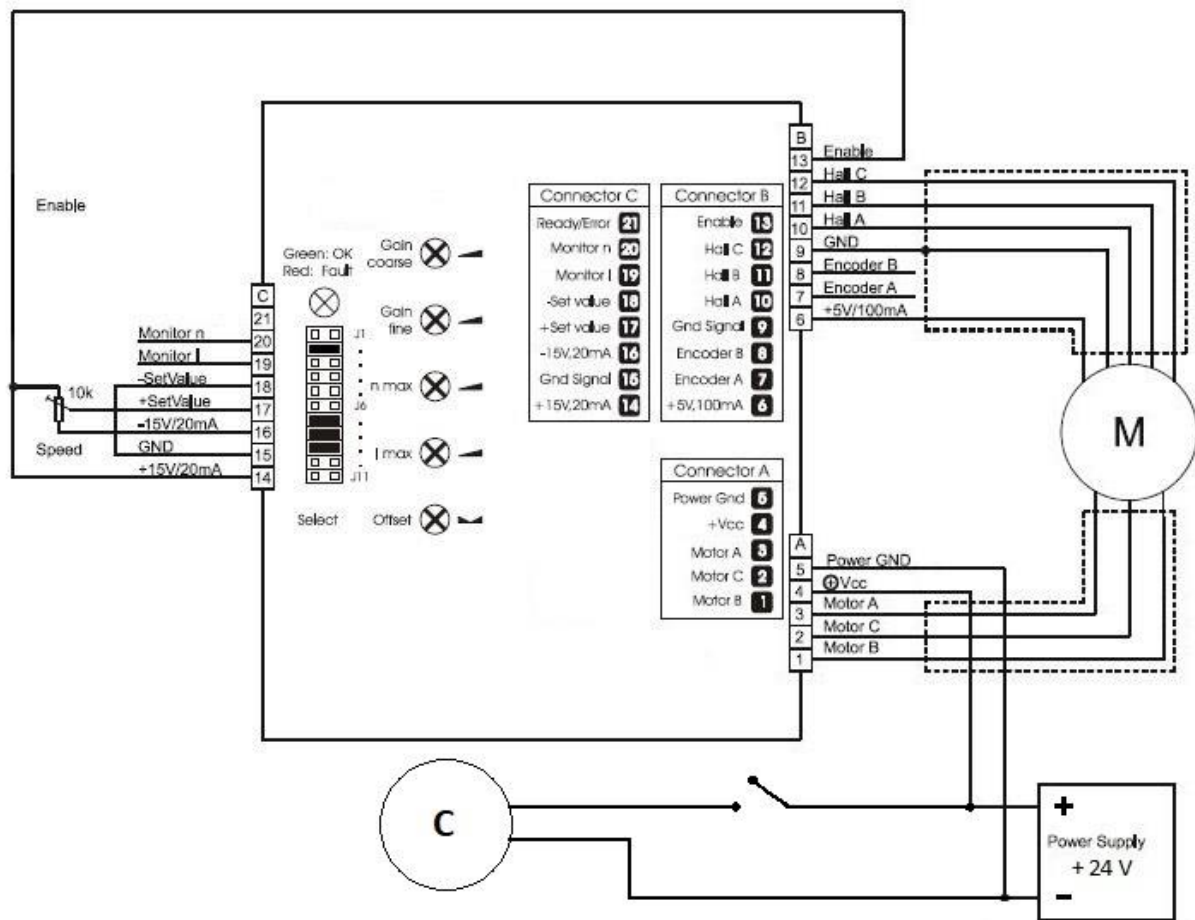


Figure 8.2.1 – Electrical circuit.

The connections made are shown in the following three tables.

Table 8.2.1 – Driver-Motor wiring.

Driver pin	Motor wire	Wire color
1. Motor B	A Coil	Black
2. Motor C	B Coil	Green
3. Motor A	C Coil	Red
6. +5 V, 100 mA	Vcc	Yellow
9. Ground	Ground	Grey
10. Hall A	S1	Brown
11. Hall B	S2	Blue
12. Hall C	S3	Orange

Table 8.2.2 – Driver-Driver wiring.

Driver pin	Driver pin
13. Enable	14. +15 V, 20 mA
15. Ground	18. -SetValue

Table 8.2.3 – Driver-Potentiometer wiring.

Driver pin	Potentiometer pin
14. +15 V, 20 mA	1 (left pin)
16. -15 V, 20 mA	2 (right pin)
17. +SetValue	3 (middle pin)

Considering our layout, the potentiometer is not directly connected to the driver, as it is housed inside a small control box together with the switch that controls the clutch power supply. The connection is therefore made between a further three-pole cable and the three corresponding pins of the connector on that box, which in turn are connected to the potentiometer itself.

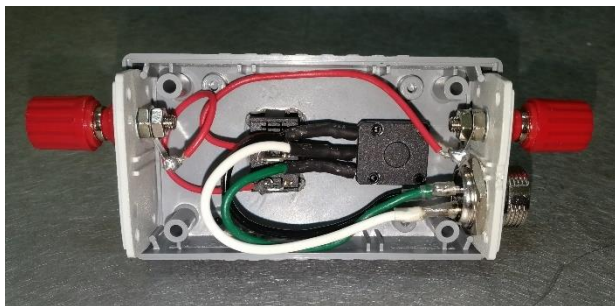


Figure 8.2.2 – Control box: inner part (left) outer part (right).

Respecting the numbering (1,2,3) of the poles of the connectors listed, and taking into account the colours of the wiring we used, the correspondence between the pins of the potentiometer and the colours of the poles of the cable used to connect the control box to the driver, is shown in table 8.2.4.



Figure 8.2.3 – Connection wire.

Table 8.2.4 – Connection wire - Potentiometer pin.

Connection wire Pin color	Potentiometer pin
Yellow	1 (left pin)
Red	2 (right pin)
Green	3 (middle pin)



Figure 8.2.4 – Preventive test of electrical connections.

8.3 Modification of system wiring

The configuration described above, created by referring to the instructions provided by the manufacturer of the driver in the case of its use with a speed control via an external potentiometer, presents a problem which is solved below by means of an alternative modification.

In the previous configuration, the potentiometer works with a total potential difference of 30 V, and the +SetValue can vary from -15 V to +15 V. As a direct consequence, when the knob of the potentiometer is exactly halfway through its stroke, the motor stands still, going from 50% of its stroke to 0% of it, there is an increase in the speed of the motor shaft in one direction, while from 50% to 100% of the stroke there is an increase in the opposite direction. This causes two problems:

- Difficulty in setting the potentiometer knob to exactly 50% to stop the motor.
- Only 50% of the knob stroke is available to carry out speed adjustment instead of 100% (as we are only interested in motor rotation in one direction, not both).

The alternative circuit is therefore proposed, and the only modification concerns the part of the wiring relating to all the connections with the pins of the driver ports numbered from 14 to 18. Since the motor shaft should rotate in the same direction as the threaded pin of the connection element between clutch and rotor described in paragraph 3.2 (so that the transfer of torque does not cause it to unscrew during operation), it could be necessary to switch the wires connected to driver ports numbered from 1 to 3, so that the desired rotation is obtained.

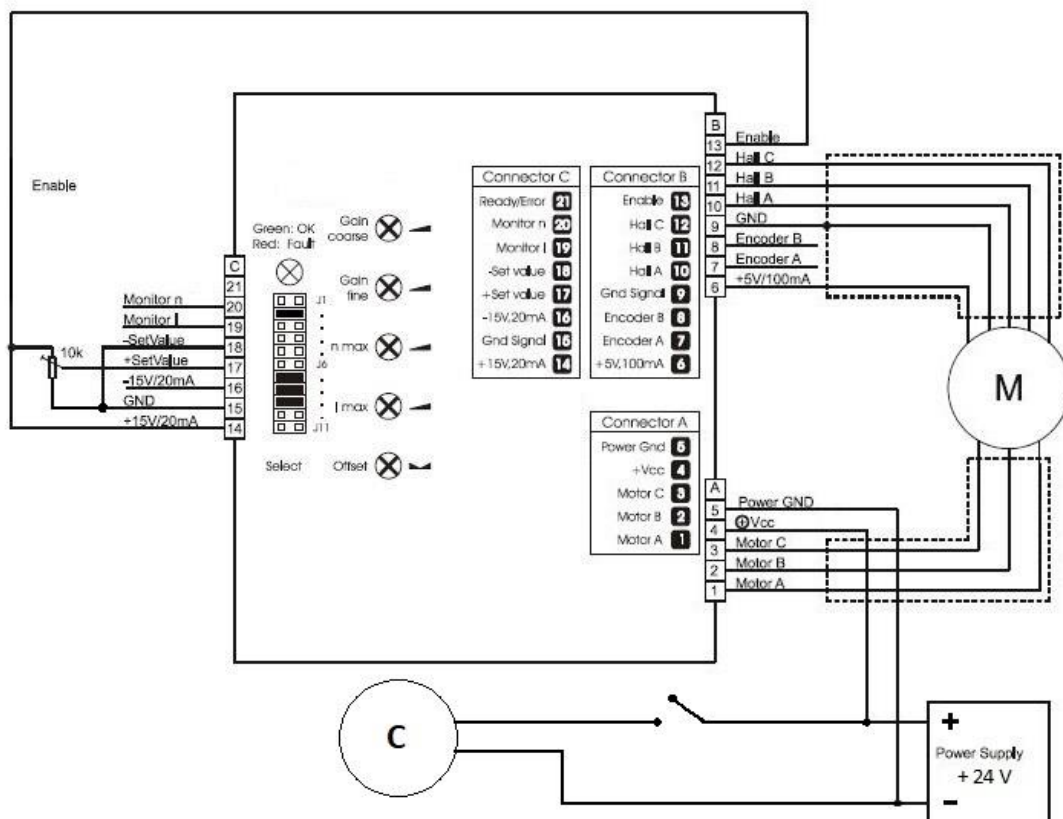


Figure 8.3.1 – Alternative electrical circuit.

9 Pre-test of optical sensors

We decided to test the operation of the optical sensors on a layout that was simpler in terms of construction but more complex in terms of dynamic behaviour. This trial made it possible to have all the data necessary to test the five sensors and to develop a Matlab script in order to obtain the exact position of the rotor in space and its angular velocity, both as a function of time, and to carry out the post-processing on its dynamic behaviour.

9.1 Pre-test layout

The components used to carry out the series of pre-tests are the following:

- magnetic rotor;
- laser tachometer;
- support structure for keyence optical sensors.

9.1.1 Magnetic rotor

The object analysed in the following pre-tests is a small rotor placed on a base, both components are made of plastic and have magnets inside. The actuation of the rotation is done manually by turning the "free end" of the rotor. This rotor and its 3D model are shown below, but only the cylindrical parts are drawn, as only some points on these parts are measured by the optical sensors.

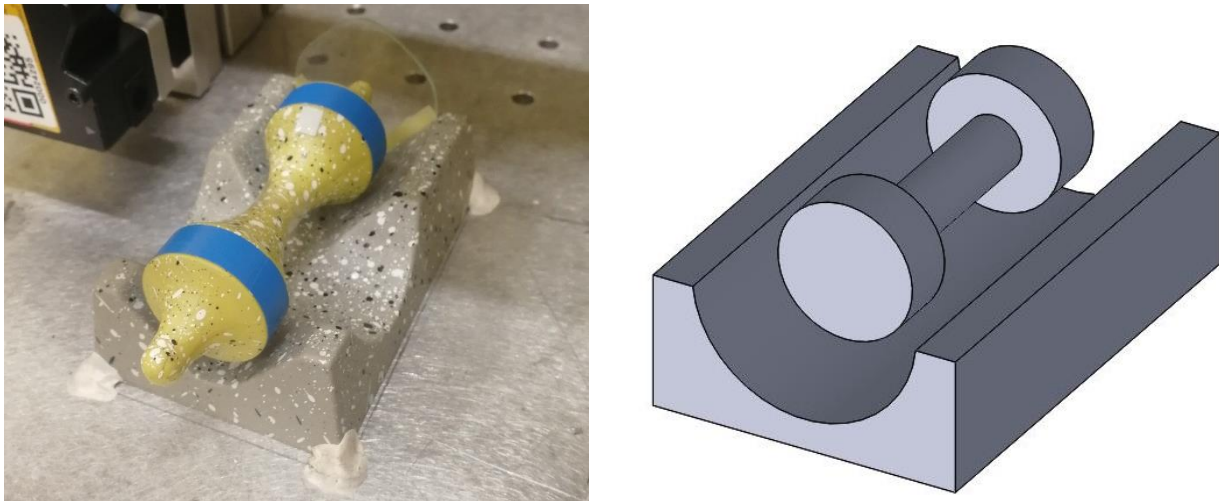


Figure 9.1.1.1 – Magnetic rotor (left) and 3D Model (right).

The interaction between the magnets of the base and the ones inside the rotor has the effect to make the latter levitating, which then rotates without any friction apart from the one of the air and the one due to the contact between one of its two ends on a plate that acts as a constraint. This constraint is necessary because the interaction of the magnets does not only cause forces in the radial direction with respect to the rotor reference system, but also axial forces, so that without the plate, the rotor would be pushed axially out of the base. In these tests, we analysed the behaviour of the rotor with two plates made of different materials: plastic and glass. The measurements made, which are shown in a later chapter, show that the material choice has a significant role in characterising the dynamics of the rotor. It is worth specifying three different effects which characterise its behaviour:

- different initial start-up conditions between tests;
- deterioration of the plastic constraint plate;
- non-symmetrical magnetic interaction in radial direction.

The tests carried out present a limited repeatability due to the initial conditions during the start-up of the rotor. In fact, its static position on the base is not always the same, as can be seen from the different positions assumed by its end in contact with the constraint plate (although these variations are small). It is important to highlight that the transmitted rotation torque is always different as it is generated manually and, as consequence, the initial rotation speeds are always different. Finally, it must be taken into account that not only rotational torque is transmitted, but due to the motion of the hand during the initial spin, a force in the radial direction is also transmitted. This force is obviously not controllable in modulus or direction and is therefore another element that prevents perfect repeatability of the tests.

Another difference between the various tests using the plastic constraint plate is its deterioration. In the initial tests it is possible to notice an anomalous trend in the vertical displacement of the rotor related to the drifting phenomenon, which in turn is linked both to the rotation of the rotor and probably to the radial force components induced already described above. In the latest tests this phenomenon was no longer evident, and the most likely explanation is the creation of a small groove by the rotor tip on the plate, so as to hinder the vertical displacement during its motion.

The base structure is constructed in such a way that the magnets inside it are placed in lateral and inferior positions with respect to the rotor, so there are no magnets above it. The consequence of this configuration is that the magnetic interaction between the base and the rotor is not radially symmetrical with respect to the latter, and the orbit traversed by the rotor during its motion is therefore not circular, but "ovoid". This trajectory is elongated upwards because, as mentioned, there are no magnets exerting a downward repulsive force on the rotor.

This behaviour can be explained starting from the analytical model of the Jeffcott rotor with anisotropic supports. This model assumes that, under the hypothesis of a reference system with the rotor axis in the z-direction, the supports can be modelled with different stiffnesses K_x and K_y . Applying this variation to the Jeffcott rotor model with isotropic supports, we obtain the following formulations:

$$K_x \neq K_y \quad (9.1.1.1)$$

$$\begin{cases} m \ddot{x}_g + K_x x = 0 \\ m \ddot{y}_g + K_y y = 0 \end{cases} \quad (9.1.1.2)$$

Where:

- m is the rotor mass;
- \ddot{x}_g and \ddot{y}_g are accelerations referred to the centre of gravity of the rotor.

The coordinates of the centre of gravity can be expressed as follows:

$$\begin{cases} x_g = x + \varepsilon \cos \omega t \\ y_g = y + \varepsilon \sin \omega t \end{cases} \quad (9.1.1.3)$$

Where ε is the distance between the centre of gravity of the moving rotor and the origin (coinciding with the position of the centre of gravity of the rotor in steady state).

Substituting in (9.1.1.2) we obtain:

$$\begin{cases} m\ddot{x} + K_x x = m \omega^2 \varepsilon \cos \omega t \\ m\ddot{y} + K_y y = m \omega^2 \varepsilon \cos \omega t \end{cases} \quad (9.1.1.4)$$

The solutions required are of the following type:

$$\begin{cases} x = x_0 + \varepsilon \cos \omega t \\ y = y_0 + \varepsilon \cos \omega t \end{cases} \quad (9.1.1.5)$$

Substituting (9.1.1.5) into (9.1.1.4) we obtain:

$$\begin{cases} x_0 = \frac{\omega^2 \varepsilon}{\frac{K_x}{m} - \omega^2} \\ y_0 = \frac{\omega^2 \varepsilon}{\frac{K_y}{m} - \omega^2} \end{cases} \quad (9.1.1.6)$$

After x_0 e y_0 are defined, it is possible to write the elliptical precession orbit of the rotor as follows:

$$\left(\frac{x}{x_0}\right)^2 + \left(\frac{y}{y_0}\right)^2 = 1 \quad (9.1.1.7)$$

In our case, the precession orbit is not perfectly elliptical because, assuming the y direction to be vertical and orthogonal to the rotor axis, the stiffness K_y of the support is different between the parts above and below the rotor. In particular, the (9.1.1.6) shows that at a lower value of K_y (corresponding to the part above our rotor) there is a greater value of upward displacement in the y direction, obtaining that "ovoid" trajectory.

9.1.2 Laser tachometer

The rotational speed of the rotor was measured by means of this sensor, already described in chapter 3.2. To simplify the construction of the measurement structure, the LT2 laser tachometer was mounted on its tripod and positioned laterally to the rotor. It is important to highlight that it has no constraints on the measurement distance as limited as those of the Keyence optical sensors. We placed a small adhesive rectangle of reflective material on the rotor, so that the laser can detect its passage at each turn and then send the respective voltage pulse as input to the SCADAS Unit.



Figure 9.1.2.1 – Laser tachometer.



Figure 9.1.2.2 – Reflective material.

9.1.3 Support structure for keyence optical sensors

The structure built for this magnetic rotor used for the pre-test of the sensors is less complicated than the one which is subsequently built for the experimental analyses on the rotor which is the main subject of this thesis. It consists of a gantry structure created using Bosch profiles on which the four optical sensors of the keyence are mounted, and before being assembled, a 3D model was made in Solidworks in order to allow the correct positioning of the sensors.

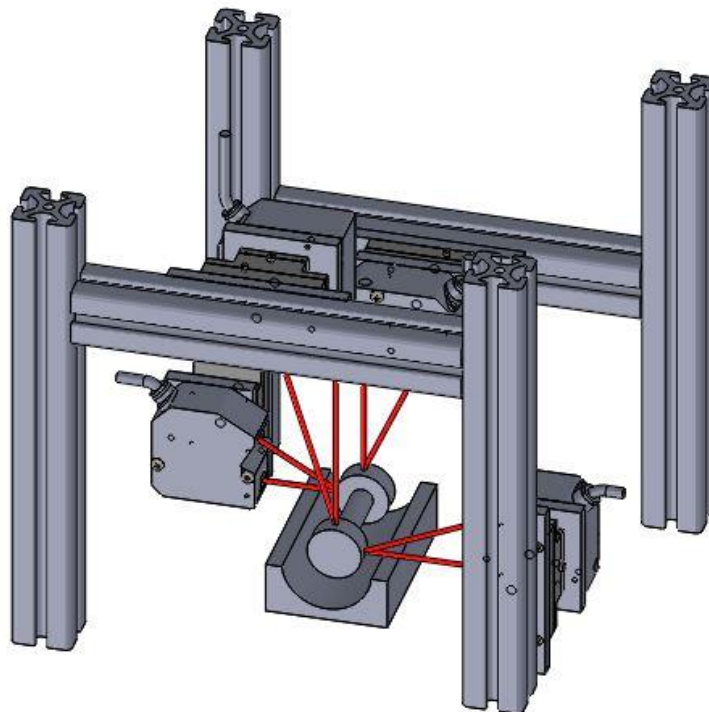


Figure 9.1.3.1 – Layout 3D model.

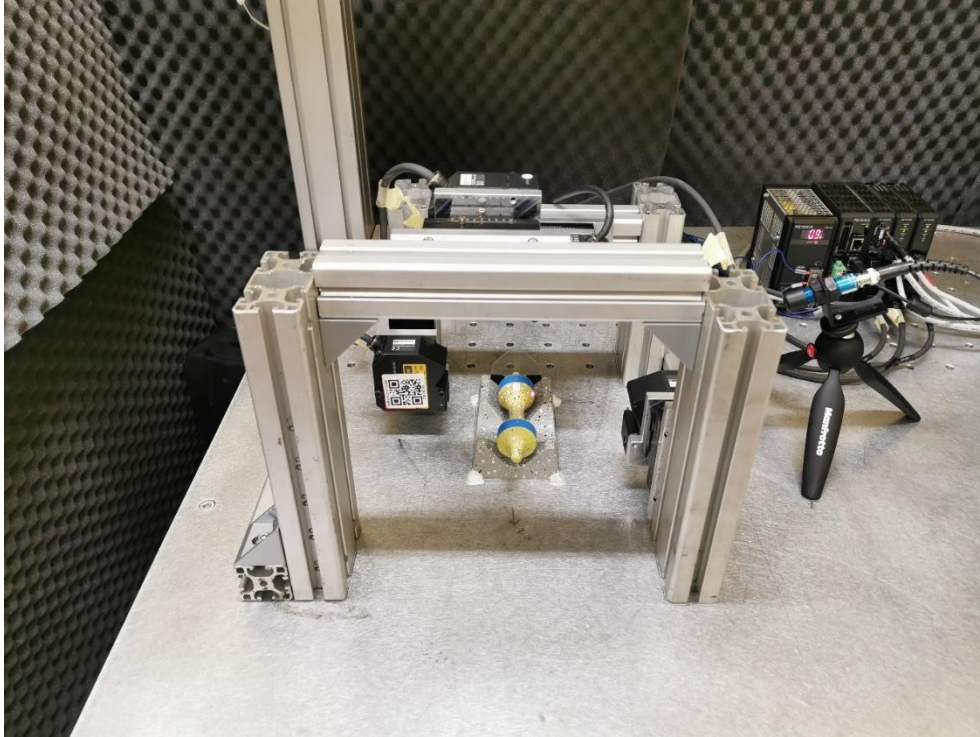


Figure 9.1.3.2 – Final layout.

After the installation and connection to the SCADAS Unit (by Siemens), the four sensors require a setup on the Testlab software (which allows to acquire the laser measurements) with the following functions:

- defining the connection with the SCADAS channels;
- setting the signal type;
- defining the sensitivity of measurements;
- indicating the position in space of the points analysed by the sensors;
- adjusting the distance from the analysed object (using Keyence software).

The setups for our layout are shown below:

	PhysicalChannelId	OnOff	ChannelGroupId	Point	Direction	Input mode	Measured Quantity	Electrical Unit	Actual sensitivity	
1	Input1	<input checked="" type="checkbox"/>	Vibration	1:1	+X	Voltage DC	Displacement	mV	1000	mV/mm
2	Input2	<input checked="" type="checkbox"/>	Vibration	1:2	-Y	Voltage DC	Displacement	mV	555.56	mV/mm
3	Input3	<input checked="" type="checkbox"/>	Vibration	1:3	-X	Voltage DC	Displacement	mV	555.56	mV/mm
4	Input4	<input checked="" type="checkbox"/>	Vibration	1:4	-Y	Voltage DC	Displacement	mV	250	mV/mm
5	Input5	<input checked="" type="checkbox"/>	Vibration	1:1	+RZ	ICP	Voltage	mV	1000	mV/V

Figure 9.1.3.3 – Channel setup.

	Parent Comp...	Name	Full Name	X (m)	Y (m)	Z (m)	XY (°)	XZ (°)	YZ (°)
1	1	1	1:1	-0.0182	0.0000	0.0325	0.0000	0.0000	0.0000
2	1	2	1:2	0.0000	0.0182	0.0335	0.0000	0.0000	0.0000
3	1	3	1:3	0.0182	0.0000	0.1050	0.0000	0.0000	0.0000
4	1	4	1:4	0.0000	0.0182	0.1005	0.0000	0.0000	0.0000

Figure 9.1.3.4 – Geometry.

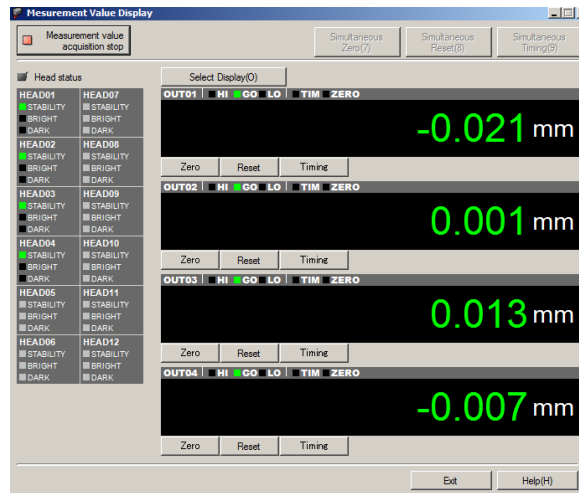


Figure 9.1.3.5 – Laser zeroing.

Before starting the tests, we applied adhesive material to the corners of the rotor base so that the rotor would not move and alter the setting.

9.2 Post-processing analysis of pre-test data

The measured data needs to be exported to Matlab so that it can be used to obtain precise information about the position in space and angular velocity of the rotor.

9.2.1 Post-processing analysis of displacements

After measuring the displacements, we post-processed them in order to obtain the position in space of the rotor axis as a function of time, so that we could create its analytical model. We investigated how to obtain the mathematical formulation of a cylinder in space, whose radius is known, using only the coordinates of the four points whose position is detected at each instant by the four optical sensors. A reference system of the type in figure 9.2.1.1 is considered in the following analysis, taking into account that the rotor axis is coincident with the z axis in stationary conditions.

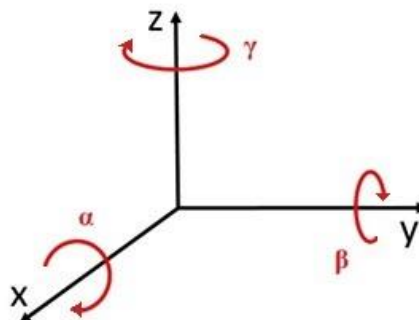


Figure 9.2.1.1 – Reference system.

The two pairs of sensors provide the displacement of two pairs of points on the rotor surface at each time instant, but always in the same two planes, whose positions depend on the mounting of the lasers. In our case, we chose to analyse two sections at the cylindrical parts of the rotor. From the coordinates

of these points during the motion of the rotor, and in correspondence with the section planes, we can determine two conics lying on these planes, that are not perfect circumferences. This happens because the section on the plane of the cylinder changes from a circumference to an ellipse due to its translation and rotations around the two axes of the reference system initially perpendicular to its axis in static condition. We decided to use rotation matrices to obtain, from these two ellipses, the equations describing the position of the circular section of the rotor in space, and therefore of the axis of the rotor itself.

The following angles of rotation are defined:

- angle α , clockwise rotation of the rotor around the x-axis;
- angle β , clockwise rotation of the rotor around the y-axis;
- angle γ , clockwise rotation of the rotor around the z-axis.

The rotation matrices around the axes are defined as follows:

$$\mathbf{R}_x = \begin{bmatrix} 1 & 0 & 0 \\ 0 & \cos \alpha & \sin \alpha \\ 0 & -\sin \alpha & \cos \alpha \end{bmatrix} \quad (9.2.1.1)$$

$$\mathbf{R}_y = \begin{bmatrix} \cos \beta & 0 & -\sin \beta \\ 0 & 1 & 0 \\ \sin \beta & 0 & \cos \beta \end{bmatrix} \quad (9.2.1.2)$$

$$\mathbf{R}_z = \begin{bmatrix} \cos \gamma & \sin \gamma & 0 \\ -\sin \gamma & \cos \gamma & 0 \\ 0 & 0 & 1 \end{bmatrix} \quad (9.2.1.3)$$

Let us assume to study a generic cylinder with an axis in the z direction under static conditions. We define the following three vectors (3×1):

- vector \mathbf{x} of the coordinates in x,y,z of the points of the undeformed circumference;
- vector \mathbf{x}' of the coordinates in x,y,z of the points of the deformed circumference measured in the two planes that make a section of the rotated and translated cylinder;
- vector $\Delta\mathbf{x}$ of the translations in the x,y,z direction. The axial translation (direction z) is zero in our case.

It is possible to change the \mathbf{x} coordinate system into the deformed \mathbf{x}' coordinate system by applying the principle of superposition of effects between the three rotations and the translation in the radial direction which is decomposed into the two translations in the directions orthogonal to the axis of the cylinder we are studying.

$$\mathbf{x}' = \mathbf{R}_x \mathbf{R}_y \mathbf{R}_z \mathbf{x} + \Delta\mathbf{x} \quad (9.2.1.4)$$

It can be assumed that the rotation around the z-axis is not influential in the problem we are analysing, since considering it as the first rotation of the cylinder, it would not change the shape of its section, for this reason we can consider the equation (9.2.1.4) only with the rotation matrices $\mathbf{R}_x \mathbf{R}_y$.

We are interested in the opposite problem: calculating \mathbf{x} from \mathbf{x}' . So, it is sufficient to invert the matrices, remembering the following properties (the first is valid because the rotation matrices are orthogonal):

$$\begin{cases} \mathbf{R}^{-1} = \mathbf{R}^T \\ (\mathbf{R}_A \mathbf{R}_B)^{-1} = \mathbf{R}_B^{-1} \mathbf{R}_A^{-1} \end{cases} \quad (9.2.1.5)$$

From the (9.2.1.4) and (9.2.1.5):

$$\mathbf{x} = \mathbf{R}_y^T \mathbf{R}_x^T (\mathbf{x}' - \Delta\mathbf{x}) \quad (9.2.1.6)$$

The (9.2.1.6) allows us to calculate the coordinates of the original points of a system moved in space. As a confirmation of this procedure, we applied it to a simple similar case. Let us consider a vector whose extremes points are (0 0 0) and (0, 0, 1) in a xyz, reference system. We apply the following rotations and translations:

- clockwise rotation $\alpha = 30^\circ$ with respect to x;
- clockwise rotation $\beta = 60^\circ$ with respect to y;
- translation $\Delta x = 0.5$ m in x direction;
- translation $\Delta y = 0.2$ m in y direction.

The new vector position, after these rotations and translations, is shown below.

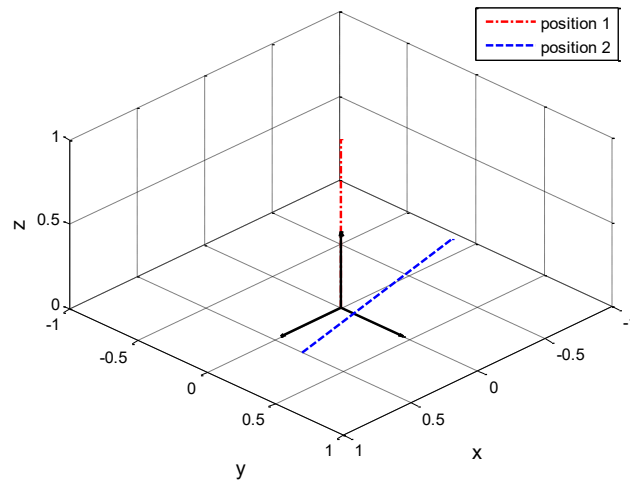


Figure 9.2.1.2 – From initial position 1 to new position 2.

Now it is possible to move the vector in such a way to reach position 3 that is the same of the initial position 1 from the previous new position (2) by applying the equation (9.2.1.6).

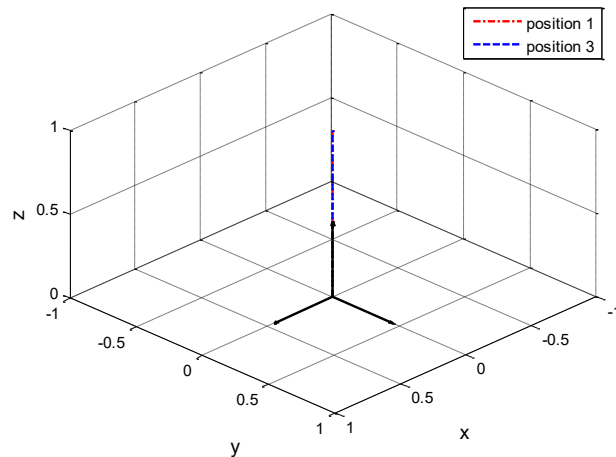


Figure 9.2.1.3 – Position 3 equal to position 1.

We proceed by introducing one more relation between the parameters: the equation of a circumference of radius equal to the cylinder one, with centre in the origin of the originally defined reference system and lying on the x-y plane of the same system.

$$\begin{cases} \mathbf{x} = \mathbf{R}_y^T \mathbf{R}_x^T (\mathbf{x}' - \Delta \mathbf{x}) \\ x^2 + y^2 = r^2 \end{cases} \quad (9.2.1.7)$$

Then, we obtain an equation in the form of a generic conic in space of the type shown below, by substituting the first equation of the system (9.2.1.8) into the second one. This resulting equation represents the circumference in space that, after being rotated and translated, generates the ellipse whose two sets of two points are measured by the optical sensors.

$$a_9 x'^2 + a_8 y'^2 + a_7 z'^2 + a_6 x' y' + a_5 x' z' + a_4 y' z' + a_3 x' + a_2 y' + a_1 z' + a_0 = 0 \quad (9.2.1.8)$$

$a_9, a_8, a_7, a_6, a_5, a_4, a_3, a_2, a_1, a_0$ are the unknowns to be found, but from the resulting equation of the system (9.2.1.7) we see that they are all functions of only four terms: $\alpha, \beta, \Delta x, \Delta y$.

$$\begin{aligned} & x^2 \cos^2 \beta + y^2 (\sin^2 \alpha \sin^2 \beta + \cos^2 \alpha) + z^2 (\cos^2 \alpha \sin^2 \beta + \sin^2 \alpha) + \\ & + 2 xy \cos \beta \sin \alpha \sin \beta + 2 xz \cos \beta \cos \alpha \sin \beta + 2 yz (\sin \alpha \sin^2 \beta \cos \alpha + \\ & - \cos \alpha \sin \alpha) - 2 x (\cos^2 \beta \Delta x + \cos \beta \sin \alpha \sin \beta \Delta y) + \\ & - 2 y (\sin^2 \alpha \sin^2 \beta \Delta y + \cos \beta \sin \alpha \sin \beta \Delta x + \cos^2 \alpha \Delta y) + \\ & - 2 z (\sin \alpha \sin^2 \beta \cos \alpha \Delta y + \cos \beta \cos \alpha \sin \beta \Delta x - \cos \alpha \sin \alpha \Delta y) + \\ & + \cos^2 \beta (\Delta x)^2 + (\sin^2 \alpha \sin^2 \beta + \cos^2 \alpha) (\Delta y)^2 + \\ & + 2 \cos \beta \sin \alpha \sin \beta \Delta x \Delta y - r^2 = 0 \end{aligned} \quad (9.2.1.9)$$

It is necessary to have a system in four equations to find these terms, and it can be obtained simply by substituting x', y', z' with the four sets of coordinates of the four points measured on the surface of the cylinder by the optical sensors.

The position of the axis of the generic cylinder in space is now defined at the various time instants of its motion. In our case, we chose to calculate the coordinates of the points of the axis as those in correspondence of the two circular sections measured by the optical sensors at steady state and those of the two ends of the rotor. The formula used, following what has been said so far, is written below:

$$\mathbf{x}' = \mathbf{R}_x \mathbf{R}_y \mathbf{x} + \Delta \mathbf{x} \quad (9.2.1.10)$$

This mathematical procedure done for a generic cylinder can easily be used without any modification for the study of our rotor.

9.2.2 Post-processing analysis of voltage pulses

Two problems were found during the operation of the laser tachometer, which was designed to measure the angular velocity of the rotor:

- No 'tacho' input channel on SCADAS unit;
- Several reflective parts on the rotor due to its colouring.

The lack of an input channel of the "tacho" type on the SCADAS unit results in the impossibility of receiving an input signal already expressed in rpm, thus allowing only information such as a series of voltage pulses received from the sensor.

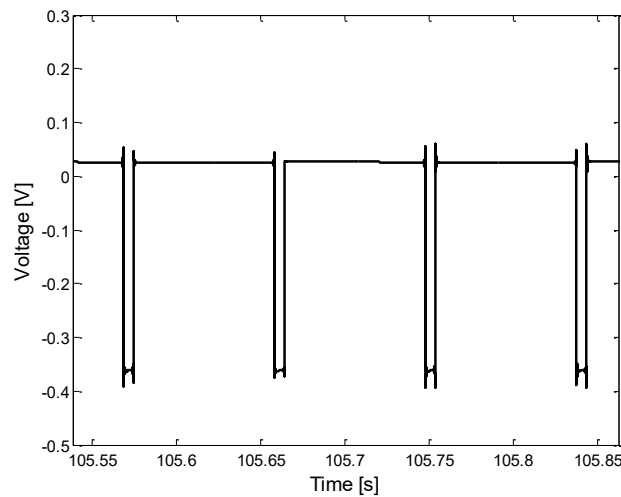


Figure 9.2.2.1 – Voltage pulses.

We wrote a Matlab script to convert these voltage pulses into an angular velocity as a function of acquisition time expressed in rpm. The functioning of this script consists in evaluating the time between two voltage pulses, identified by setting an appropriate threshold value, which will be equal to the rotation period that can be converted into an angular speed expressed in rpm. Considering that the voltage pulses acquired during each revolution are two, one for the moment when the sensor detects the reflective piece of material and the other when it returns to aim at the non-reflective surface, only one of these two pulses must be considered during each revolution. Since this rotor, at the end of its slowdown, stops rotating and begins to oscillate, a series of small peaks in speed are recorded at the end of the stop transient, because during the pendulum motion the piece of reflective material is detected twice at short intervals due to the reversal of the direction of the pendulum motion.

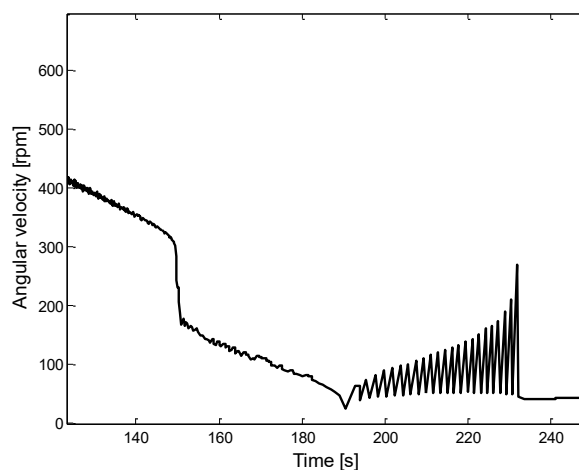


Figure 9.2.2.2 – Angular velocity measured during motion of the rotor as a pendulum.

The second problem found is the presence of multiple reflective parts of the rotor due to its colouring, which causes a random detection of unwanted voltage pulses when the rotor assumes certain positions during its rotation. This causes angular velocity peaks that do not conform to reality, so a Matlab

script was created to cut them. It works as a filter as soon as it detects a velocity value between two successive instants that exceeds a threshold that is set appropriately. When this threshold is exceeded, the velocity value is set equal to the one of the previous instant, since the sampling frequency is high enough to assume that the variation of velocity is almost negligible between the two adjacent instants detected.

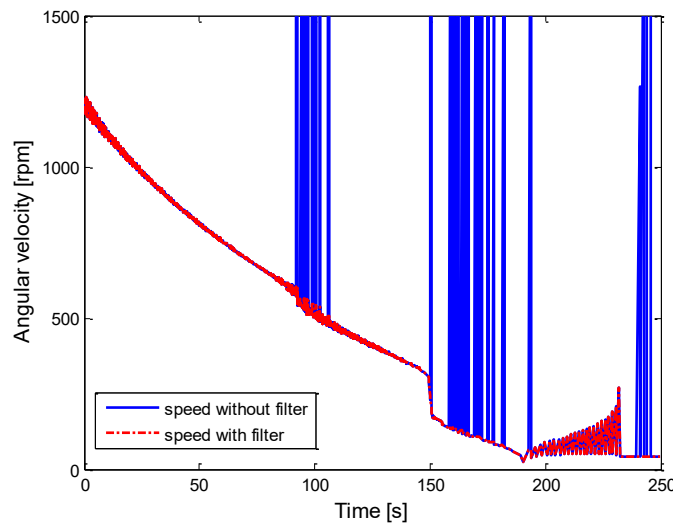


Figure 9.2.2.3 – Comparison between angular velocity without filter and with filter.

9.3 Tests results

We carried out two series of tests:

- 28/10/2021: tests 1-12 (with plastic plate),
- 01/11/2021: tests 13-16 (with plastic plate), tests 17-21 (with glass plate).

It is possible to divide these twenty-one tests into three different groups according to the type of results obtained:

- Test 1-9 (plastic plate, drifting);
- Test 10-16 (plastic plate, no drifting);
- Test 17-21 (glass plate, no drifting).

In all the tests conducted, regardless of the group to which they belong, it is possible to note the dynamic instability condition which causes a high increase in displacements in the radial direction, due to the resonance. During this phase, due to the magnitude of the oscillations, collisions occur between the rotor and the support base which cause considerable dissipation of kinetic energy, thus reducing the time required for the rotor to stop.

The graphs of the tests results show some cases in which displacements continued to be observed despite the interruption of speed detection, as if the rotor had remained stationary. In reality, when the speed becomes equal to zero, the rotor is still moving like a pendulum, but compared to the previous seconds, so much kinetic energy has been dissipated that its oscillations do not have such a large angle as to allow the laser tachometer to intercept the reflective material, which therefore does not send any electrical impulse.

The following graphs show displacements measured in two different sections of the rotor defined by the position of the sensors: section 1 is located at a distance of 30 mm from the constraint plate, while section 2 at a distance of 100 mm.

9.3.1 Test 1-9 (plastic plate, drifting)

In this group of tests carried out with the plastic constraint plate, the rotor had a particular dynamic behaviour caused by its end in contact with the plate constraint. The displacement shows a periodic increase in its value followed by a fast decrease as soon as the rotor tip reaches a limit position, as it can be seen from figure (9.3.1.4). The cause of this phenomenon is probably the interaction between the constraint friction and the force components in the radial direction given during the initial spin of the rotor. The phenomenon is clearly more visible in the displacements at section 1 since it is closer to the plastic plate. The figures shown refer to test 8.

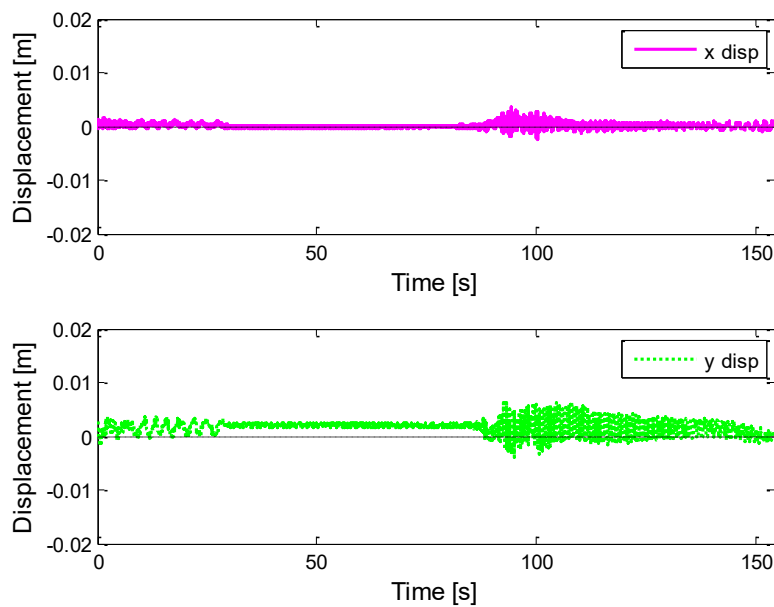


Figure 9.3.1.1 – Displacements section 1.

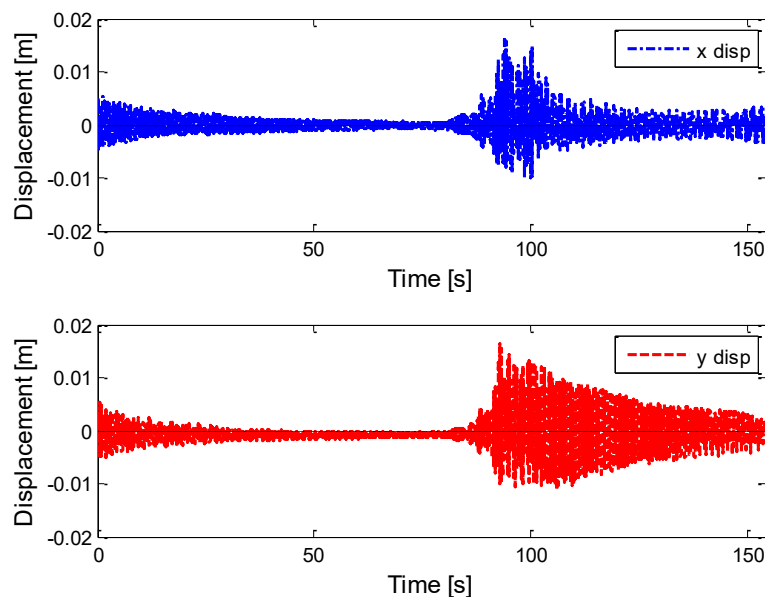


Figure 9.3.1.2 – Displacements section 2.

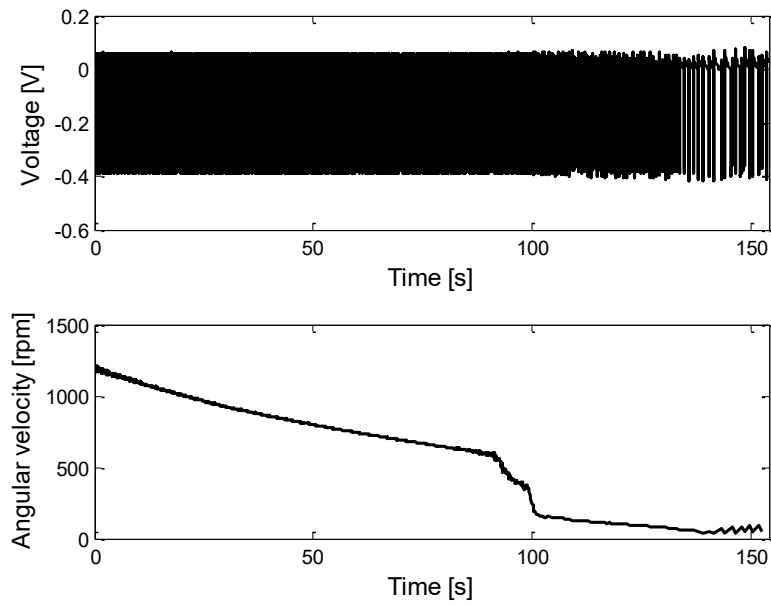


Figure 9.3.1.3 – Voltage pulses and angular velocity.

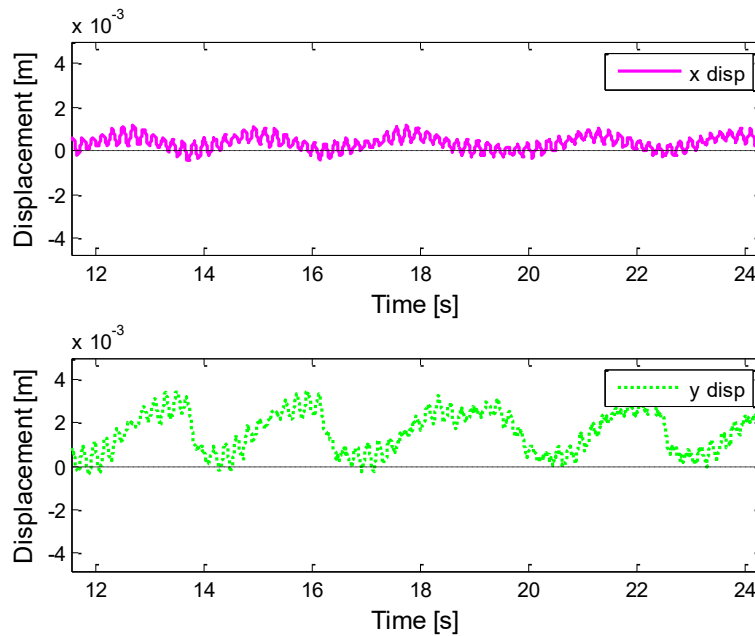


Figure 9.3.1.4 – Displacements section 1 detail (drifting).

9.3.2 Test 10-16 (plastic plate, no drifting)

The drifting phenomenon no longer occurred from test number 10 onwards, and since the same hand-actuation procedure continued to be used, although not perfectly repeatable, this was due to the creation of a small groove on the plate which significantly reduced the area in which the rotor tip moved. The figures shown refer to test 12.

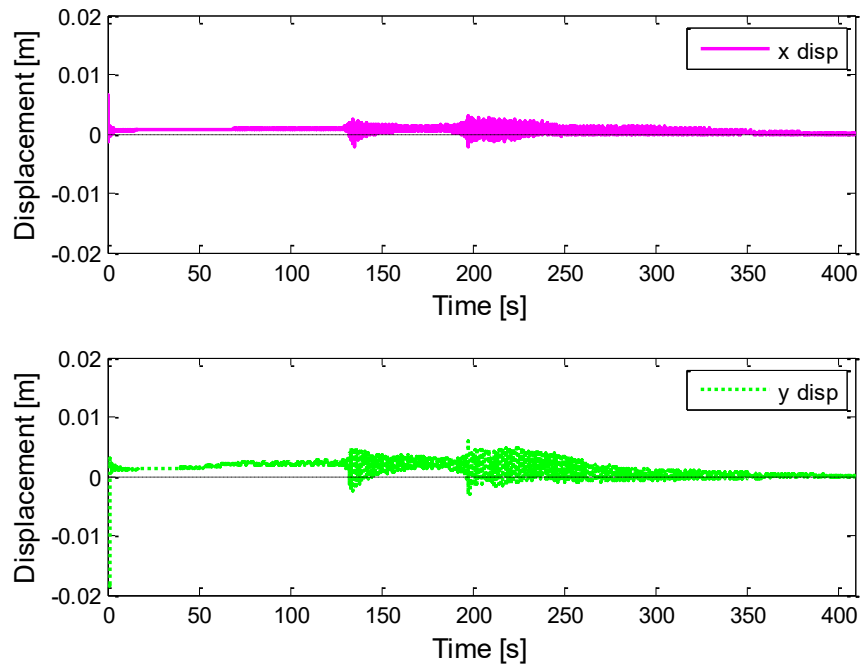


Figure 9.3.2.1 – Displacements section 1.

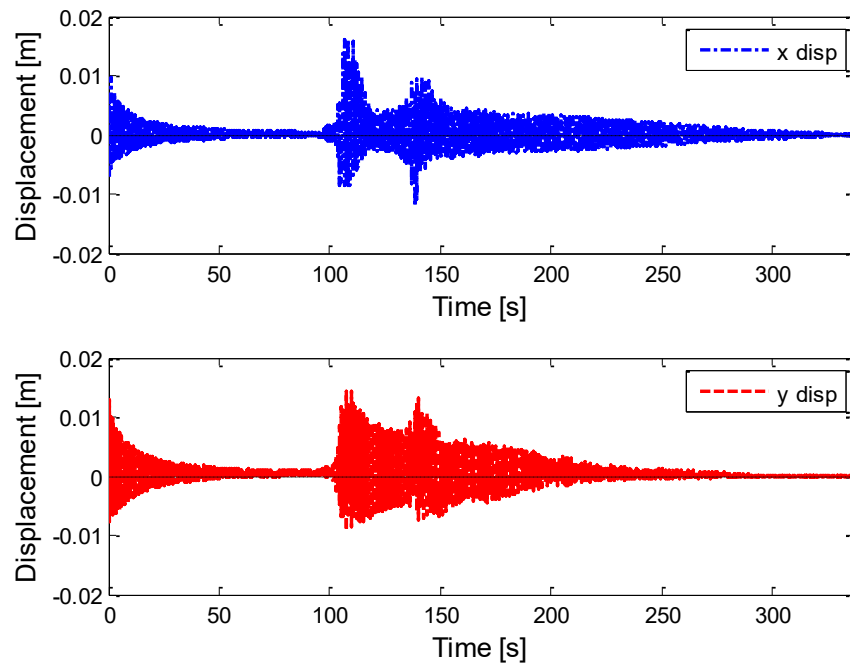


Figure 9.3.2.2 – Displacements section 2.

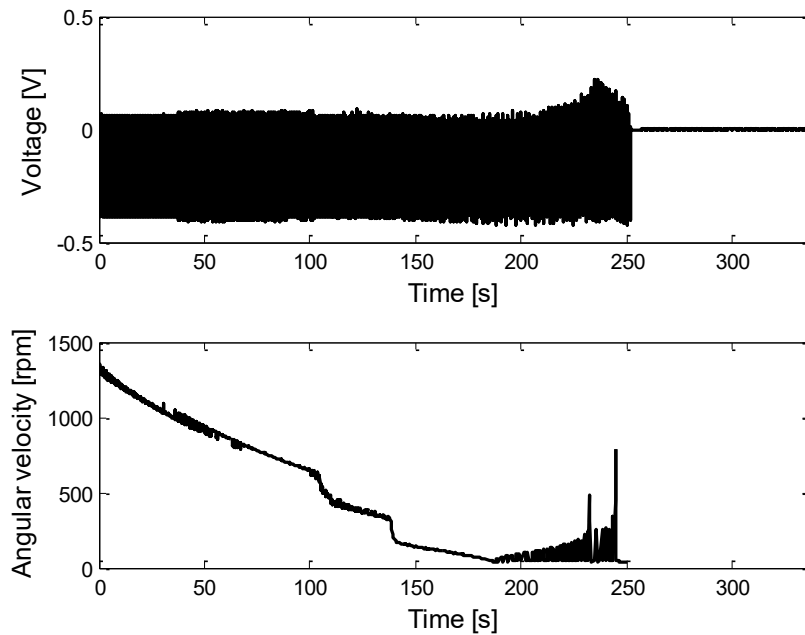


Figure 9.3.2.3 – Voltage pulses and angular velocity.

9.3.3 Test 17-21 (glass plate, no drifting)

We carried out the last group of tests replacing the plastic plate with a glass one to analyse the effect the constraint material had on the system. The results showed better dynamic behaviour, with a higher initial speed reached with respect to the tests with the plastic plate, which, in addition to the reduction in friction with the rotor tip, increased the time required for the rotor to stop. The figures shown refer to test 17.

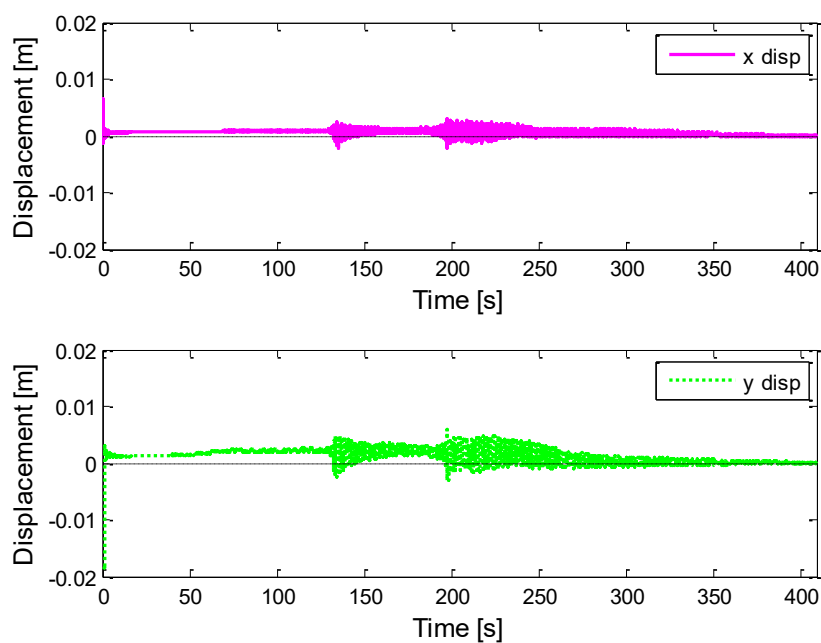


Figure 9.3.3.1 – Displacements section 1.

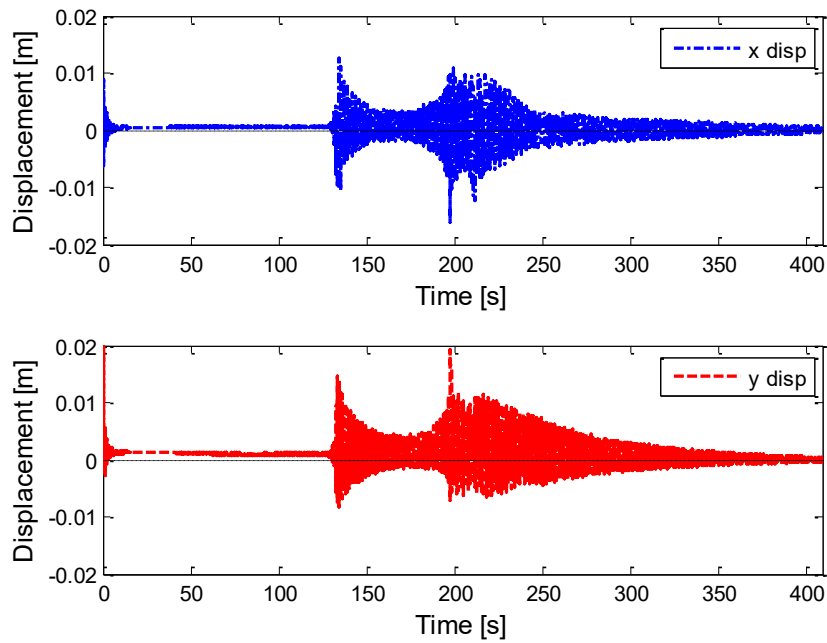


Figure 9.3.3.2 – Displacements section 2.

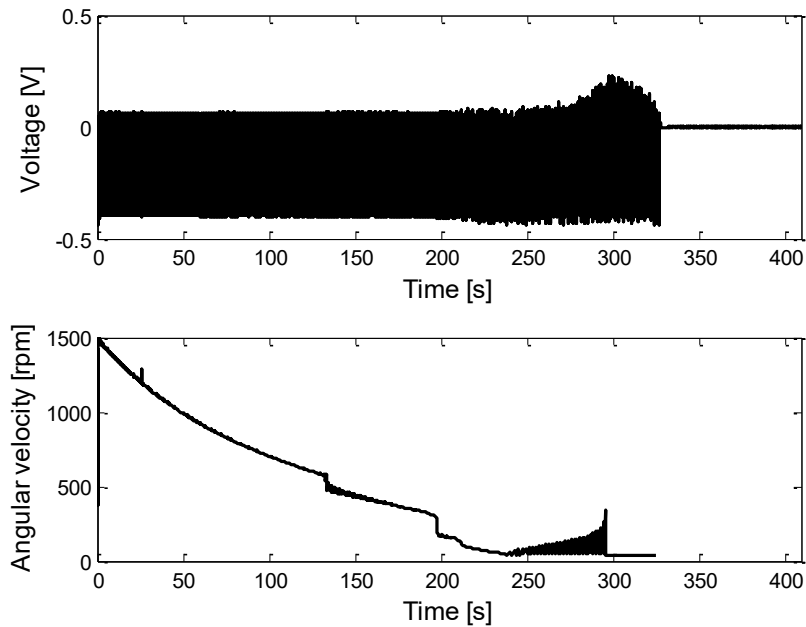


Figure 9.3.3.3 – Voltage pulses and angular velocity.

9.3.4 Analysis of dynamic rotor behaviour

In order to analyse how the magnetic rotor behaves during its operation, we consider it appropriate to study the rotations and translations data of its axis calculated as explained before, instead of using the displacements detected by the individual sensors. The graphs below show the values of parameters of test 17, whose measurements made by the lasers are shown in the previous paragraph.

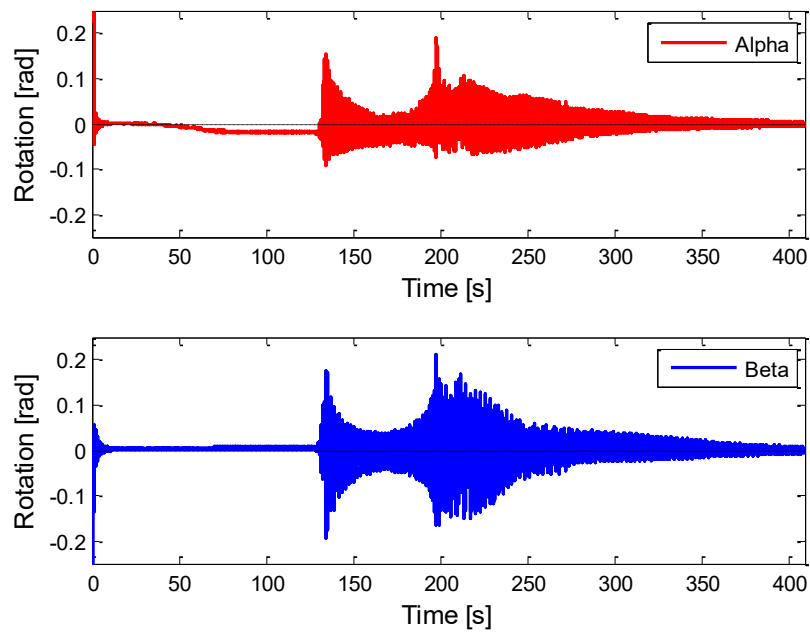


Figure 9.3.4.1 – Rotations alfa (around x axis) and beta (around y axis).

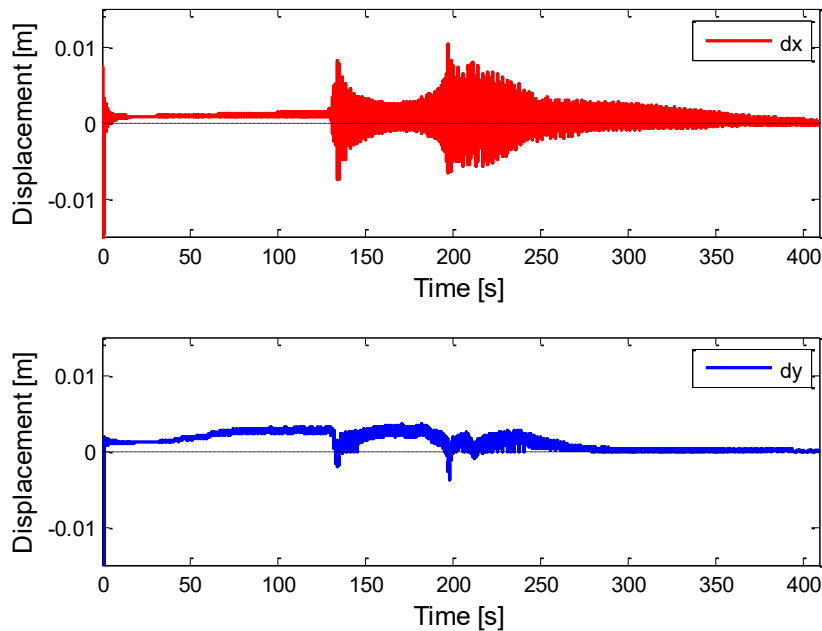


Figure 9.3.4.2 – Translations dx and dy.

The large variations in the initial values of the parameters are data errors caused by starting the measurements when the rotor was already in motion, thus needing a short time interval before stabilising the measured data.

We can easily identify areas of instability due to resonance by studying the displacement of the axis in space. The parameter we chose to study is the angle of alpha rotation around the x-axis as it clearly shows the zones mentioned above. We can identify the instant of time in which there is a large increase in its value and read the angular velocity at the correspondent time from the graph of the latter.

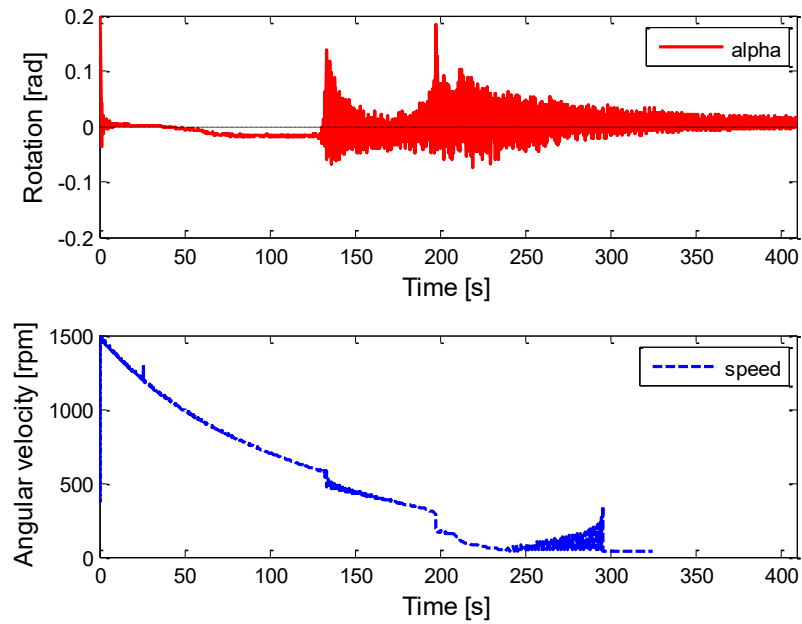


Figure 9.3.4.3 – Rotation alfa (around x axis) and beta (around y axis).

The first resonance peak occurs for a rotational speed of about 525 rpm.

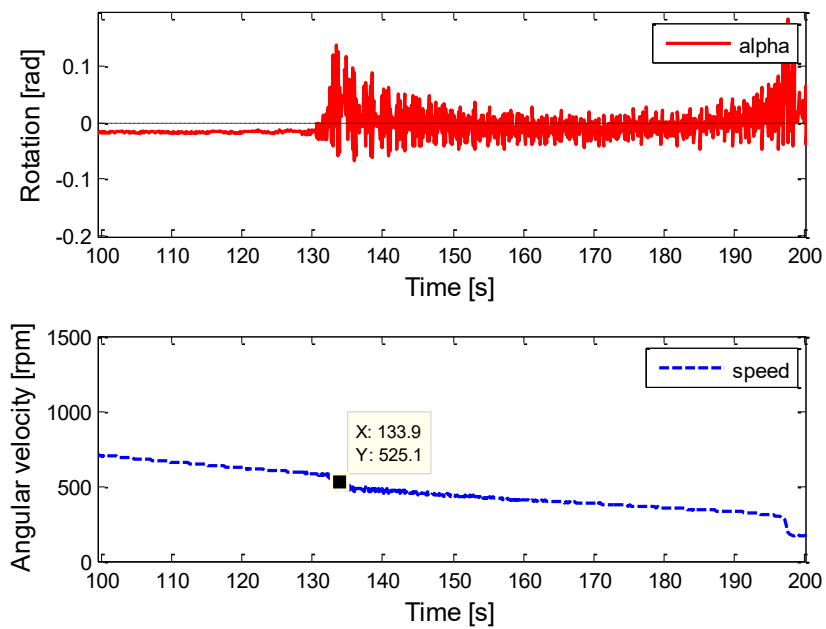


Figure 9.3.4.4 – First resonance.

The second resonance peak occurs for a rotational speed of about 235 rpm.

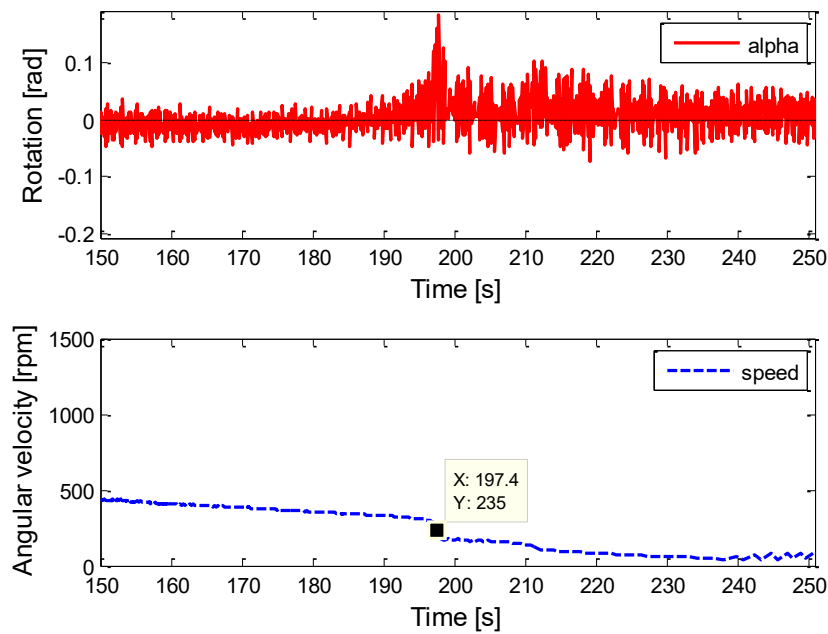


Figure 9.3.4.5 – Second resonance.

Finally, we noticed a further peculiar behaviour of the rotor with regard to its inclination in certain phases of its operation: the alpha angle assumes negative values after about 45 seconds from the start of the measurement, while showing a stable dynamic behaviour. This means that the rotor rotates slightly inclined downwards, probably due to the contact between its end and the tie plate. We can see this behaviour not just from the angle alpha, but also from the vertical displacement values measured by the optical sensors: the y-displacements measured by sensor 2 in section 1 (the one closest to the plate) are greater than those measured by sensor 4 in section 2.

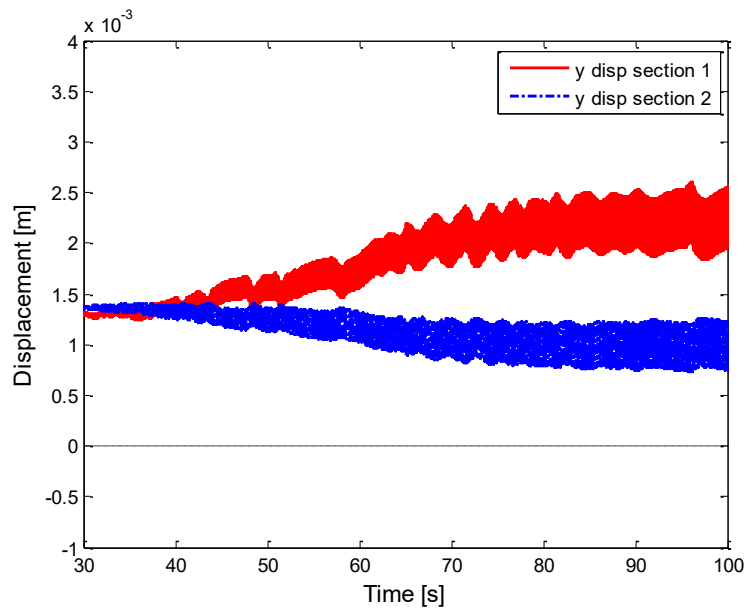


Figure 9.3.4.6 – y displacements measured in section 1 and 2.

9.3.5 LUPOS model

We used the displacement data collected by the optical sensors and the geometrical considerations given in chapter 9.2.1 to create a Matlab model of the rotor's motion in space during the tests. We created this model by means of the software LUPOS, developed by Prof. Bonisoli E. and his research team, which is a parametric FEM code that has the aim to merge together different simulative characteristics:

- Providing a complete open source 3D FEM code suitable for analysing elements formulations, assembly approaches, reduction techniques in a complete parametric scheme;
- Allowing parametric analyses and integrating results, giving all matrices details and formulations;
- Integrating this parametric FEM code in Multi-Body and nonlinear integration processes such as Simulink.

In order to create this model, it is necessary to define the nodes whose displacements are analysed as a function of time, to specify their degrees of freedom, to define the geometry with which they are connected, and to provide data on the displacements of the nodes as a function of time. The nodes chosen are points of the rotor axis, and the points on which the sensors carried out their measurements.

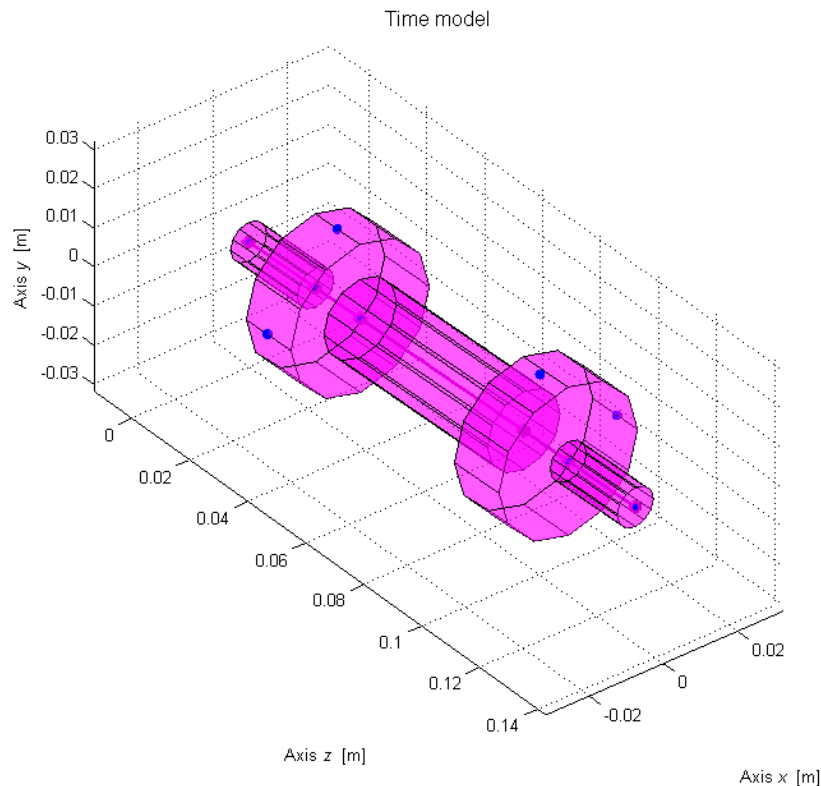


Figure 9.3.5.1 – LUPOS model of the magnetic rotor.

9.3.6 Analysis in frequency domain

In order to study the behaviour of the magnetic rotor in frequency domain, we post-processed the acquired data (measured with a frequency sample equal to 8.192 kHz) by means of the Fast Fourier

Transform. The analysis was carried out on the following complex coordinates in order to consider the global contributions of the two translations Δx and Δy and the two rotations α (around x axis) and β (around y axis), taking into account to define these coordinates as both forward and backward.

Complex forward coordinates:

- $r = \Delta x + i\Delta y$
- $\eta = -\beta + i\alpha$

Complex backward coordinates:

- $r^* = \Delta x - i\Delta y$
- $\eta^* = -\beta - i\alpha$

The result of the Fast Fourier Transform applied to the complex forward coordinate r in a time window between $t_1 = 40$ s e $t_2 = 60$ s, is shown below.

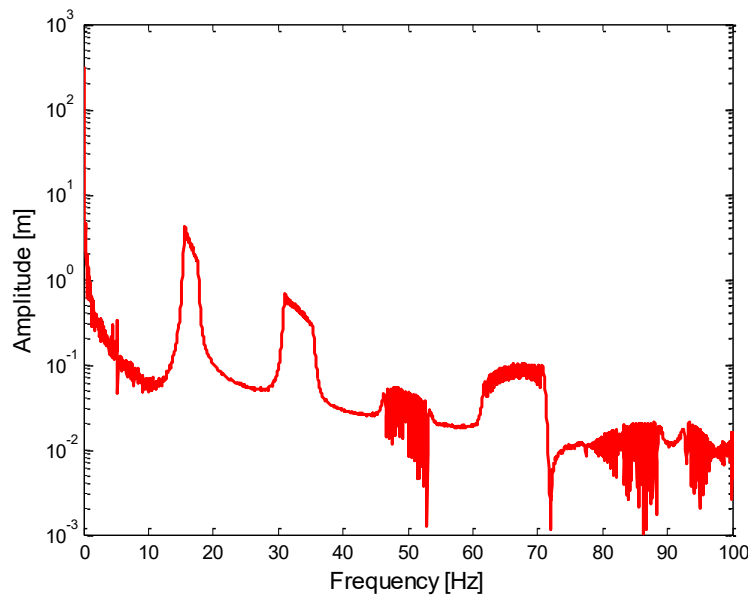


Figure 9.3.6.1 – FFT of the complex coordinate r (with $T_w = [40 \text{ s} : 60 \text{ s}]$).

We notice how the modes have a range of variability that depends on the slope of the harmonic to which they are related, while keeping the same T_{window} . Since the higher are the frequencies relative to a harmonic, the greater will be the slope of the harmonic, we observe from the frequency axis that at 70 Hz there is a wider frequency variability with respect to the harmonic whose frequencies in the graph are around 35 Hz, which in turn has a greater variability than the harmonic whose frequencies in the graph are around 17.5 Hz. Increasing T_{window} this phenomenon is accentuated, decreasing it the opposite happens.

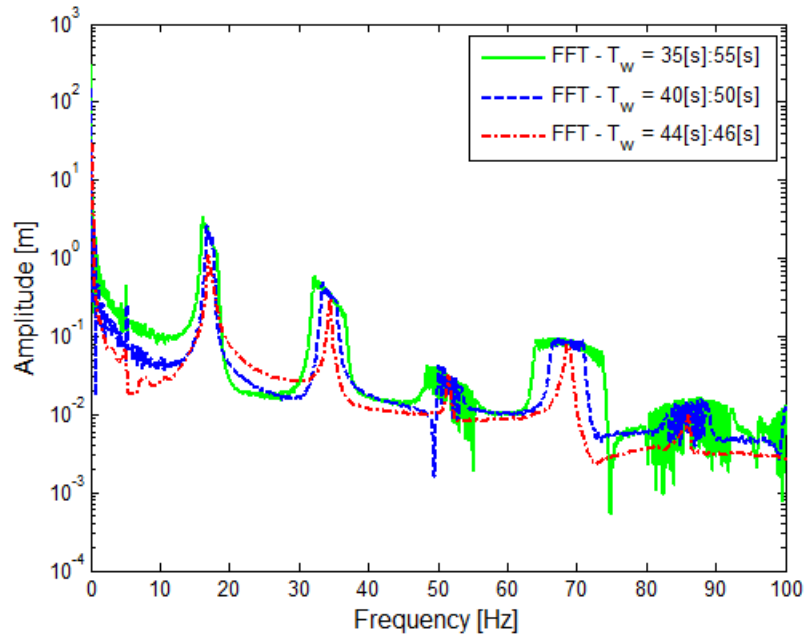
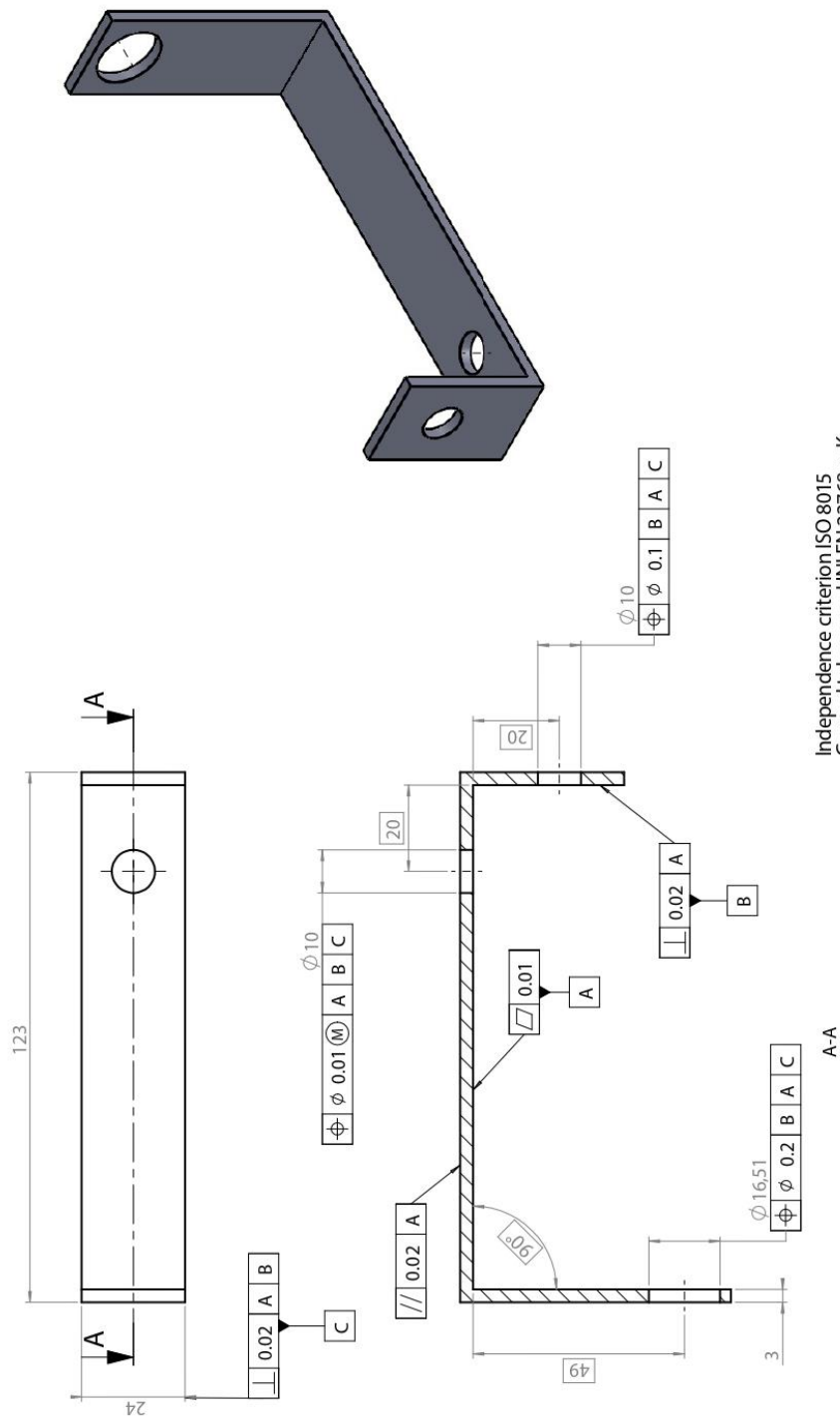


Figure 9.3.6.2 – Comparison of FFT on different T_w .

In addition, the previous figure shows how a harmonic that decreases in a non-linear way with a non-constant derivative, as the T_{window} varies, exhibits a non equal increase/decrease between the two parts that delimit its range of assumed frequencies. This variation will be greater for the part at higher frequencies.

Appendix

The drawings of the components that were projected to create the magnetic rotor test rig are shown in the following pages. We decided not to include drawings of modifications made to existing parts with technical drawings that had already been made in other previous thesis works.



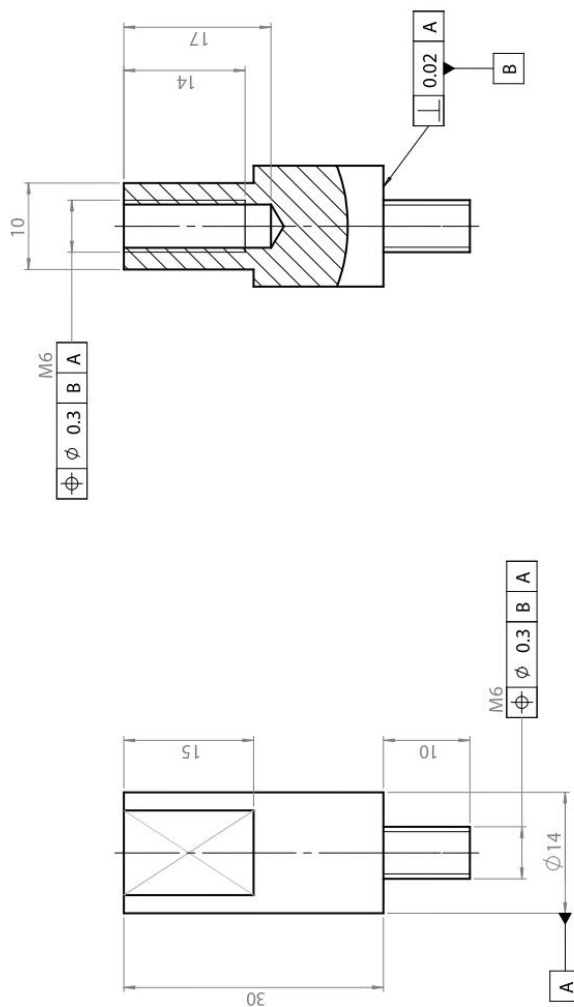
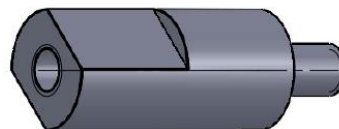
Independence criterion ISO 8015
General tolerances UNI EN 22768-mK

#	-	MATERIAL	Aluminium	STUDENT	Build	19/09/2021 12:16:13
SUBJECT		DESCRIPTION	Bracket_custom	COURSE	SCALE	1:1
					DATE	15/10/2021
					SURFACE TEXTURE	WEIGHT (kg)
					Ra 3.2	
					PAPER	Drawing N.
					A3 1/1	



Politecnico di Torino

Politecnico di Torino - Corso Duca degli Abruzzi, 24 - 10129 TORINO



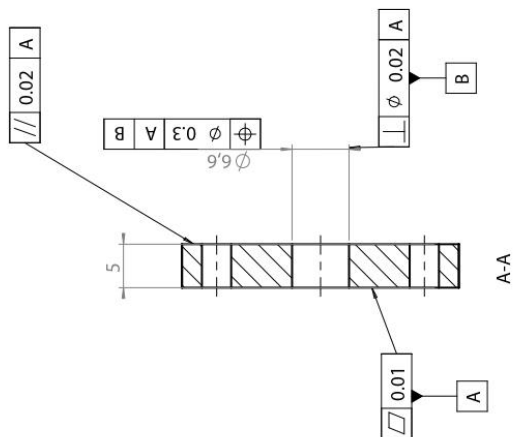
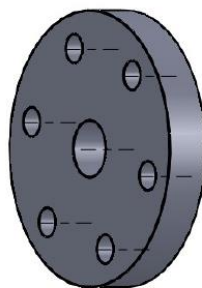
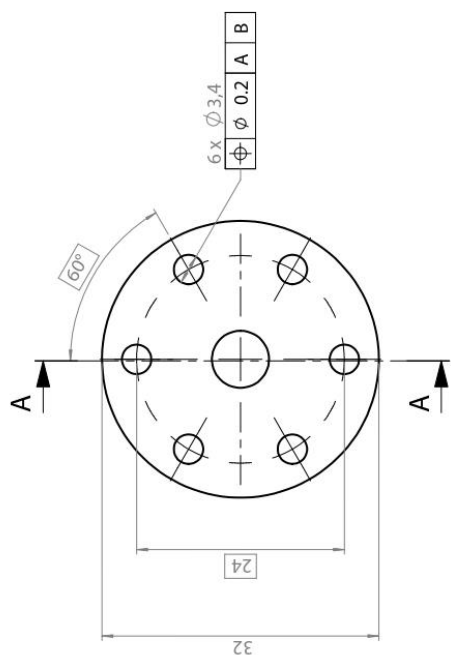
Independence criterion ISO 8015
General tolerances UNI EN 22768-mk

#	-	MATERIAL	Aluminium	STUDENT	Build	07/09/2021 11:38:13
SUBJECT				COURSE	SCALE	2:1
DESCRIPTION			Connection_clutch_rotor_down		DATE	15/10/2021
				SURFACE TEXTURE	WEIGHT (kg)	
				$Ra 3.2$		
				PAPER	Drawing N.	
				A3 1/1		




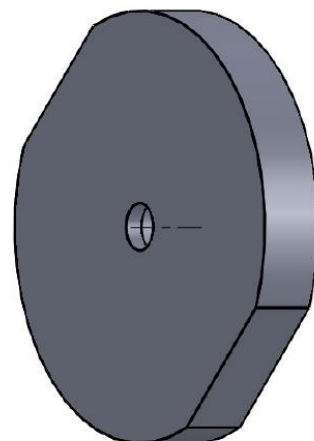
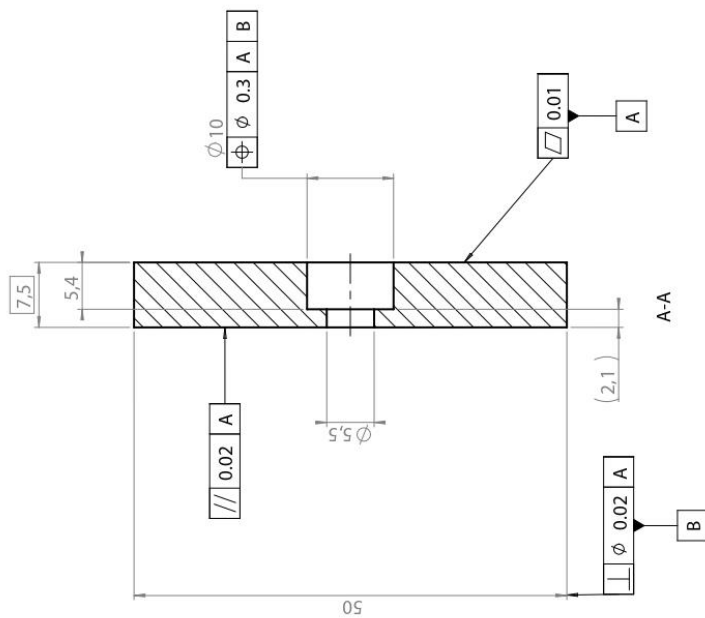
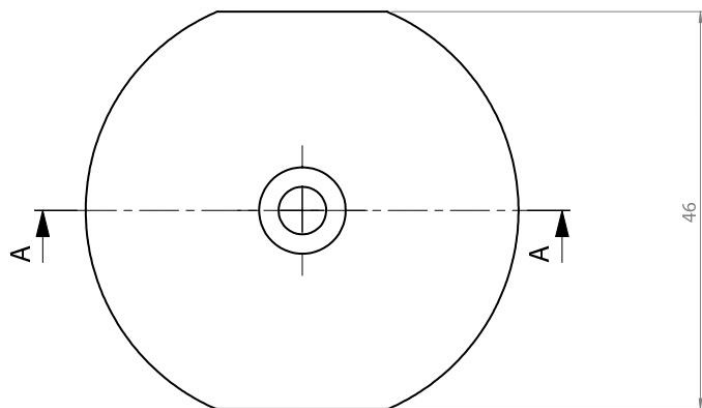
Politecnico di
Torino

Politecnico di Torino - Corso Duca degli Abruzzi, 24 - 10129 TORINO



Independence criterion ISO 8015
General tolerances UNI EN 22768-mK

#	-	MATERIAL	Aluminium	STUDENT	Build	18/07/2021 172903
SUBJECT				COURSE	SCALE	2:1
DESCRIPTION			Connection_clutch_rotor_up		DATE	15/10/2021
 Politecnico di Torino Consorzio degli Abruzzi, 24 - 10129 TORINO				SURFACE TEXTURE	WEIGHT (kg)	
				Ra 3.2		
				PAPER	Drawing N.	
				A3 1/1		



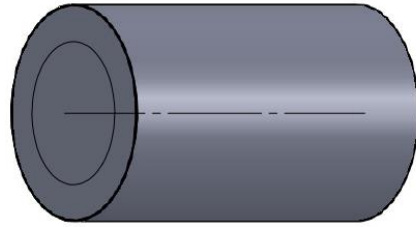
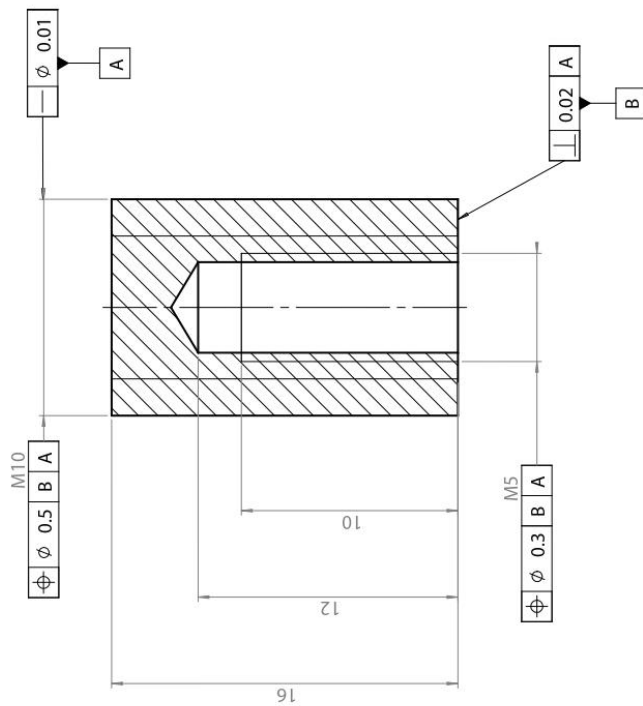
Independence criterion ISO 8015
General tolerances UNI EN 22768-mK

#	-	MATERIAL	Aluminium	STUDENT	Build	07/09/2021 172209
SUBJECT				COURSE	SCALE	2:1
DESCRIPTION			S_cylinder_down_1		DATE	15/10/2021
				SURFACE TEXTURE	WEIGHT (kg)	
				Ra 3.2		
				PAPER	Drawing N.	
				A3 1/1		



Politecnico
di
Torino

Politecnico di Torino - Corso Duca degli Abruzzi, 24 - 10129 TORINO



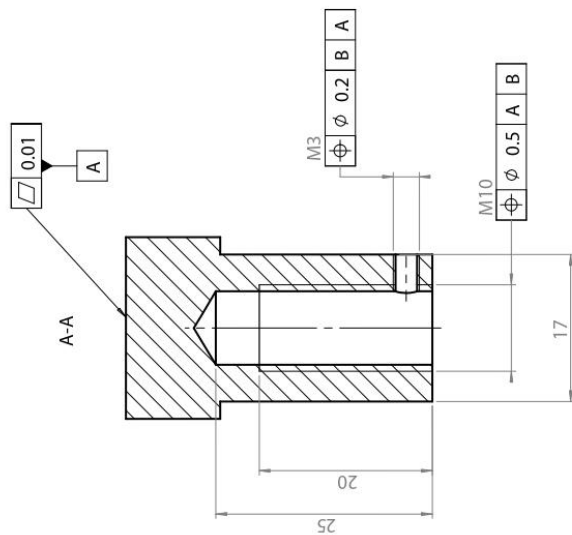
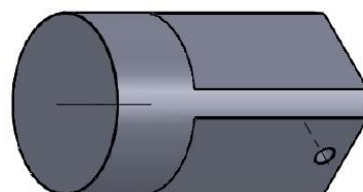
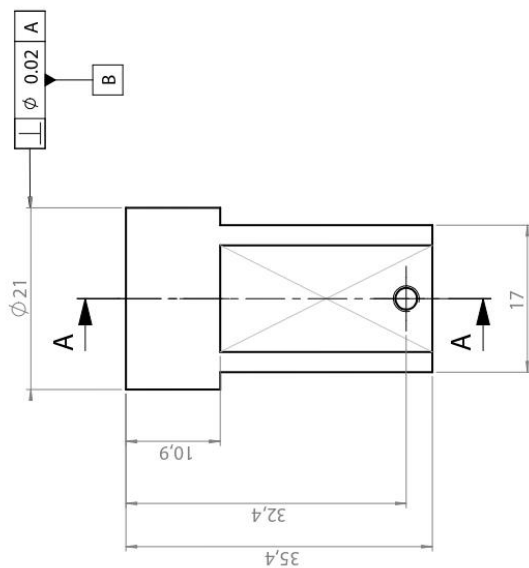
Independence criterion ISO 8015
General tolerances UNI EN 22768-mK

#	-	MATERIAL	Aluminium	STUDENT	Build	07/09/2021 172209
SUBJECT		DESCRIPTION	S_cylinder_down_2	COURSE	SCALE	5:1
					DATE	15/10/2021
					SURFACE TEXTURE	WEIGHT (kg)
					Ra 3.2	
					PAPER	Drawing N.
					A3 1/1	




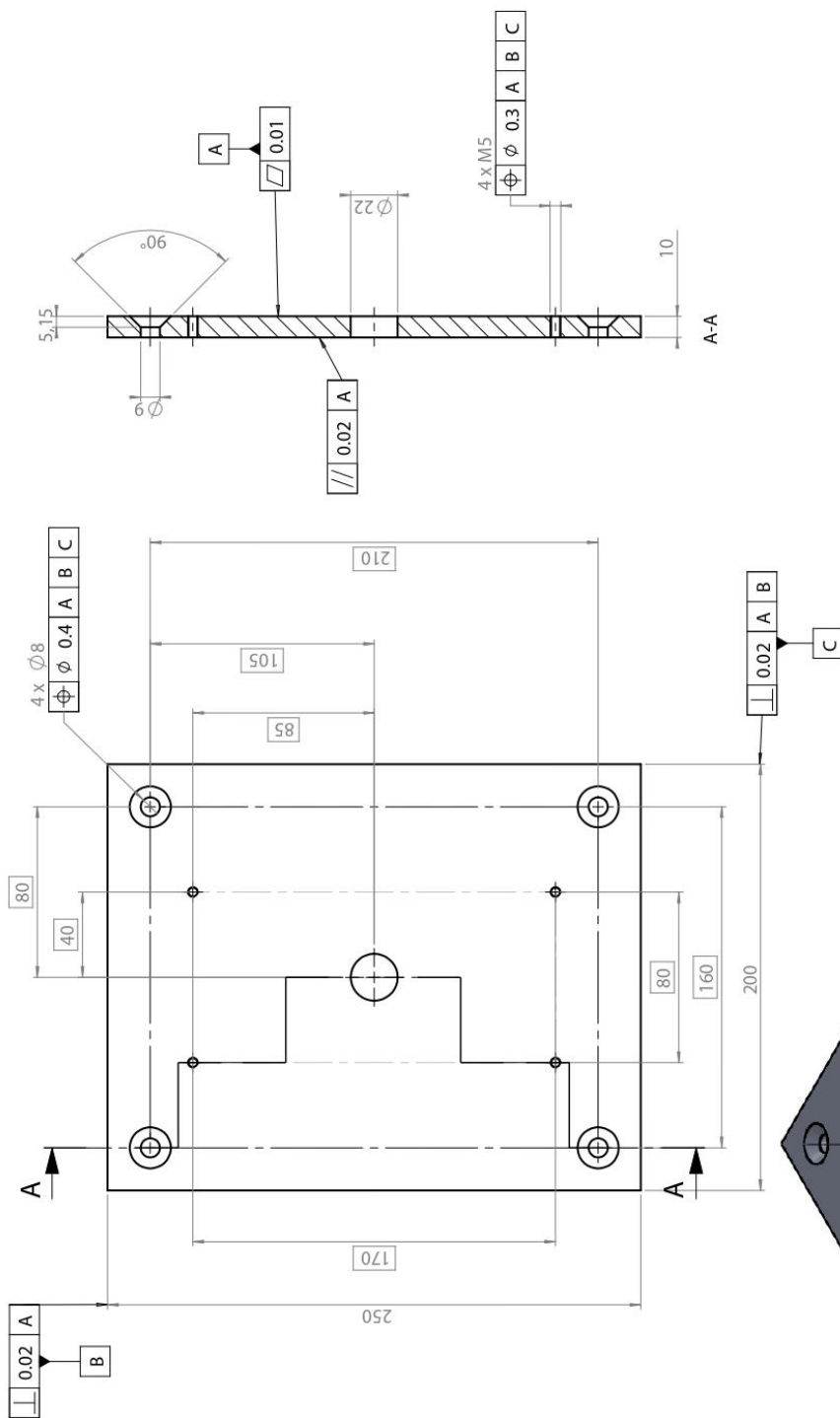
Politecnico
di
Torino

Politecnico di Torino - Corso Duca degli Abruzzi, 24 - 10129 TORINO




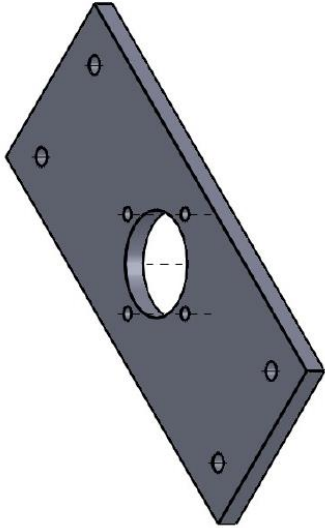
Independence criterion ISO 8015
General tolerances UNI EN 22768-mk

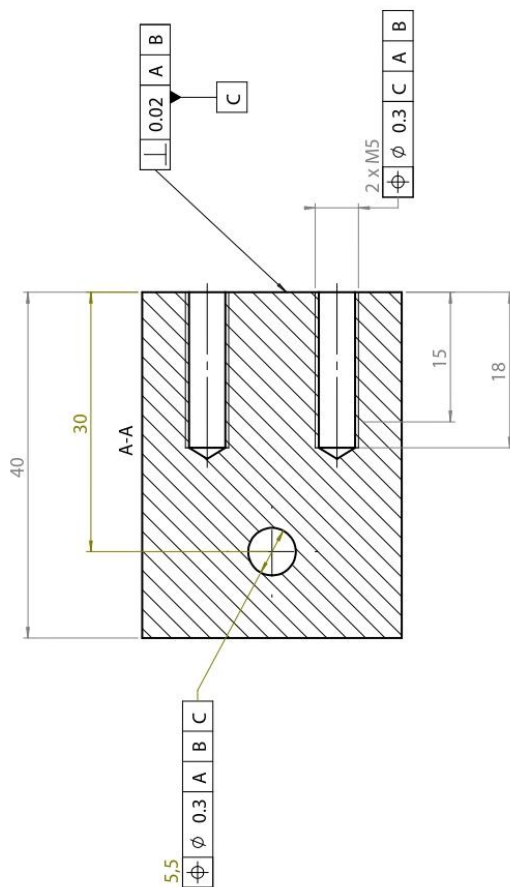
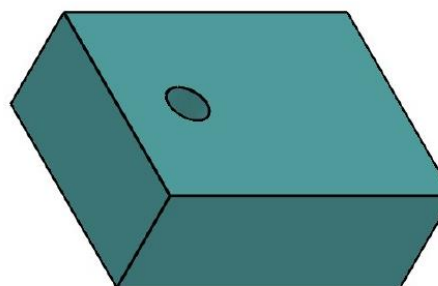
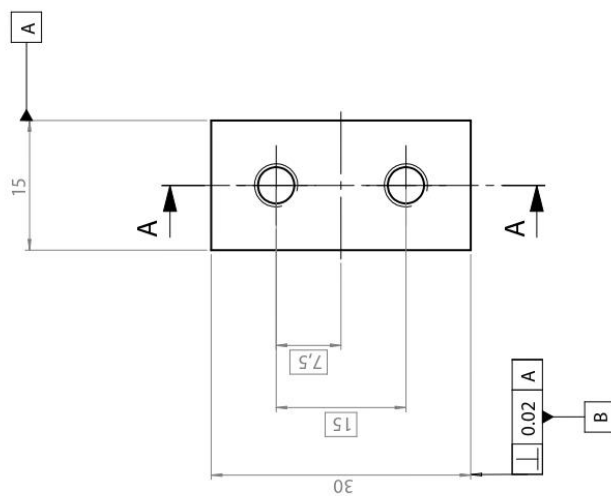
#	-	MATERIAL	Aluminum	STUDENT	Build	14/09/2021 10:28:19
SUBJECT				COURSE	SCALE	2:1
DESCRIPTION	S_cylinder_top				DATE	15/10/2021
		 Politecnico di Torino		SURFACE TEXTURE	WEIGHT (kg)	
				Ra 3.2		
				PAPER	Drawing N.	
				A3 1/1		



Independence criterion ISO 8015
General tolerances UNI EN 22768-mK

#	-	MATERIAL	Aluminium	STUDENT	Build	20/08/2021 180129
SUBJECT				COURSE	SCALE	1:2
DESCRIPTION			S_lower_plate		DATE	15/10/2021
		 Politecnico di Torino - Corso Duca degli Abruzzi, 24 - 10129 TORINO		SURFACE TEXTURE	WEIGHT (Kg)	
				Ra 3.2		
				PAPER	Drawing N.	
				A3 1/1		





Independence criterion ISO 8015
General tolerances UNI EN 22768-mk

#	-	MATERIAL	Delrim	STUDENT	Build	14/09/2021 11:45:37
SUBJECT				COURSE	SCALE	2:1
DESCRIPTION	Stator_block				DATE	15/10/2021
		Politecnico di Torino		SURFACE TEXTURE	WEIGHT (kg)	
				Ra 3.2		
				PAPER	Drawing N.	
				A3 1/1		

Reference

- [1] Costantino Gagliardi, Analysis of rotor configurations, M.Sc. Thesis, Politecnico di Torino, Department of Mechanical and Aerospace Engineering.
- [2] Bonisoli E., "LUPOS: LUMped Parameters Open Source FEM code", Tutorial v.2021-09-16, Politecnico di Torino, Department of Mechanical and Aerospace of Mechanical and Aerospace Engineering, 2021.
- [3] Fasana A., Marchesiello S., *Meccanica delle vibrazioni*, CLUT, Turin, 2006.
- [4] Bonisoli E., Delprete C., "Nonlinear and linearised behaviour of the Levitron", *Meccanica*, 2015.
- [5] Marchesiello S., corso di "Dinamica dei sistemi meccanici", Politecnico di Torino, Department of Mechanical and Aerospace Engineering, 2018.